Syed Mohammad Mujtaba

Analysis and Implementation of Energy Management System on Concept Design of Gløshaugen Microgrid

Master's thesis

NTNU
Norwegian University of Science and Technology
Faculty of Information Technology and Electrical Engineering
Department of Electric Power Engineering

Master's thesis in MSc. Electric Power Engineering

Supervisor: Irina Oleinikova

July 2020

NTNU
Norwegian University of Science and Technology

Syed Mohammad Mujtaba

Analysis and Implementation of Energy Management System on Concept Design of Gløshaugen Microgrid

Master's thesis in MSc. Electric Power Engineering
Supervisor: Irina Oleinikova
July 2020

Norwegian University of Science and Technology
Faculty of Information Technology and Electrical Engineering
Department of Electric Power Engineering

NTNU
Norwegian University of
Science and Technology

Syed Mohammad Mujtaba

Analysis and Implementation of Energy Management System on Concept Design of Gløshaugen Microgrid

Master Thesis

Trondheim, July 2020

Supervisor: Irina Oleinikova

Norwegian University of Science and Technology
Faculty of Information Technology and Electrical Engineering
Department of Electric Power Engineering

ABSTRACT

Distributed Energy Sources (DERs) have been the focus of the modern power industry as they are proven to be a more efficient and reliable source of energy supply. Renewable Energy Sources (RES) and other DERs are integrated into the grid at the distribution level to set up a Microgrid (MG). The main objective of this thesis was to develop a concept design of NTNU Gløshaugen campus as a microgrid; implement energy management system with PVs and batteries to achieve peak-shaving; and improve the stability of the microgrid during load variations and after fault clearance. Data from the existing grid network was used to model the campus on ETAP-16. Time-based AC/DC Load flow and transient stability simulations were performed to analyze the system behaviour under different conditions. The burden on the utility grid was reduced significantly after the integration of PVs and batteries during peak hours. The adequate operation of batteries resulted in achieving a flat utility output power curve when the demand was high. The stability of the system was improved with the generator's exciter AVR control for the worst-case scenario. As a result, the bus and generator parameters were reaching their steady-state values within a reasonable time.

Acknowledgement

I would first like to express my highest regards and gratitude to Masumeen A.S. and all the people who inspired me, encouraged me, enriched me, believed in me and guided me throughout the journey of my masters at the Norwegian University of Science and Technology. First in the list is my supervisor Irina Oleinikova for her continued support and guidance throughout the process. She ensured to steer me in the right direction while I have all the tools and resources available to carry out this work.

I would like to extend special thanks to all the professors and the faculty members of NTNU especially, Erik Næss and Pedro Crespo from SINTEF and CityExChange for providing me with the necessary information and data for completing my thesis.

In the end, I would like to thank my parents and the rest of my family and friends who have prayed for me, supported, tolerated and encouraged me throughout this work. Without their passionate participation and input, the thesis could not have been successfully completed.

Table of Content

List of Figures

List of Tables

ABBREVIATIONS

MG	Microgrid
DG	Distributed Generation
DER	Distributed Energy Resources
RES	Renewable Energy Sources
CHP	Combined Heat and Power
PV	Photovoltaics
ESS	Energy Storage System
NTNU	Norwegian University of Science and Technology
ETAP	Electrical Transient Analyzer Program
AC	Alternating Current
DC	Direct Current
BEMS	Building and Energy Management System
EMS	Energy Monitoring System
PCC	Point of Common Coupling
MPPT	Maximum Power Point Tracking
IGBT	Insulated-Gate Bipolar Transistor
CHP	Combined Heat and Power
AVR	Automatic Voltage Regulator
LTC	Load Tap Changer
LF	Load Flow
LFA	Load Flow Analysis
NR	Newton Raphson
PSS	Power System Stabilizer
EMS	Energy Management System
LTC	Load Tap Changer
DSM	Demand Side Management
BMS	Battery Management System
SSS	Small Signal Stability
LGS	Large Signal Stability

1 INTRODUCTION

As the energy demand is increasing due to electrification, fulfilling the ever-increasing demand rises severe concerns amongst the government and concerned relevant organizations. The conventional approach of energy production (using thermal/coal powerplants) has been contributing to severe damages to the environment in terms of global warming. Figure 1-1 represents the global warming index for over 100 years obtained from NASA [1]. The decline in fossil fuel and its negative impact on the environment has forced engineers and scientists to look for alternatives in the field of power systems. These problems have motivated the scientists to study in detail the concept of alternative energy sources such as solar energy, wind energy, Combined Heat and Power (CHP) systems, energy storage systems and micro-turbines relative to the conventional power generating sources.

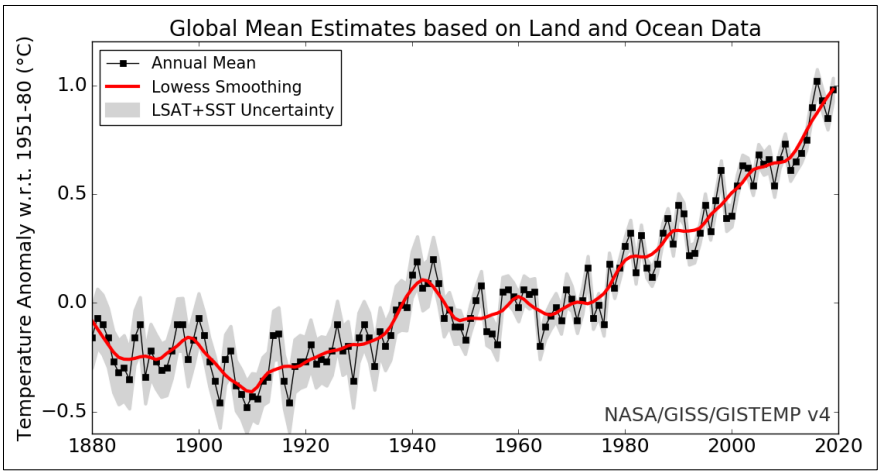

Figure 1-1 Global warming index over 100 years

As the generation, transmission and distribution network is ageing with time, the integration of Renewable Energy Sources (RES) into the existing grid comes as a robust and reliable solution. Furthermore, the innovation introduced the concept of on-site generation, meaning that the generating sources located close to the load to avoid transmission losses. This concept of on-site generation is labelled as Distributed Energy Resources (DER), which involves a variety of power source types. Hence the generation type is called Distributed Generation (DG).

Despite the RES having environmental and operational advantages over fossil fuels, high installation and maintenance costs come as an obstacle to the widespread use of renewable generation worldwide [2]. To achieve the objective of having a carbon-free environment, governments have defined targets for the reduction of greenhouse gasses, an increase in shares of RES and improvements in the energy efficiency for the future [3]. Figure 1-2 represents the global demand and the contribution of the expected energy sources that may fulfil the demand

until 2050 [4]. With the contribution of renewable energy sources (RES) growing in the power industry, experts predict that the RES will have a share of around 80 % of total power generation in 2050.

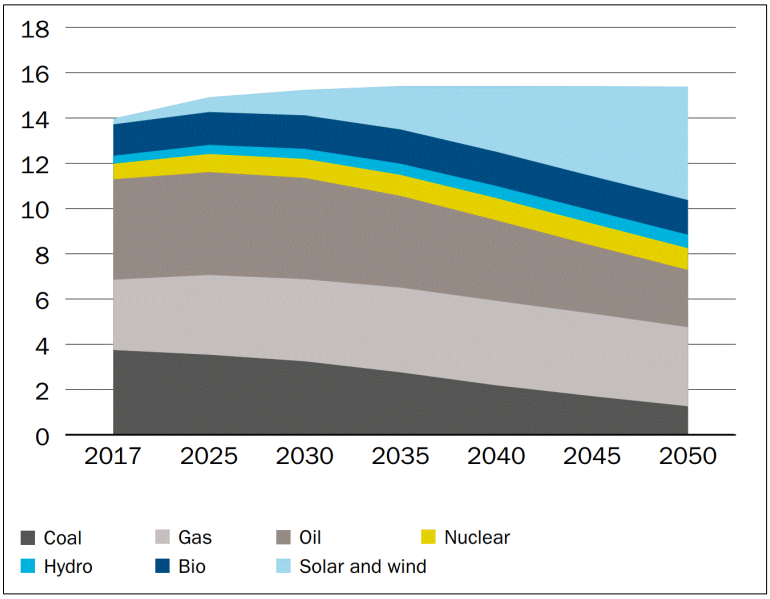

Figure 1-2 Global energy balance in primary energy from 2019 until 2050

1.1 Distributed Generation

Under the centralized generation paradigm, electricity is produced mainly at extensive generation facilities, located at a distance from the consumers. The electricity is then shipped through the transmission and then the distribution grids to reach the end consumers, i.e. loads. This process contributes to losses in the transmission and distribution network that comes for a cost. On the other hand, the decentralized systems involve distributed generation that is relatively complex but has more advantages once implemented [3].

Distributed generation has been defined differently by various organizations. P. A. Daly defines DG as small-scale, environmentally-friendly technologies such as micro-turbines, photovoltaics (PV), wind turbines and batteries as energy storage system (ESS) – that are installed at the distribution level to serve the consumers in defined premises [5]. Where the integration of RES plays a role in the provision of active power, mainly, the microturbines and internal combustion engines provide the system with voltage stability and reduction of reactive power losses [5]. One of the main advantages of having DERs is that the transmission losses that occur while transporting electricity reduce since the generation units are located close to the electrical load. A system with well-planned and operated DGs can also contribute to energy efficiency, economic savings and greater reliability [5].

1.2 Microgrid

While the implementation of deploying DERs on-site can reduce the need for the distribution grid enhancement, controlling a large number of DG units create various new challenges for managing and operating the network efficiently and safely. This issue is partially addressed by microgrids when connected to the AC grid, as they coordinate DERs in a more decentralized manner, thereby reducing the burden on the main grid and allowing them to provide more flexibility [6]. Furthermore, microgrids can isolate themselves from the main grid acting as a standalone system, providing electrical energy in regions of developing countries where the conventional AC grids are either unreliable or unavailable [7]. Since the evolution of microgrids shows significant advantages, Norway also has had some projects related to the development of microgrids in various regions. According to a report by 'Smart Innovation Norway', Hvaler Energy Park, consisting of 1200 square meters of PV facility and one wind turbine, became the first full-scale microgrid in 2017. The microgrid can operate under island mode when the local power grid is down and can run until the grid is back to normal, switching the microgrid back to the grid-connected mode of operation. The facility expects to run on its own for approximately six months, from spring to fall [8].

1.3 +CityXChange Project

Positive City XChange is a smart-city project hosted by the Norwegian University of Science & Technology that leads the consortium with the LCTK (Lighthouse Cities Trondheim Kommune) and Limerick City. The project is funded by the EU Horizon 2020 research program named 'Smart Cities and Communities'. The aims of the project are to develop a framework for enabling an improvised structure of a common energy market that is supported by a connected community [9]. The technical part of the project focuses on integrating local distributed RES and ESS (Energy Storage System) in the distribution grid and connecting building systems to energy communities and power markets. Another area of focus on the optimization of energy system operation along with mobility solutions [10].

The seventh work package of the project (DP07) focuses on the development of microgrids to balance and optimize the energy in the positive energy block through microgrids. The demonstration areas in Trondheim are Sluppen-Tempe, Brattøra and the NTNU Gløshaugen campus facilities. Figure 1-3 represents the satellite view of the main areas where the pilot projects are being carried out. The main research area of this thesis is the modelling and analysis of the Gløshaugen campus as a microgrid.

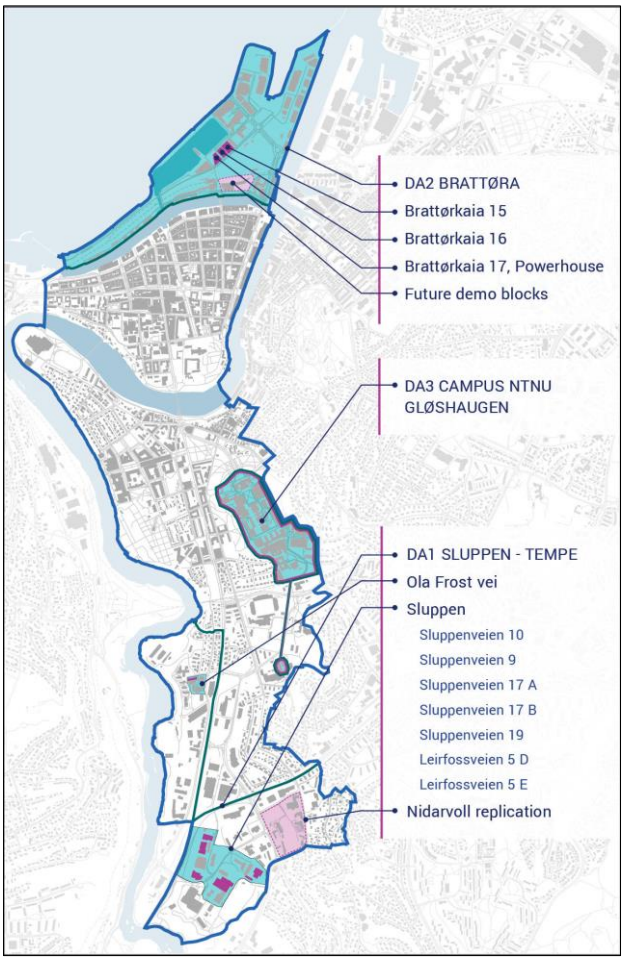

Figure 1-3 Satellite view of the demonstration areas of CityXChange project (Source: cityxchange.eu)

1.4 NTNU Gløshaugen Campus

The NTNU Gløshaugen campus comprises of a total of 35 buildings, covering approximately 300,000 square meters and the expansion of the campus is expected to occur during 2020-2022 [11]. The largest building with the most energy consumption is the Realfagbygget covering an area of approximately 60,000 square meters, followed by the rest of the building blocks. As mentioned by Olav Fosso in [12], the Norwegian grid supplies 400 Volts and 230 Volts at the distribution level in most of the areas. The Gløshaugen campus includes electrical and heating loads that operate on both 400 and 230 Volts depending on the equipment and buildings. According to the Building and Energy Management System (BEMS) and Energy Monitoring System (EMS) available at NTNU, there are 79 electricity meters and 46 heating meters installed on campus [11]. This thesis will use the data for electrical loads from [11] assuming that there would be minor adjustments as the campus facilities have not seen any major expansion until the year 2020. The technical minutiae of the campus will be addressed in later chapters of this thesis report.

The concept microgrid of Gløshaugen was developed on electrical power system analysis and operation software ETAP-16. ETAP is the most comprehensive software for power system design, simulation, operation, control, monitoring, optimization and automation [13]. It can perform multiple studies, mainly Load Flow (AC and DC, balanced and unbalanced, time-domain), Short Circuit studies, Transient Stability. ETAP is used by various industries specializing in different areas of the power system design as it is user friendly and includes all the tools for designing a power system of any size. ETAP has the edge over other few power system software as it has a relatively shorter simulation time which allows the user to alter and improve their design in a shorter time. The software capabilities and functionalities will be further explained later in this thesis in the methodology chapter.

1.5 Aims and Objectives

The aims and objectives of this thesis were divided into three main parts.

1. The first objective was to develop the concept design of the Gløshaugen campus as a microgrid using the existing grid data and assumption.
2. The second objective was to implement the Energy Management System (EMS) by integrating the RES and Energy Storage System (ESS).
3. The third objective of the thesis was to study, analyse and stabilize the system during load variation and fault clearance.

This thesis is structured in eight chapters.

CHAPTER 1: This chapter includes the Introduction and the motivation for this thesis. Brief introduction about the CityXChange project

CHAPTER 2: This chapter discusses the background theoretical knowledge regarding the overview of microgrids and the role of the main components in a microgrid.

CHAPTER 3: System analysis overview of the study performed on two main operational functions, Energy Management System (EMS) and Transient Stability Analysis. These functions will be the basis of the simulations carried out in chapter 5 of this thesis report.

CHAPTER 4: Discussion regarding the methodology and the approach used for developing the concept model of Gløshaugen. The chapter also includes how the data was collected and used.

CHAPTER 5: The development of the concept design model with a detailed explanation of each element used in the model. Final complete model on which the simulations were carried out after eliminating all the errors.

CHAPTER 6: Results and discussions on the EMS and Transient stability analysis performed on the model. Comparison of scenarios with instantaneous and time-domain load flows over 24-hours.

CHAPTER 7: Conclusion and potential improvements and modifications that could be made to the model for future work.

CHAPTER 8: References used for the literature review and theoretical background for the thesis.

2 MICROGRID SYSTEM OVERVIEW

Although Thomas Edison introduced the first microgrid in 1882, the shift towards a liberalized approach with RES and DG integration into distribution grid introduced the modern and optimized concept of microgrids. As of today, the definition of a microgrid is unclear. The various organization have defined microgrids based on their perspectives and opinions. Following are the definitions of microgrid provided by IEEE, Conseil International des Grandes Réseaux Electriques (CIGRE) and the US Department of Energy DoE:

- **US DoE** - A microgrid is a group of interconnected loads and distributed energy resources within clearly defined electrical boundaries that acts as a single controllable entity concerning the grid. A microgrid can connect and disconnect from the grid to enable it to operate in both grid-connected or island-mode [14].
- **IEEE** - A group of interconnected loads and distributed energy resources with clearly defined electrical boundaries that act as a single controllable entity concerning the grid and can connect and disconnect from the grid to enable it to operate in both grid-connected or island modes [15].
- **CIGRE** - Microgrids are electricity distribution systems containing loads and distributed energy resources, (such as distributed generators, storage devices, or controllable loads) that can be operated in a controlled, coordinated way either while connected to the main power network or while islanded [16].

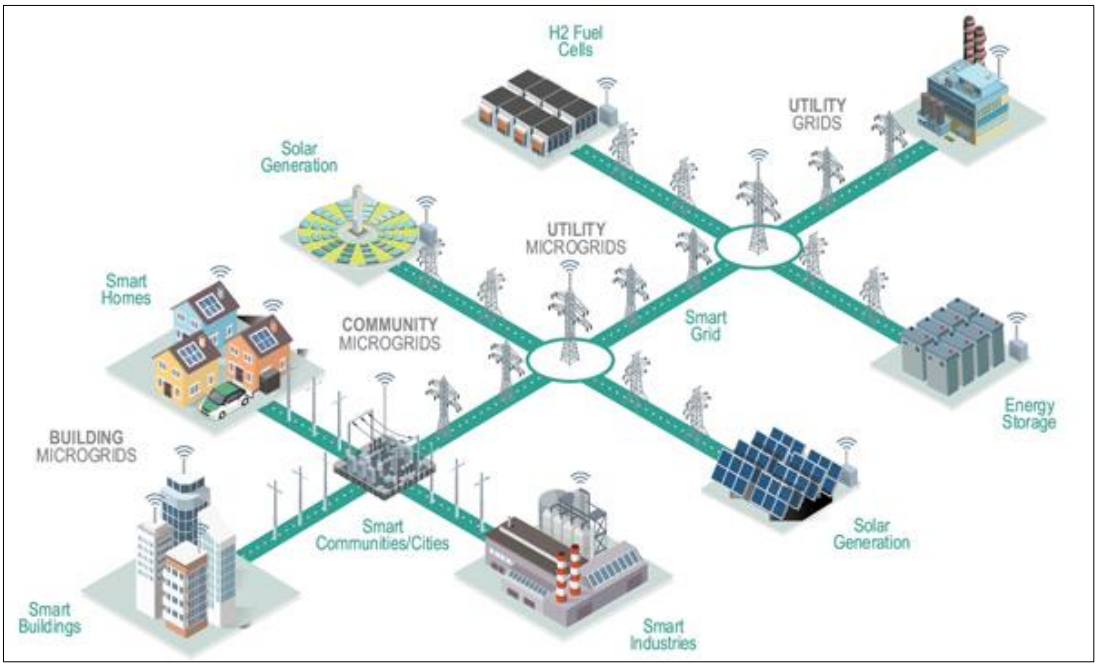

Figure 2-1 An illustration of a microgrid with energy generation and consumption sources (Source – SEIA and SEPA).

Solar Energy Industries Association (SEIA) [17] has created a simplified graphical representation of a generic microgrid, as illustrated in Figure 2-1. From grid point of view, one of the main advantages of a MG is that within the power system it is treated as a controlled entity, i.e. It can be considered as a single aggregated load while under operations. This ensures the easiness in the controllability in compliance with grid codes. In the view of the consumers, MG fulfils their requirement of meeting their demands of electrical and heat energy with the privilege of having uninterruptible power supply at all times [3, 18].

A typical microgrid may consist of several types of equipment interconnected with each other to create a power system network which couples with the grid at the Point of Common Coupling (PCC). The choice of equipment such as power electronic converters, transformers, relays and circuit breakers to interconnect the DERs and the loads with the microgrid is made depending on whether the microgrid is operated in AC, DC or AC/DC technology [15].

2.1 Classification of Microgrids

As a microgrid consists of numerous micro-generating sources, some, e.g. solar, produce DC power while the rest produce AC power directly without any need of connecting a converter. Different configurations depend on the technical topologies to couple the RES and meeting the load demand. Microgrids can be classified into mainly two types of configurations, based on the nature of the voltage that is fed to the load. The microgrid can thus be specified as either AC microgrid, DC microgrid or hybrid AC-DC Microgrids.

2.1.1 AC Coupled Microgrid

This configuration is defined by various DGs, RES and ESS linked to a universal AC bus through their interfacing converters together with the load. In this structure, both AC and DC loads are connected (with or without converters) to a common AC bus. Figure 2-2 represents the configuration of a centralized AC coupled microgrid [19].

Another approach is the decentralized AC-coupled approach for the MG connection. In the decentralized AC microgrid, the architecture of the system is such that all the technologies individually connect to the load directly. The energy sources can thus connect to the load regardless of their location. The disadvantage of this configuration is that it makes the power control challenging to manage. The centralized system is chosen over the decentralized configuration as a common choice due to its controllability [20].

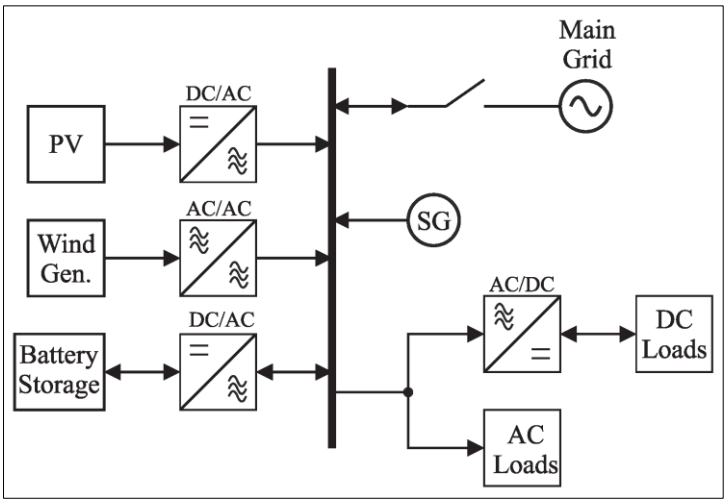

Figure 2-2 AC coupled microgrid

2.1.2 DC Coupled Microgrid System

The development of DC microgrid system has shown to gain much interest for the researchers according to the recent trends [21]. In the DC combination, all energy sources are connected to the DC bus via converters. Figure 2-3 presents the schematic of a DC-coupled microgrid [22].

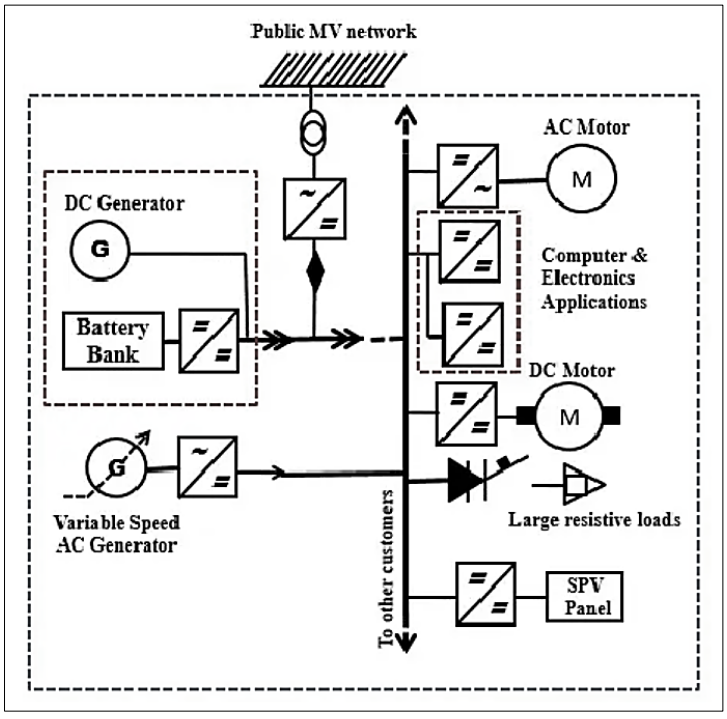

Figure 2-3 DC-coupled microgrid

When compared to an AC microgrid, DC microgrids have fewer converters in the microgrid which can provide significant energy-shavings. Another advantage of the DC system is that it solves some of the control issues in a microgrid. One example of such an advantage is that the DGs do not require synchronization, and the controls are directly based on the DC bus voltage.

Most of the modern equipment and appliances operate under DC power, which is an additional benefit of having a DC microgrid [22].

2.1.3 Hybrid AC-DC Microgrid

The concepts of AC and DC coupled microgrids mentioned in the sections above, create the possibility to have a combination of AC and DC coupled microgrid system using bidirectional converters. A mixed couple system can reduce the number of DC-AC-DC and AC-DC-AC conversion of power in an individual AD or DC microgrids. The schematic of a hybrid mixed couple AD-DC system is shown below in Figure 2-4 [23].

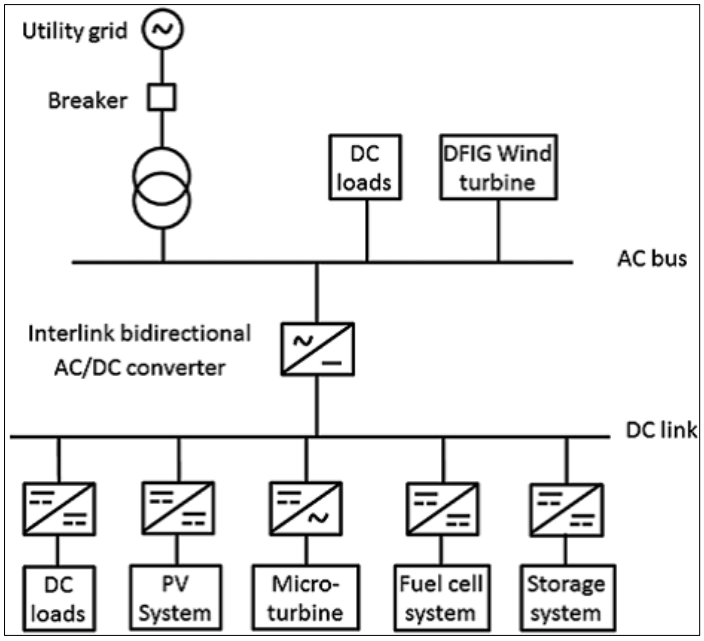

Figure 2-4 AC-DC Hybrid microgrid

A significant disadvantage of for using such type of configuration is that the system efficiency depends highly on the type and number of connected generating units and loads. Hybrid microgrid systems are most suited for isolated installations that are smaller in size with wind and PV generation as major sources of power supply [22].

2.2 Components of Microgrid

This subchapter discusses various components and equipment that may be used to develop a microgrid. Although many small detailed components share equal importance as the large ones, only the common technical elements or the ones used for modelling the Gløshaugen MG are discussed in detail here. Renewable energy sources (PV/Wind) and their integration into the grid at distribution level has a significant influence on microgrid operation, reliability and efficiency, hence requiring theoretical analysis of functionality. Other components to be analyzed include micro synchronous generators, power electronic converters, Transformers,

load and most importantly, batteries. The description of electrical loads, cables and transformers are discussed briefly; however, the PV, wind turbine, power electronics, synchronous generators and batteries are discussed in detail.

***Transformer*:** The transformers are used at all levels of the AC power system. A transformer can either step up or step down the voltage to the desired output value. Adequate sizing of the transformer (rating and impedance) will avoid overloading in the system. Modern transformers come with the Automatic Voltage Regulators (AVR) built in to adjust the range of the voltage through stepping the Load Tap Changer (LTC). The settings used for the transformers for the Gløshaugen campus MG will be explained in chapter 5.

***Load*:** In the Gløshaugen MG, there are two types of loads, static and lump load. The static load is 100% resistive and does not require only active power to operate. The inductive load is presented as a lumped load where ETAP allows the power factor and the inductive ratio to be adjustable accordingly.

***Cables*:** The cables are one of the crucial elements in a microgrid or a distribution grid. The sizing of the cables must be in accordance with the voltage level, maximum power transfer to the load from the generating unit and provision of short circuit current for a specific period. ETAP has a built-in library with a list of cables having the type and rating as the parameters to set before carrying pout the simulations. The cables should be selected adequately so that the system does not experience any abnormal behaviour.

2.2.1 Synchronous Generator

The synchronous generator is the heart of a power system as it is the main source of generation for any size of the system. A few synchronous generators that are commonly used in a power system network are namely steam turbo, hydro, gas turbo and diesel generators. There are two fundamental modes of operation when the generator is connected in the grid-connected operation are:

- P-V control – Constant active power and constant voltage at the terminals
- P-Q control – Constant active and reactive power

The governor control in a generator calculates the required torque for the generator to supply active and reactive power to the grid while following the grid frequency. In the P-V mode of operation, the exciter of the generator manages the current flow from the field windings in order to achieve voltage regulation via reactive power generation [24]. Synchronous generators have the ability to produce both leading and lagging vars depending on the field excitation. If the

generator is overexcited, it produces vars, where else in case of under-excitement, the synchronous generator absorbs vars [25].

2.2.2 Photovoltaic (PV) Generation Units

A photovoltaic array is a combination of PV cells connected in series and parallel to produce rated output voltage and current for a particular solar array. The resultant output voltage when the cells are connected in series is equivalent to the sum of individual voltages of the cells. However, when the modules are connected in parallel, the resultant output current is equal to the sum of individual currents of the cell. The photovoltaics act as DC voltage sources, producing DC power as its output while current and voltage being interdependent to each other. Figure 2-5 shows the interdependency of the current VS voltage and voltage VS power.

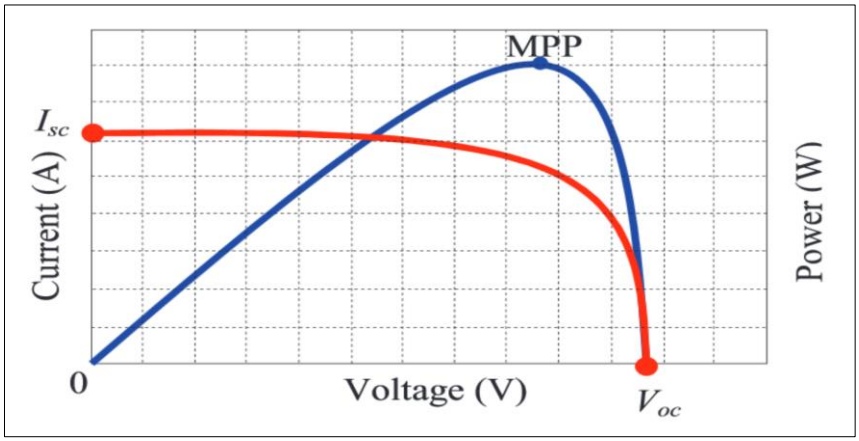

Figure 2-5 Current VS voltage VS power of a PV cell

2.2.2.1 Mathematical Model for PV cells

The two-diode circuit model presented by Z. Salam [26] is shown in Figure 2-6 below.

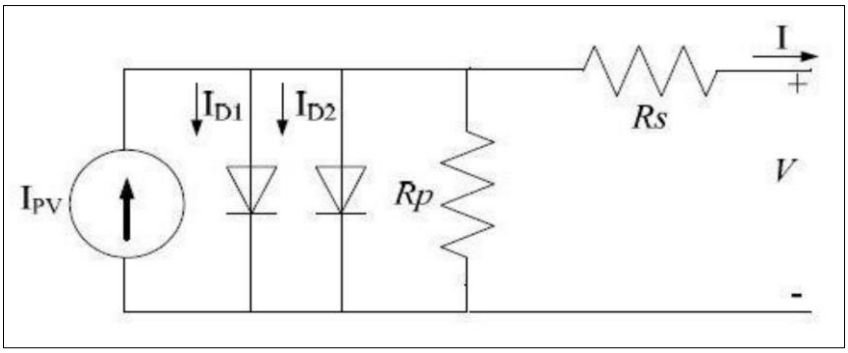

Figure 2-6 Circuit model of a two-diode PV cell

The equation gives the output PV current as:

$$I = I_{PV} - I_{d1} - I_{d2} - \frac{(V + IR_s)}{R_p} \quad (1)$$

Where,

$$I_{d1} = I_{01}\left[exp\left(\frac{V + IR_s}{a_1 V_{T1}}\right) - 1\right] \quad (2)$$

$$I_{d2} = I_{02}\left[exp\left(\frac{V + IR_s}{a_2 V_{T2}}\right) - 1\right] \quad (3)$$

Where,

- I_{01} and I_{02} are the reverse saturation current of diodes 1 and 2
- V_{T1} and V_{T2} are the thermal voltages of diodes 1 and 2 and
- a_1 and a_2 are the ideality constant for both the diodes respectively

2.2.2.2 Maximum Power Point Tracking (MPPT)

The PV output voltage depends on the current flowing through it. As the current flow in the PV cell increases, the output voltage across the terminals decreases, as shown in Figure 2-5. There is a particular combination of voltage and current where the output power reaches a maximum value and starts to decrease as the voltage increases further. This point of maximum output power value is called Maximum Power Point (MPP). Maximum power is obtained from the Solar panels using charge controllers, and this technique is called MPPT, Maximum Power Point Tracking. In a microgrid, MPPT technique is applied to the PV array where a reference signal is sent to the inverter (Active/reactive power controlled) to operate the PV array at MPP. Hence, the inverter output power is approximately equal to the maximum rated power of the PV array [26].

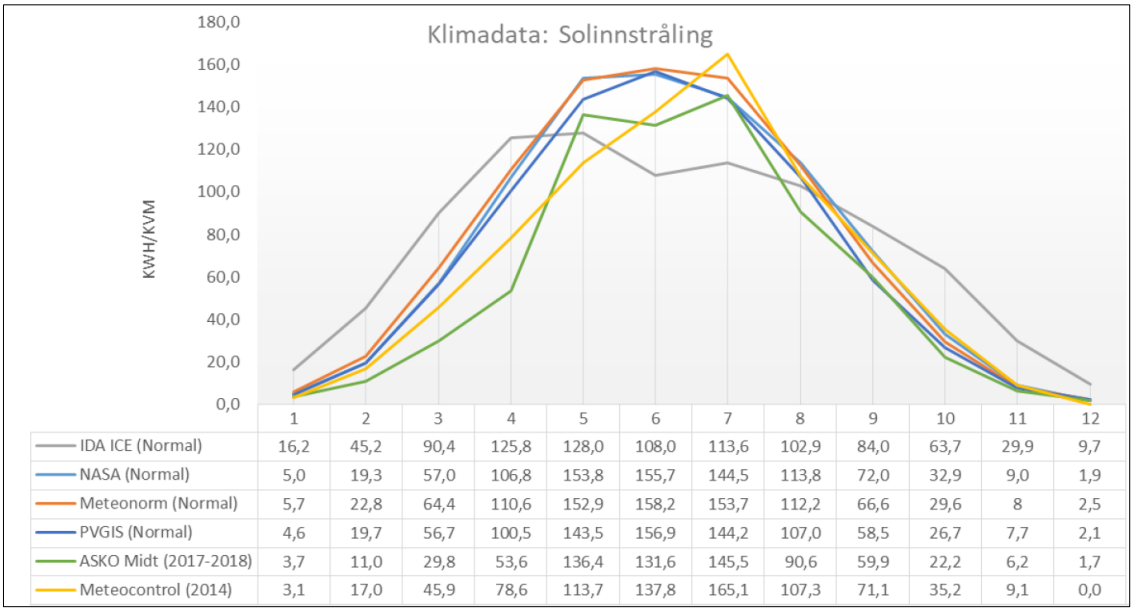

	1	2	3	4	5	6	7	8	9	10	11	12
IDA ICE (Normal)	16,2	45,2	90,4	125,8	128,0	108,0	113,6	102,9	84,0	63,7	29,9	9,7
NASA (Normal)	5,0	19,3	57,0	106,8	153,8	155,7	144,5	113,8	72,0	32,9	9,0	1,9
Meteonorm (Normal)	5,7	22,8	64,4	110,6	152,9	158,2	153,7	112,2	66,6	29,6	8	2,5
PVGIS (Normal)	4,6	19,7	56,7	100,5	143,5	156,9	144,2	107,0	58,5	26,7	7,7	2,1
ASKO Midt (2017-2018)	3,7	11,0	29,8	53,6	136,4	131,6	145,5	90,6	59,9	22,2	6,2	1,7
Meteocontrol (2014)	3,1	17,0	45,9	78,6	113,7	137,8	165,1	107,3	71,1	35,2	9,1	0,0

Figure 2-7 Solar radiation throughout the year from various databases

The power generation from a PV system is highly dependent upon the angles between the modules and the sun and the solar radiation, i.e. the higher the intensity of the radiation, the higher will be the output power [27]. For the Gløshaugen campus, Multiconsult had obtained weather statistics from various reputable sources. Figure 2-7 represents the solar radiation profile of Trondheim through multiple databases.

The best practice is to use the worst-case scenario to design the system. The values from NASA and Meteonorm are relatively similar with a percentage difference of approximately 2% in the year 2018. The irradiation for the Gløshaugen campus can be varied on ETAP depending on the specific season of the year.

According to Multiconsult [27], if every building in Gløshaugen have PVs installed on their roofs, then there is a possibility to achieve an annual electricity production of approximately 3.638 GWh depending on the rating and size of panel installed.

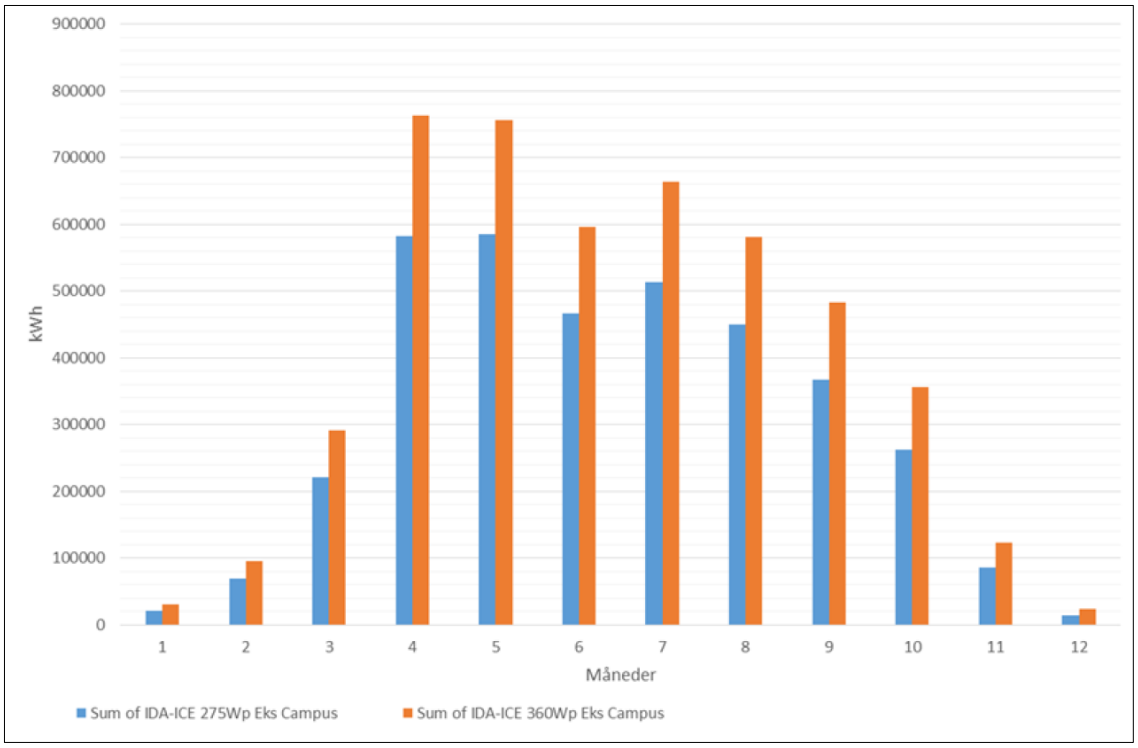

Figure 2-8 Energy production comparison of 275Wp and 360Wp panels (Climate data IDA ICE)

The above Figure 2-8 represents the comparison of the 275Wp and 360Wp rated solar panels which are likely to be used for the Gløshaugen campus. If highly efficient panels such as 360Wp are used, the possibility of annual production is expected to rise to 4.610 GWh of energy.

2.2.3 Energy Storage System

One of the main concerns of using RESs in a microgrid is that it suffers from intermittency as it is highly dependent on the climate condition. Other issues that come with RESs are stability

issues, frequency/voltage control and unbalanced loads, leading to reduced power quality [28]. This is where the energy storage (ESS) technology becomes indispensable and critical as it instantly compensates for the interim power shortfall. In a MG, the ESS suppresses any power fluctuations to deal with imbalance challenges between the supply and demand side. Several forms of ESS have been studied in the recent past. These include batteries (lithium-ion), Supercapacitors, flywheel energy storage and superconducting magnetic energy storage. The typical details of the ESS technologies available today are given in Table 1 below.

Table 1 ESS technologies available for microgrid applications

Type	**Efficiency** (%)	**Energy Density** (Wh/kg)	**Power Density** (W/kg)	**Response** Time (ms)	**Cycle Life** (time)	**Cost** ($/kWh)
Battery	60 - 80	2 – 200	25 - 1000	30	200 - 2000	150 - 1300
SMES	95 - 98	30 – 100	1e4-1e5	5	1e6	High
Flywheel	95	5 – 50	1e3-5e3	5	> 20,000	380 - 2500
SuperCap	95	< 50	4000	5	> 50,000	250 - 350

Lithium-ion batteries are nowadays the most popular types as they have one of the best energies to weight ratio and a slow loss of charge when not in use. The use of such batteries will be made while modelling the campus later in chapter 5. The equation below represents the charging and discharging of the battery [29].

$$C(t+1) = C(t) - \triangle t {P_t}^E \tag{4}$$

Where ${P_t}^E$ is the power supplied by the battery bank during time t, and $\triangle t$ is the duration time of a single interval. The value of ${P_t}^E$ is positive when the battery bank is discharged and negative when the battery bank is charged up [29]. The battery bank in a microgrid should also satisfy the following constraints.

Output power limits:

$$\left|{P_t}^E\right| \leq {P_E}^{max} \tag{5}$$

Stored energy limits:

$$C_{min} \leq C(t) \leq C_{max} \quad (6)$$

And Starting limits:

$$C(0) = C_S \quad (7)$$

Where,

$P_E{}^{max}$ – Maximum charge or discharge rate

$C(t)$ – Energy stored in the battery at time t

C_S – Initial stored energy in the battery

C_{min} – Minimum energy stored in the battery

C_{max} – Maximum energy stored in the battery

2.2.3.1 Battery Sizing

Choosing a battery energy storage system causes concerns regarding the minimal sizing of the batteries in a system. A suitable battery bank with optimal power and energy rating could not only help in peak shaving when the demand is high but also store energy from the RESs and supply during intermittency hours [29]. After the establishment of peak-shaving process, the minimum power supplied by the battery bank is obtained by the equation below [29].

$$E_{dis}^{min} = \int_0^T \left(P_{load}^i - P_{grid}^i{}^{max}\right)\delta t\,, \qquad P_{load}^i \geq P_{grid}^i{}^{max} \quad (8)$$

Where,

T – End of the time set (hours/days/weeks)

δt – Time interval (hours)

P_{load}^i – System load at time i

P_{grid}^i – Traditional and renewable energy power at time i

$P_{grid}^i{}^{max}$ – Maximum power supplied by all generating units in the system

When the power generated by the RESs in the system exceeds the demand, the batteries should go in the charging mode. Then the minimum energy needed to charge the batteries is given as:

$$E_{charge}^{min} = \int_0^T \left({P_{grid}^{i}}^{min} - P_{load}^{i} \right) \delta t \,, \qquad {P_{grid}^{i}}^{min} \geq P_{load}^{i} \tag{9}$$

Where ${P_{grid}^{i}}^{min}$; is the minimum power supplied by the RES in the power system.

Finally, the minimum size of the battery bank can be obtained by the equation below [29]:

$$E_{ESS}^{min} = max\left(\frac{E_{dis}^{min}}{\eta_d}, \eta_c \cdot E_{charge}^{min} \right) \tag{10}$$

Where,

η_d – The discharge rate of the battery bank.

η_c – Charge rate of the battery bank.

$\frac{E_{dis}^{min}}{\eta_d}$ – The minimum charge density of the battery bank.

$\eta_c \cdot E_{charge}^{min}$ – Charge energy of the battery bank.

2.2.4 Wind Turbine Generators

Wind turbine generators (WTG) are one of the fastest-growing sources of electrical power generation. The high growth rate of WTGs is due to the availability of substantial wind resources worldwide, carbon-free generation source and technical development. The increase in the integration of wind turbines within the distribution systems can cause several concerns and adverse impact on the behaviour of the system [30]. The power output of the wind turbine depends on the principles of aerodynamics parameters such as wind speed, air density, turbine radius and pitch angle [31]. The formula below describes the energy contained in the wind in the form of kinetic energy [31]:

$$P_w = 0.5 \cdot \rho \cdot A \cdot v^3 \cdot C_p \tag{11}$$

Where

- ρ is the air density.
- A is the area normal to the wind speed.
- v is the velocity of the wind.
- C_p is a coefficient that represents the amount of wind energy that is converted to mechanical power by the turbine.

Figure 2-9 below depicts the output power of a wind turbine relative to the wind speed [31].

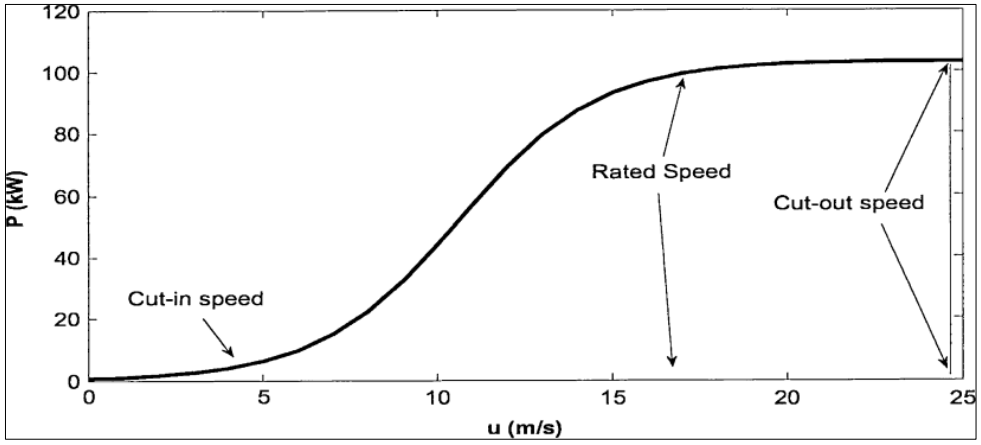

Figure 2-9 Power Vs wind speed curve for a typical wind turbine

According to the report published by Multiconsult, the annual mean wind speed is roughly 3.5 m/s. Most of the relatively smaller wind turbines are not able to start production until the wind speed is approximately 3.0 – 3.2 m/s [27]. In the case of Gløshaugen, campus, Quinta20 model wind turbine could contribute very little to the total energy production. Gløshaugen, building roofs are not strong enough to have large wind turbines installed, and the small roof-mounted wind turbines are not a good alternative for utilizing the roof space when the option of the PV installation is available. The expected total annual production, if wind turbines are installed at Gløshaugen, were estimated to be 7100kWh with 20kVA rated (WTG) and 29,300kWh with 99kVA rated WTGs in total [27].

2.2.5 Power Electronic Converters

Power electronics allows the conversion of AC power to DC power and vice-versa, as shown in Figure 2-10 below [32]. Each power electronic interface consists of a power converter having semiconductor switches with primary electric elements such as transformers, capacitors, resistors, inductors and diodes. It also consists of a control unit that manages power flowing in the system and the conversions of current and voltages [32].

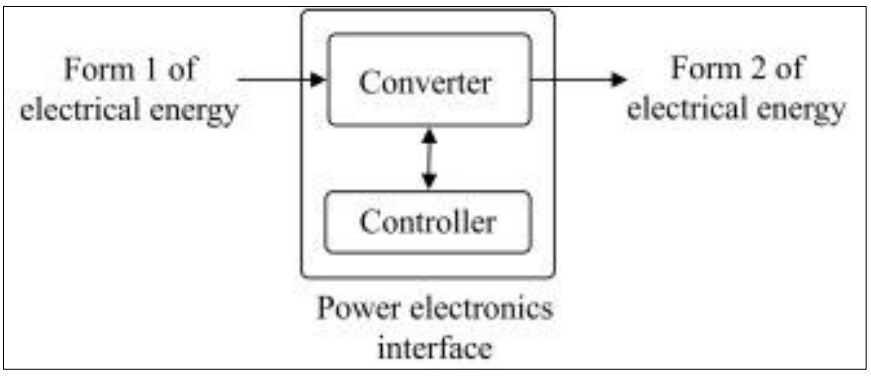

Figure 2-10 Representation of a PE interface

The converter may have different frequencies, voltage levels and voltage and current types on either side. In some cases (e.g. battery charging and discharging), the power converter, should also be able to allow the bidirectional flow of power. Still, mostly the converter designs are unidirectional, i.e. they intake power from the generating sources and the output power from the inverters is fed to the loads. Power electronic converters can be classified based on the input and output types of the currents and voltages.

2.2.5.1 DC-DC Converters

The DC-DC inverter has the same form of voltage and current at both its input and output side; however, the converter generates controlled DC voltages and currents as the output. This type of converter is prevalent in DC microgrid applications or the AC/hybrid microgrids when the ESS is integrated into the network [32].

2.2.5.2 AC-DC / DC-AC Converter

This AC-AC type of converter is known as 'rectifier', and it transforms AC to DC with a controlled output voltage. A controlled rectifier based on semiconductor switches can also be used to attain a higher degree of controllability and allowance of bi-directional power flow [32].

Another specific term used for the DC-AC converters is inverters. They are fed with DC input and generate AC outputs with controllable frequency, magnitude and phase. Inverters are vital in many industrial applications, especially in motor operation, where it is essential to control the torque and speed of the induction motors. Figure 2-11 Shows the AC-DC converter topology for a three-phase system [33].

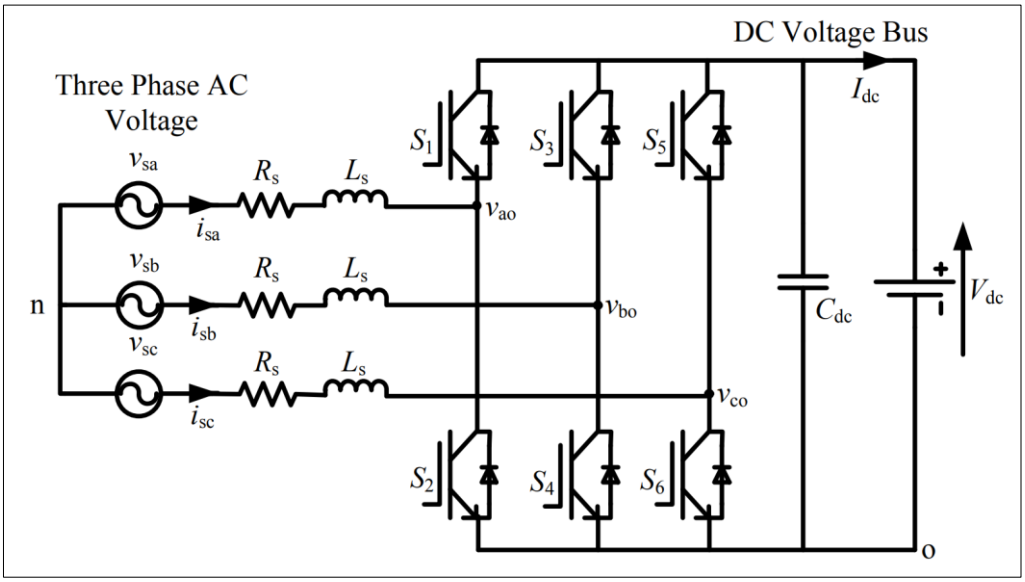

Figure 2-11 Three-phase bidirectional AC-DC converter topology

The AC-DC bidirectional converter consists of 6 IGBT switches ($S_1 - S_6$) as shown in Figure 2-11. The IGBTs are connected to 3-phase voltage supply via resistance R_s and series filter inductance L_s. In order to keep the voltage V_{dc} constant, a DC capacitor C_{dc} is connected across the DC voltage bus. The bidirectional converter operates as both rectifier and inverter [33]. ETAP has a variety of options where the functionality of the converter can be selected for modelling the power system network. The possible mode of operations that can be chosen is AC operating mode, swing mode and voltage control mode. The converter settings will be defined in the model described in chapter 5.

2.2.6 Micro Turbines

A micro-turbine is a Combined Heat and Power (CHP) unit that consists of four main components such as turbine, alternator, compressor and a combustor [34]. A microturbine is the backbone of the microgrid, especially in cold regions where the electricity and heat are produced at the same time. The advantages of having a micro-turbine in the system are that it has high power density, zero carbon emission, low maintenance, high reliability, high durability and it is relatively lighter in weight compared to other turbines [35].

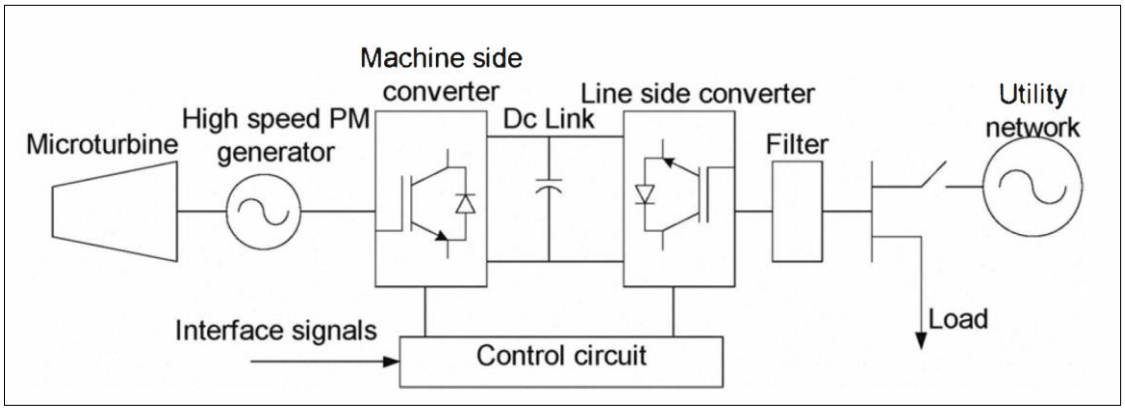

Figure 2-12 Schematic of a micro-turbine generator with back to back converters

Figure 2-12 represents the schematic of a typical microturbine connected system with back to back voltage source inverters. In a grid-connected MG system, this topology allows power to flow in both directions, i.e. from the converter to the grid and vice-versa [36].

ETAP is a complete power system software, and it does not have tools for modelling a CHP or a microturbine explicitly, however, there is an option of modelling a synchronous generator with detailed minor parameters to observe the functionality of the system. The Gløshaugen campus consists of a few CHP units, but this thesis will only focus on the electrical generation and consumption.

2.3 Microgrid System Analysis

Today's power system is considered as a complex interconnected network consisting of several entities. Likewise, the system can be studied in detail under different conditions. These conditions provide an in-depth analysis of the behaviour of the system, which allows the operator to take corrective measures. Some of the conventional analysis include AC/DC power flow, short circuit fault analysis, transient stability, harmonic analysis and overall protection analysis of the system.

2.3.1 Transient Stability Analysis

Power system stability refers to the ability of a power system, for a specified initial operating condition, to regain a state of operating equilibrium after being subjected to a physical disturbance, with the condition that most system variables are bounded for the entire system to remain intact [37]. Power system stability can further be classified into different types, depending on the nature and period of disturbance [38]. Figure 2-13 represents the classification of power system stability with the causes and effects [38].

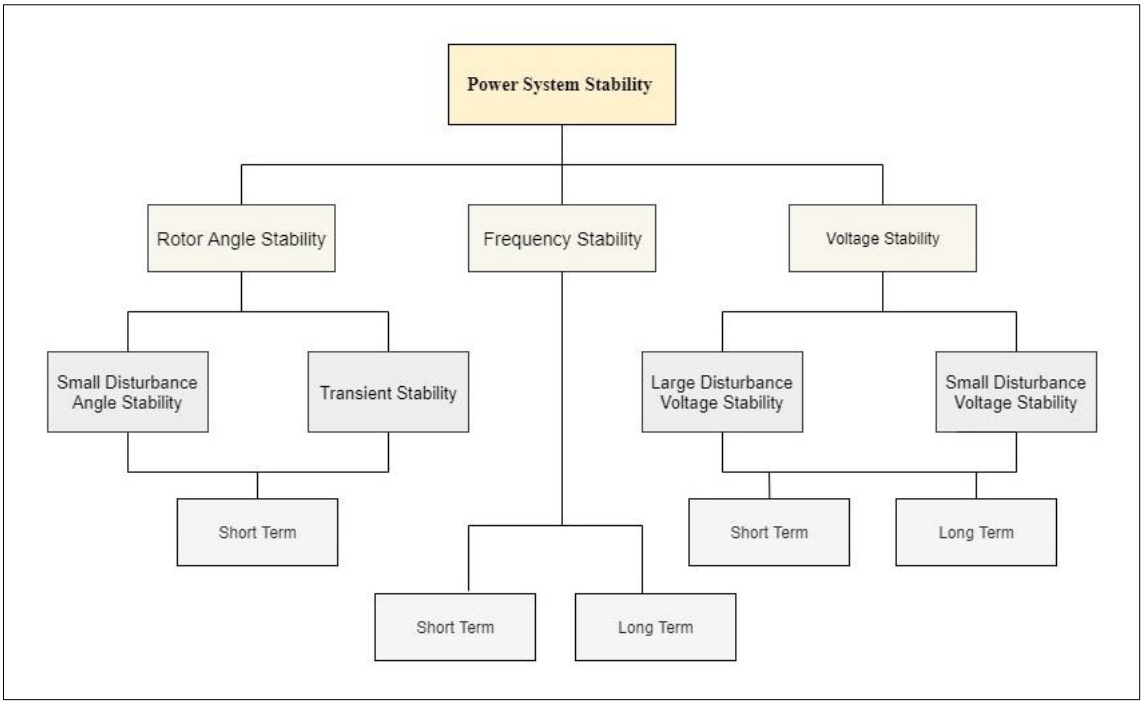

Figure 2-13 Classification of power system stability

In microgrids, transient analysis becomes essential due to the presence of micro-sources that have current limitations, limited synchronous units and reactive support. The possible stability issues a MG can have are listed in Figure 2-14 [38].

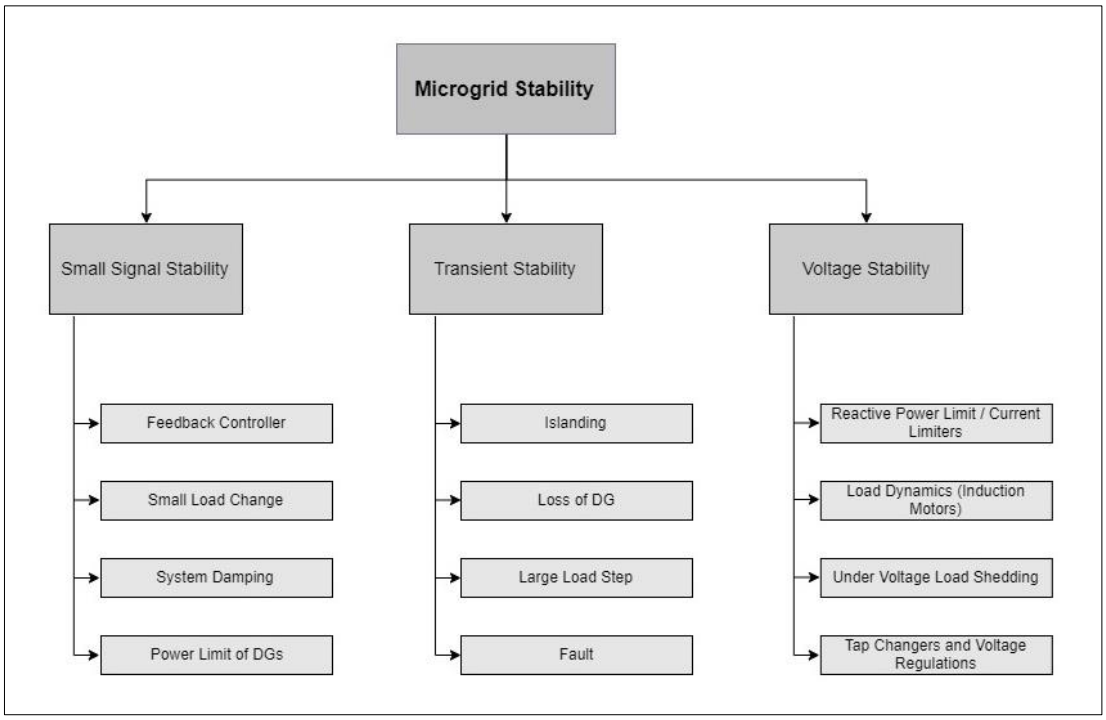

Figure 2-14 Different stability issues in a MG

Other vital factors required for understanding the transient stability analysis are the stability limits, cause and consequences of instability in the power system, and the improvements that could be made to stabilize the system. These factors are discussed briefly for a better understanding of the Gløshaugen campus model.

2.3.1.1 Small Signal Stability

Small Signal Stability (SSS) has been a critical issue in MGs due to the unique characteristics of RES and their integration. The system experiences oscillations with growing or undamped phenomena sue to the lack of synchronism or damping. The utility grid is expected to provide stability as multiple generators are running in the conventional large power plants. The unstable oscillations could occur at any point of location within the network against the whole interconnected power system. Small signal stability is defined as the ability of the system to gain the synchronism back after the occurrence of a small disturbance. SSS falls under the category of rotor angle stability, as shown in Figure 2-13. The two main factors that contribute to small signal instability are the variation in loads and generation [39]. While the small-signal stability is associated with small disturbances in the system, transient stability issues occur when there are large disturbances such as fault at any point, loss of generation or loss of load. A huge impact on the load may also lead to transient stability problems depending on the size of the system network.

2.3.1.2 Stability Limits

For a power system, there are mainly two types of steady-state limits, 1) Steady-state stability limit and 2) Transient stability limit.

Steady-State Stability Limit: It is the stability of the system in the event of small or gradual changes in the system during operation. Transient stability calculation can be used to find the stability of the system under steady-state operation and/or if there are any disturbances involved. After the occurrence of small or gradual disturbances, the system is said to be steady-state stable, if all the synchronous machines in the system attain either their steady-state or pre-disturbance operating condition. A synchronous machine is said to be within the stability limit if its power angle is below 90° [40].

Transient Stability Limit: Transient stability is the stability of the system during and after an event of a significant or sudden disturbance in the system. Example of such type of disturbance could be loss of generation, line tripping, sudden changes in the load or short-circuits. If the system encounters a severe disturbance and all synchronous machines attain their steady-state operating condition within a specific time, the system can then be called a transient stable system. A synchronous machine is said to be within the stability limit if its power angle is below 180° [40].

2.3.1.3 Causes and Consequences of instability Problem

Instability can be caused by many reasons depending on the events occurring and the size of the power system network. A few problems that may cause instability in the system are:

- Short-circuit at any point in the system.
- Loss of connection to the utility system.
- Loss of generation (micro-sources in a MG).
- Integration of RES into a MG.
- A sudden substantial increase in the generation or load (step change).
- Impact loading in case of static loads and motors.
- Starting of a large-size motor compared to the generation capacity.
- Capacitors or line switching operation.

Instability in a power system can have severe consequences that may lead to shutting down processes to avoid further damage to the system. Instability may cause [40]:

- Permanent damage to the equipment
- Areawide blackout (Power outage)

- Malfunctioning of protective devices and relays.
- Low voltage conditions.
- Load interruptions.

2.3.1.4 Power System Transient System Improvements

It is essential to analyze the cause of instability to improve the stability of a power system, as it helps in deciding what enhancements or improvements should be made to the system. Some typical improvements that could be made are [40]:

- Improvement in system design and its configuration.
- Increasing synchronization power.
- Addition of exciter and governor in synchronous generator with specified parameters.
- Application of (PSS) Power System Stabilizer.
- Addition of load-shedding scheme.
- Addition of adequate system protection, i.e. system separation, fast fault clearance etc
- Selection of appropriate rotating equipment by improving voltage regulator and exciter characteristics, reducing transient reactance, using induction motors and increasing moment of inertia.

Transient stability analysis is a time-based simulation. ETAP allows its users to create multiple events and specify the actions at different time instants. It was assumed that the Gløshaugen model is supported entirely by reliable grid connections with high inertia. However, to study system dynamics related to stability, the use of a generator in the model was made at one of the main buses as backup energy sources.

2.3.2 Energy Management System of a Grid-Connected Microgrid

One of the core aspects that contribute to the development of MGs is the Energy Management System of a MG. It holds the responsibility of making the right decisions for generation, consumption and transaction of energy. EMS in MGs faces new challenges due to the requirement of bi-directional energy and data flow within the system. Energy Management System manages the energy within the MG and transactions with the upper network (grid) to satisfy environmental, technical and economic constraints [41, 42]. EMS is responsible for collecting information, controlling DERs and ESS devices, analyzing and selecting the best possible strategy for the MG operation, forecasting of the RES generation and load consumptions. Some fundamental responsibilities of the EMS in a microgrid are listed below [41]:

- Determine the amount of energy produced by generating units and energy consumed by the loads connected.
- Ensure that the balance is kept between supply and demand for energy.
- Ensure proper implementation of riles for connecting the MG to the upper distribution network.
- Make sure that the existing resources are utilized optimally.
- Minimize the overall cost of operation.
- Separation of the MG with the utility in case of an emergency.
- Provision of an appropriate control strategy to reconnect the MG to the upper network after island mode operation.

When the microgrid is in the grid-connected mode, the aim is to optimize the power flow and maximize the benefit, while in the island mode of operation, EMS focuses the most on the reliability of the MG. EMS can be applied for both long and short term operations and has a vital role in power balancing. In order to balance the power, the MG desires to achieve the following goals [41]:

- Voltage regulation at all buses.
- Frequency regulation of the system.
- The capability of controlling loads.
- Avoiding mismatch between supply and demand.
- Providing adequate dynamic response for the MG (Voltage and frequency recovery after transients).
- Ensuring high power quality at the demand side.
- Resynchronizing after disturbances (transient states) in order to connect to the upper (utility) grid.

The long-term application of EMS tries to pursue the following goals [41]:

- Scheduling of DGs and ESS units to control the exchange of power with the network, maximizing the production of RESs, reducing losses and minimizing production costs.
- Recovering the interrupted loads by performing demand response programs.
- Considering DER constraints and environmental impacts.

2.3.2.1 Energy Peak Shaving with Local Storage

The uneven electricity consumption by the customers usually results in load peaks. The power system capacity is designed to supply the energy demand during peak hours while during the rest of the day, the system is not being utilized at its maximum capacity. The customers are charged with extra fees for keeping the power system up with the peak demand, i.e. the customers pay for their maximum peak load [43]. The six main method programs used for EMS with the help of DSM are shown in Figure 2-15 [44]. The most common methods used are load shifting and peak clipping. In the load shifting method, the non-critical loads are operated during the off-peak hours while the important loads are kept under operation during peak hours. In the peak clipping method, the consumption profile remains the same while the ESS compensates for the extra load during peak hours.

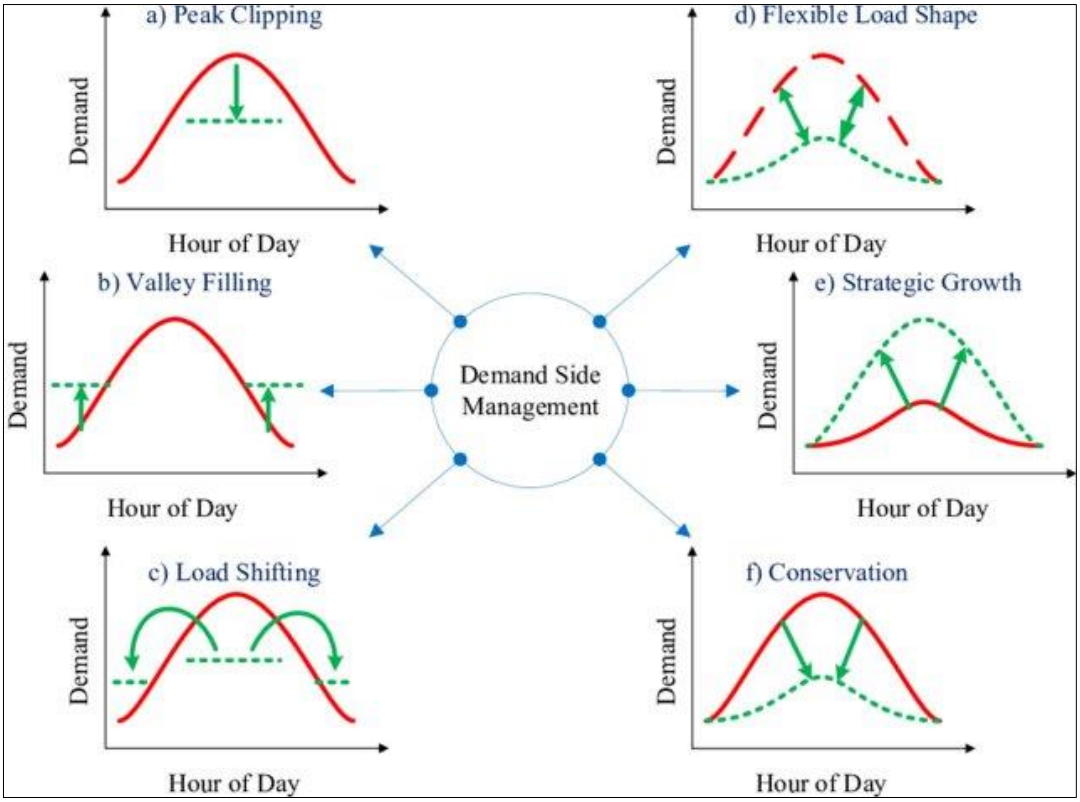

Figure 2-15 Demand Side Management methods used for controlling loads

With the help of ESS and RES, peak loads can be reduced, which may result in reduced energy fee. The Battery Management System (BMS) controls the ESS to charge during off-peak hours and discharge during the hours when the demand is at peak. Similarly, the PVs help in supplying energy during the daytime, especially in the commercial buildings where the demand and the irradiance, both are highest roughly around noon. Figure 2-16 represents the effect of ESS on peak shaving with the help of generation [43].

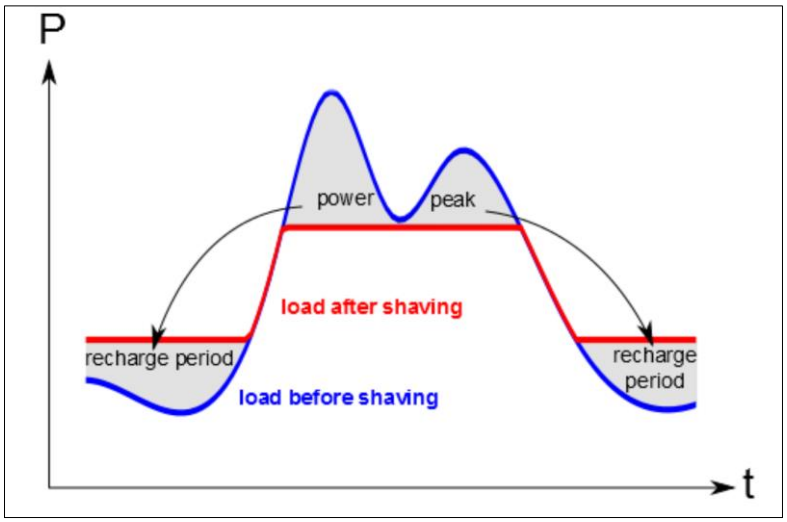

Figure 2-16 Principle of peak-shaving

A demand limit is usually specified for the ESS control instead of calculations performed for charging and discharging targets for every point in time. This control strategy of defining limits is known as peak clipping method. The upper cut-off line and the lower cut-off line on the consumption curve are specified, and the ESS operation is set to be dependent on the load consumption. Figure 2-17 shows the peak-clipping method where the red region above the green dotted (upper limit) line represents the peak that is clipped via discharging of the batteries and the red region below the red dotted line (lower limit) represents the charging of the batteries during off-peak hours. The area in between the limits is called the 'hysteresis zone', within which the excessive discharge or recharge cycle is prevented [45]. The limits are usually varied seasonally and are updated depending on the load forecast.

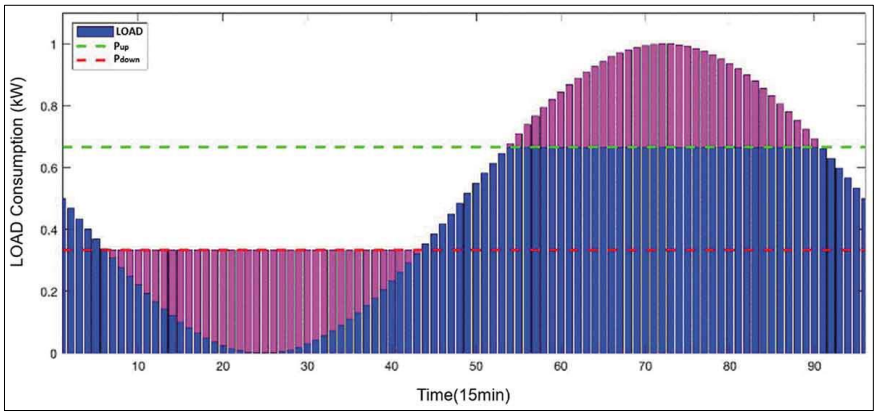

Figure 2-17 Peak-cut disposition method also known as the peak-clipping method

3 METHODOLOGY

Power system simulations can be carried on various modern software programs. Each software is unique in its way, and the focus of all the software developers is to provide a user-friendly interface. Depending on the standards, different countries make use of different software within the power industry. A few typical software programs used in the power industry are SimPowerSystem PSCAD, ETAP, PowerFactory etc. For microgrid applications, HOMER is also considered to be one of the most efficient software for power system simulations. Power system analysis is also performed by scripting via programming languages such as Python, MATLAB, Simulink etc. Nonetheless, Graphical User Interface is preferable by a majority of the industries as it is relatively less time consuming to design and run simulations of a power system network.

ETAP is one of the most comprehensive software for power system design, simulation, control, operation, monitoring, automation and optimization. Its unique functions include load flow analysis, real-time simulator, short-circuit at fault, transient studies, dynamic load shedding and cost optimization [13]. Another advantage of using ETAP is that it creates an automatically generated report containing all details of results and simulations performed on the designed network. The alert messages generated, highlight the alarms due to the possible mistakes or errors made by the user while designing.

3.1 Methods for Analysis

This thesis focused on analyzing and studying the AC/DC load flow, transient stability and energy management system (via time-domain load flow with load profiling) for the Gløshaugen MG. ETAP and other similar power system software programs provide a platform to carry out the above-mentioned system analysis with different configurations.

3.2 Load Flow Analysis

Load flow or power flow studies play an important in planning, control and economic scheduling of already developed power systems as well as the enhancement of the future power systems. The purpose of load flow analysis is to determine the voltage levels and angles at each bus and also the real and reactive power flow in every line of the system [46]. The four main quantities associated with each bus in the system are voltage magnitude $|V|$, phase angle δ, active power and reactive power as P and Q. The load flow formulation, on basis of which ETAP performs the simulation is shown below:

The apparent power injected into the network by a generating source into a bus (i^{th} bus) is given by the following equation:

$$S_i = P_i + jQ_i = V_i I_i^* \tag{12}$$

Where V_i is the voltage of i^{th} bus with respect to ground, and I_i^*represents the complex conjugate of the current I_i injected into the i^{th} bus. Simplifying the conjugate from (12) gives the equation below:

$$S_i^* = P_i - jQ_i = V_i^* I_i \tag{13}$$

Substituting the equation below in (13)

$$I_i = \sum_{k=1}^{n} Y_{ik} V_k \tag{14}$$

Then,

$$S_i^* = P_i - jQ_i = V_i^* \sum_{k=1}^{n} Y_{ik} V_k \tag{15}$$

To get the real and reactive power, we equate the equations above to get the following

$$Real\ Power = P_i = R_e \left\{ V_i^* \sum_{k=1}^{n} Y_{ik} V_k \right\} \tag{16}$$

$$Reactive\ Power = Q_i = -I_m \left\{ V_i^* \sum_{k=1}^{n} Y_{ik} V_k \right\} \tag{17}$$

Voltages and admittance in their polar form are represented as

$$V_i = V_i \angle \delta_i, \qquad V_i^* = V_i \angle -\delta_i\ , \qquad Y_{ik} = Y_{ik} \angle \theta_{ik} \tag{18}$$

Finally, real and reactive power can then be expressed as in the equation (19) and (20). The equations of real and reactive power below are also known as static load flow equations and are nonlinear, i.e. only numerical solutions are possible.

$$Real\ Power = P_i = V_i \sum_{k=1}^{n} Y_{ik} V_k \cos\left(\theta_{ik} + \delta_k - \delta_i\right) \tag{19}$$

$$Reactive\ Power = Q_i = V_i \sum_{k=1}^{n} Y_{ik} V_k \sin(\theta_{ik} + \delta_k - \delta_i) \quad (20)$$

There are four types of load flow calculation methods available on ETAP. The methods include Newton-Raphson, Adaptive Newton-Raphson, Accelerated Gauss-Seidel and Fast-Decoupled. A brief description of the load flow calculation methods is discussed in the next subsection.

3.2.1 Newton-Raphson Method

In the Newton-Raphson method, the following load flow equation is formulated and solved iteratively [46].

$$\begin{bmatrix} \triangle P \\ \triangle Q \end{bmatrix} = \begin{bmatrix} J_1 & J_2 \\ J_3 & J_4 \end{bmatrix} \begin{bmatrix} \triangle \delta \\ \triangle V \end{bmatrix} \quad (21)$$

Where,

$\triangle P$ – Real power mismatch vector between calculated and specified value.

$\triangle Q$ – Reactive power mismatch vector between calculated and specified value.

$\triangle V$ – Incremental bus voltage magnitude

$\triangle \delta$ – Incremental bus voltage angle

$J_1, J_2, J_3\ and\ J_4$ – Jacobian matrix

The advantage of using this method on ETAP is that it has a fast convergence speed compared to the rest of the load flow calculation methods. For direct control of the precision specified for the LF solution, NR method also has the convergence criteria specified, which ensures the convergence of active and reactive power mismatches at the bus. The typical convergence criteria for the NR method was set to 0.001MW and MVAr. NR method is the most common LF calculation method and is always recommended as the first choice for any system [47].

3.2.2 Adaptive Newton Raphson Method

Adaptive NR method is an improved NR method which introduces fine steps for iteration whenever a divergence condition is encountered. For some systems where the NR method fails to reach a solution, the smaller increments in the adaptive NR method may help to converge and reach a solution. The only disadvantage of using this technique is the reduction in the calculation speed because of the small incremental steps in the solution. The test results have proved that the adaptive NR method is more effective in the transmission and distribution system that involves convergence with negative series reactance [47].

3.2.3 Accelerated Gauss-Seidel Method

The accelerated Gauss-Seidel method uses the system nodal voltage equation $[I] = [Y_{Bus}][V]$ for deriving the following LF equation to solve it iteratively.

$$[P + jQ] = [V^T][Y^*_{Bus}][V^*] \tag{22}$$

Where,

$P\ and\ Q$ – Specified active and reactive power

V – Bus voltage

Y_{Bus} – System admittance matrix

V^T – Transpose of voltage

Unlike the NR method, this method

In comparison with NR and Fast-Decoupled, the Accelerated Gauss-Seidel Method has relatively low demands for the initial voltage values of the bus. The accelerated Gauss-Seidel method checks the tolerance of the bus voltages between two consecutive iterations in order to control the solution precision. The voltage magnitude precision was set on its typical value of 0.000001 pu.

The speed of convergence in this method is relatively slower than NR; however, if an appropriate acceleration factor is applied, there is a significant increase in the convergence. The acceleration factor ranges from 1.2 – 1.7 [47].

3.2.4 Fast Decoupled Method

In Fast Decoupled method, a minor change of bus voltage does not change the real power at the bus. Likewise, an insignificant change in the voltage angle will not affect the reactive power significantly at the bus. The LF method from the NR equation is then simplified to two separate sets of LF equations, that are solved iteratively.

$$\begin{aligned}[\triangle P] &= [J_1][\triangle \delta] \\ [\triangle Q] &= [J_4][\triangle V]\end{aligned} \tag{23}$$

The advantage of using this method of LF calculations is that it requires less memory storage (approximately half of NR calculation) and has faster calculation speed compared to the NR method. The accuracy of this method is not as good as the NR method. The faster calculation

time makes it a favourable solution in large power systems with many transmission lines and cables [47].

3.3 Data Collection

The main challenge in developing and modifying an existing system is to attain the necessary information and data regarding the specifications and ratings of the equipment within the power network. Further challenges arose due to the COVID-19 pandemic as it was nearly impossible to meet and discuss with the concerned engineers and technicians about the Gløshaugen power network and distribution grid. However, data such as the Gløshaugen grid map, SLD, Cable data, transformer capacities etc. was received online through persons involved in the cityXchange project. The yearly electricity consumption data for Gløshaugen was taken from the master thesis done by Aleksandra Stretenovic in 2012. The data was noted down from BEMS (Building & Energy Management System) and ERM (Energy Remote Monitoring) available at NTNU. The electricity consumption was observed from 79 electricity meters installed on the Gløshaugen campus. The main electricity meter is installed at the campus by TrongerEnergi as they are the supplier of energy.

4 GLØSHAUGEN MICROGRID MODEL

This thesis aims to analyze the Gløshaugen campus as a MG and analyze the effect of PVs and ESS's integration into the network to show Energy Management System and the stability of the MG. The NTNU Gløshaugen campus comprises of 35 buildings covering an area of approximately 300,000 square meters. The aerial view of the NTNU Gløshaugen campus is shown in Figure 4-1 [27]. The premises include classrooms, auditoriums, offices, cafes, Laboratories and sports facilities. The largest building is the Realfagbygget which also has the highest energy consumption out of all the remaining buildings.

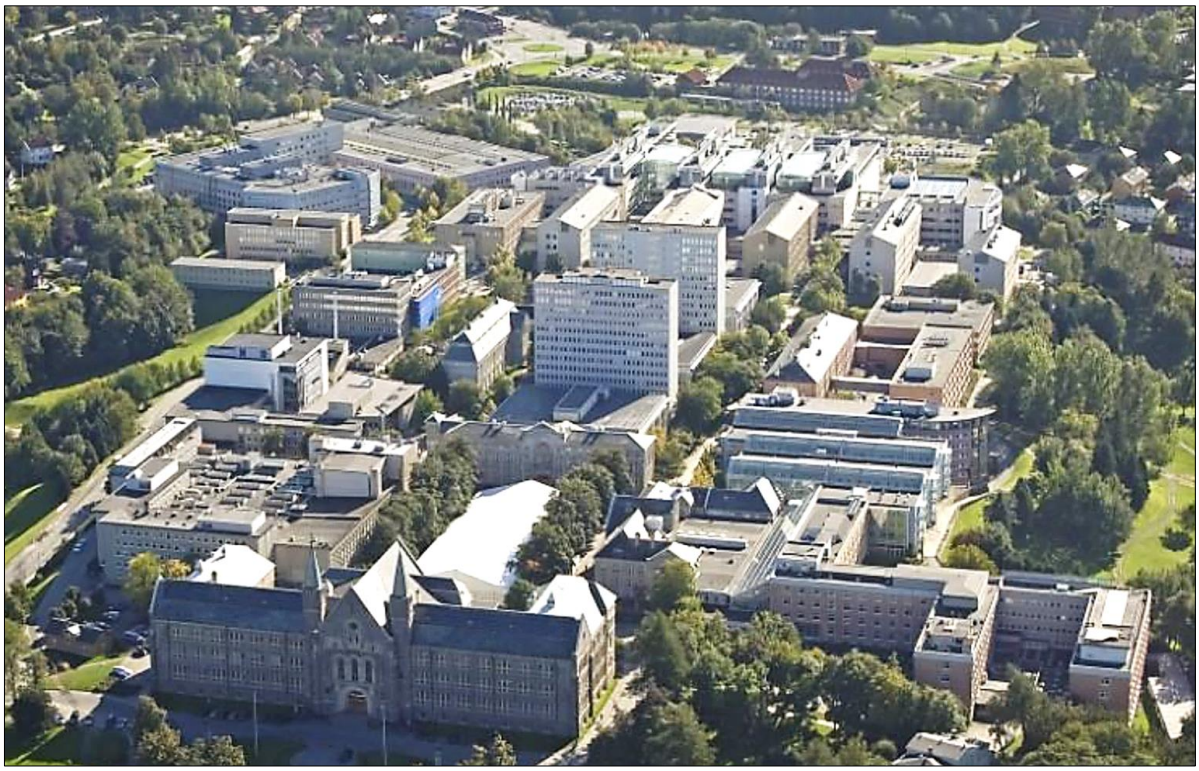

Figure 4-1 Aerial view of NTNU Gløshaugen campus (Source: Multiconsult)

Gløshaugen campus has an interconnected electrical network at the distribution level. The network is spread within the campus and across until Valgrinda (Gløshaugen Nord) via medium voltage cables. All the buildings interconnect to provided redundancy for every building in the event of a fault at any location. Gløshaugen has access to both 230 Volts and 400 Volts at the campus. There are a total of 27 locations where specific buses/nodes are associated with each building. The remaining eight smaller buildings connect to a bus of a relatively larger building next to it. Figure 4-2 represents the Gløshaugen map (top view) showing all the buildings and electrical interconnections. From Figure 4-2, the arrows represented in fuchsia colour are the connections from the main grid of 12 kV. In total, there are six connections from the main grid, where connections PA-2E, PA-4E and MO-6E are connected directly to Varmeteknisk building

(0330), PA-23 to EFI building (0300) and PA-5E and PA-12E to Realfagbygget (1996) respectively. Table 2 gives the name and the code number associated with each building.

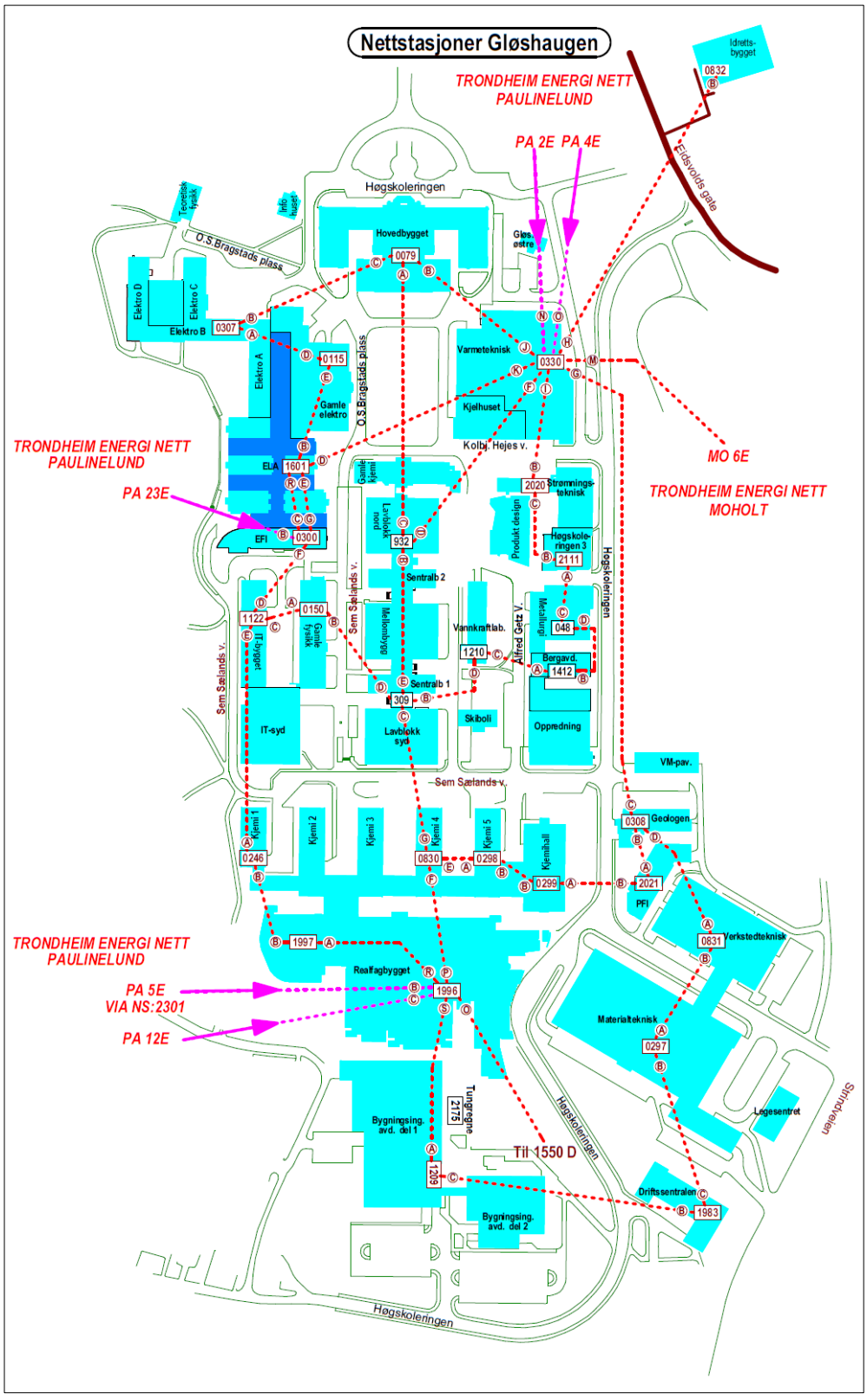

Figure 4-2 Gløshaugen map showing all the buildings and connections (view from top)

Table 2 Code number associated to each connection at the building

No.	Building No.	Building Name
1	0079	Hovedbygningen
2	0330	Varmeteknisk
3	2020	Stromnings Teknisk
4	0048	Metallurgi
5	0831	Verkstedteknisk
6	0297	Materialteknisk
7	0246	Kjemi 1
8	0830	Kjemi 4
9	0298	Kjemi 5
10	0299	Kjemihall
11	1122	IT Bygget
12	0150	Gamle Fysikk
13	0300	EFI
14	0309	Sentral Byg 1
15	0932	Sentral Byg 2
16	1210	Vannkraftlab
17	0115	Gamle Elektro
18	1601	ELA
19	0307	Elektro B, C & D
20	1412	Bergavd
21	0832	Idrett-S Bygget
22	1209	Bygningsing avd
23	2111	Hogskoleringen 3
24	1996	Realfagbygget
25	2021	PFI
26	0308	Geologen
27	1983	Driftssentralen

4.1 Single Line View of Gløshaugen Grid

The use of Single Line Diagram (SLD) of the existing campus made on PSCHEMATIC was used to model the Gløshaugen MG on ETAP. The SLD was divided into two parts, *"Gløshaugen Nord"* and *"Gløshaugen Syd and sydområdet"*. Figure 4-3 and Figure 4-4 represents the SLD of "*Gløshaugen Nord"* and *"Gløshaugen Syd and sydområdet"* respectively. The complete view of the whole SLD is given in the APPENDIX A. The MG was modelled only for the Gløshaugen Nord and part of Gløshaugen Syd. The power system network connected from 1996 REA to 1515 SIB, shown in Figure 4-4, was not modelled in this thesis.

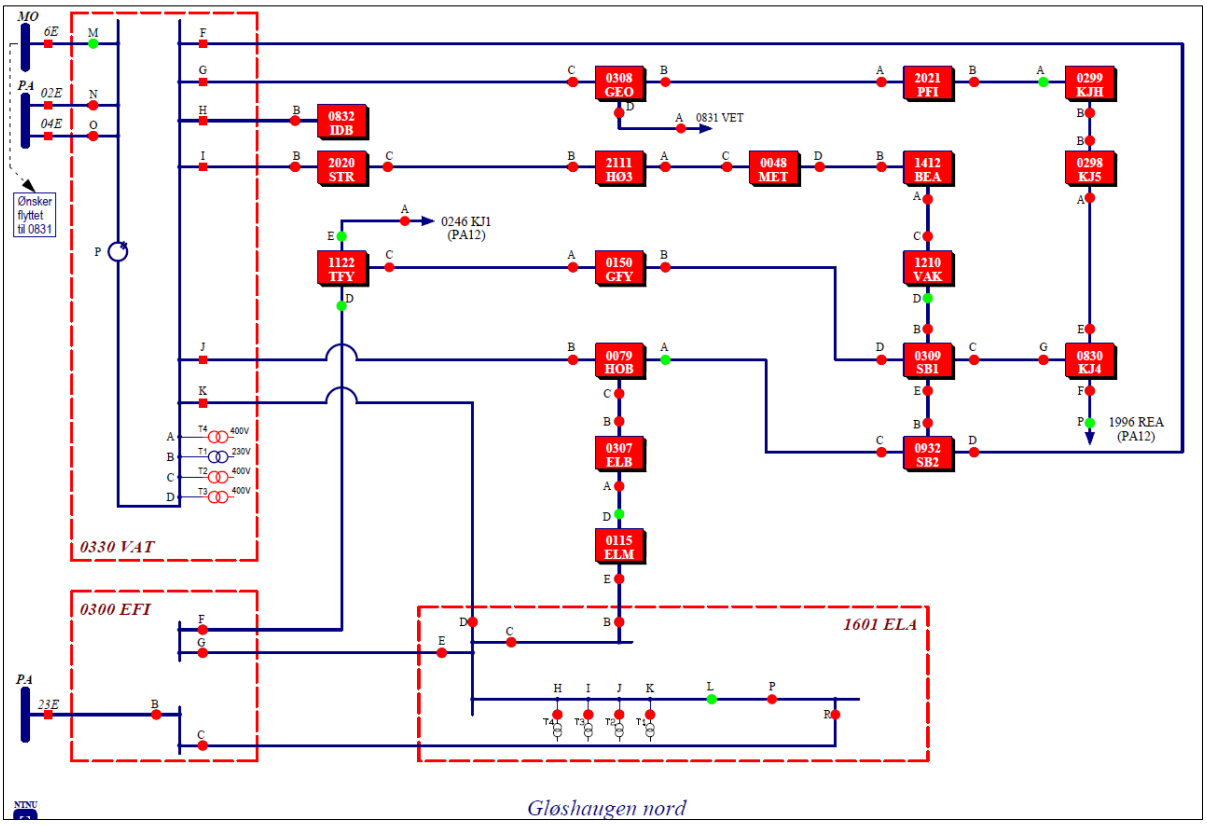

Figure 4-3 SLD representation of Gløshaugen Nord

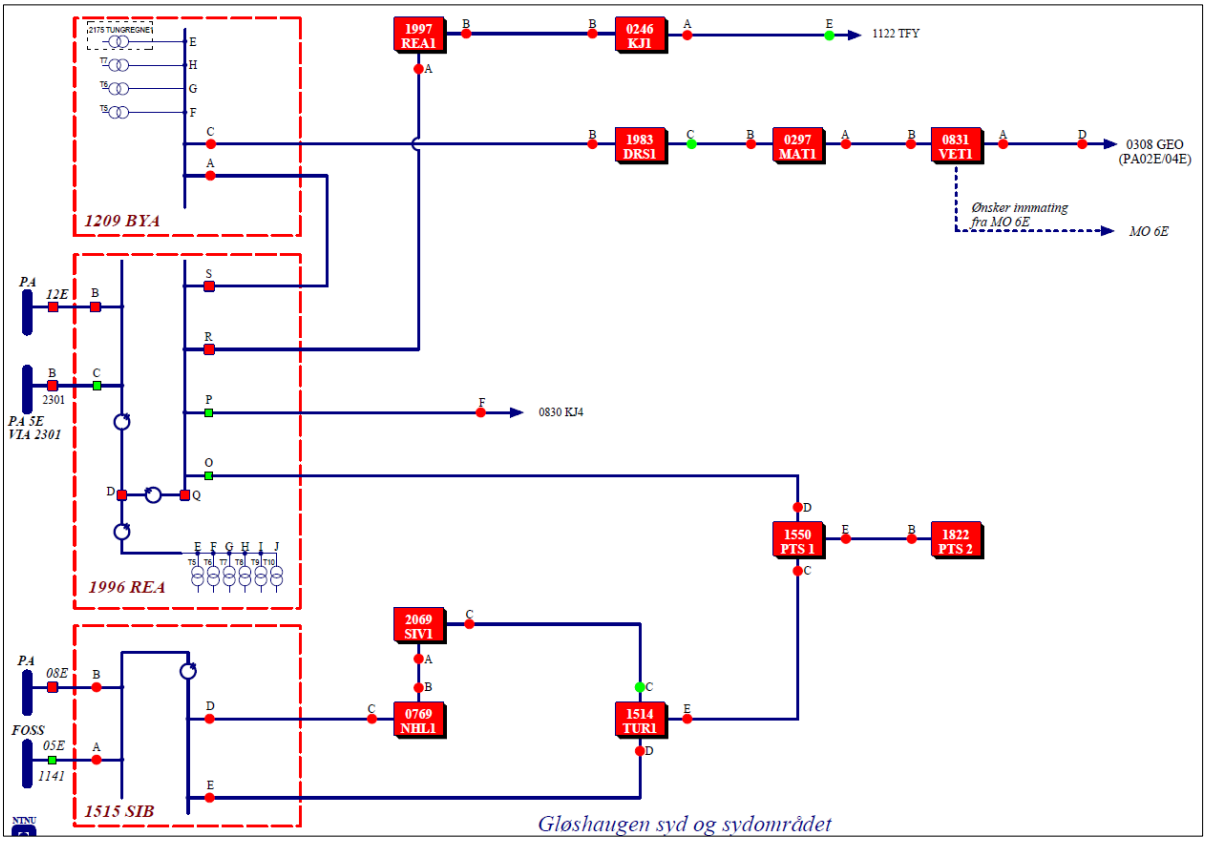

Figure 4-4 SLD representation of Gløshaugen Syd and Sydområdet

Each building in the SLDs above was assigned with a code number (referred in Table 2) and an abbreviation associated with it. The nodes in the figures above represent the connection type with cables and transformers, circuit breakers and switches, as shown in Figure 4-5. The green and red colour of the nodes represents the status of the connections the instant when the screenshot was captured from the real-time graphical display. Figure 4-5 illustrates an example of legends representing the connection type for building 0330 Varmeteknisk.

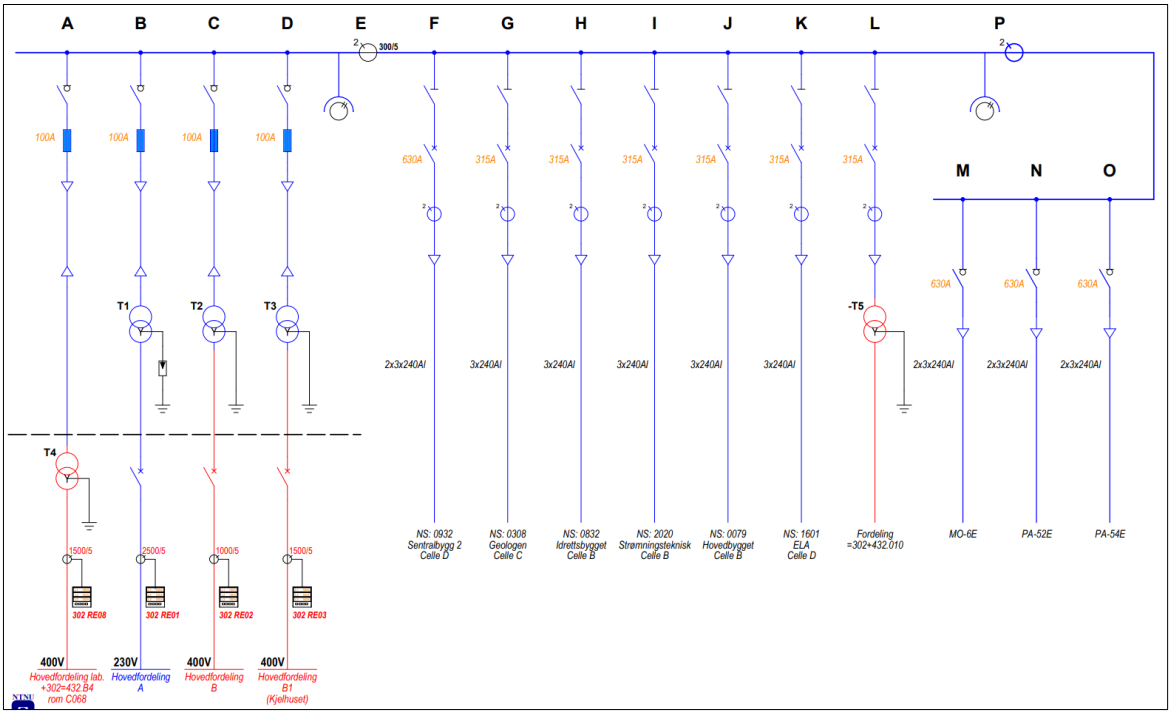

Figure 4-5 Legends representing the type of connections from building 330 VAT (Varmeteknisk)

The Gløshaugen distribution grid map along with the SLDs was analyzed and compared to decide the elements needed for modelling the grid on ETAP. As mentioned in the methodology of this chapter, elements from AC and DC toolbox were used to develop a concept design of the Gløshaugen campus MG. The next section describes in detail the AC/DC elements used to build the MG model.

4.2 Description of Elements Used in ETAP for Modeling the MG

ETAP comes with a variety of options with the help of which, the power system of any size or type can be modelled using simple basic elements from the toolbox in the software. The elements were connected to create a Single Line Diagram (SLD) of the power system for carrying out simulations under different conditions. Every element is unique and has its settings and parameters assigned to it according to the requirements of the system. The ratings of the elements were based on the data provided for the modelling. Complete data of elements with their ratings are attached in the appendices, while some necessary information regarding

settings and parameters will be discussed in this section. The eleven different elements used to model the grid on ETAP are described in the subsections below.

4.2.1 Utility Grid

Utility grids are the main and the most significant source of power supply in the distribution network. Utilities are capable of supplying both active and reactive power to the loads as per their requirements. The Norwegian grid is considered to be very stable and healthy to provide required power by the loads with excellent power quality. The main grid supplies power with a relatively higher voltage of 12kV, which is stepped down through transformers to feed the residential load. The Gløshaugen grid network is connected to the main grid through 6 different connections as described earlier and shown in Figure 4-2. The connections 'Mo-6E', 'PA-2E' and 'PA-4E' feeds the network via Varmeteknisk building (0330). PA-23E can be seen connected directly to EFI building (0300), and two connections from the main grid to the Realfagbygget was observed, namely, PA-5E and PA-12E. Due to the unavailability of grid data, it was assumed that the grids were in an extremely healthy state. Hence, the Short-Circuit (SC) ratings of the grid were specified to a high value of 50MVAsc for all three grids in the model. The MVAsc ratings can also be reduced in order to check the transient stability of the network. Only three out of six grid connections were assumed to be under operation, and the remaining were kept isolated for redundancy purposes. On the ETAP model, the isolation was done by opening the CBs of the respective grid connection. The Gløshaugen grid network was assumed to feed the load via MO-6E, PA-23 E and PA-5E utility connections. The power grid editor in ETAP allows the grid to operate in different modes. Figure 4-6 represents the grid settings and parameters added from power grid editor.

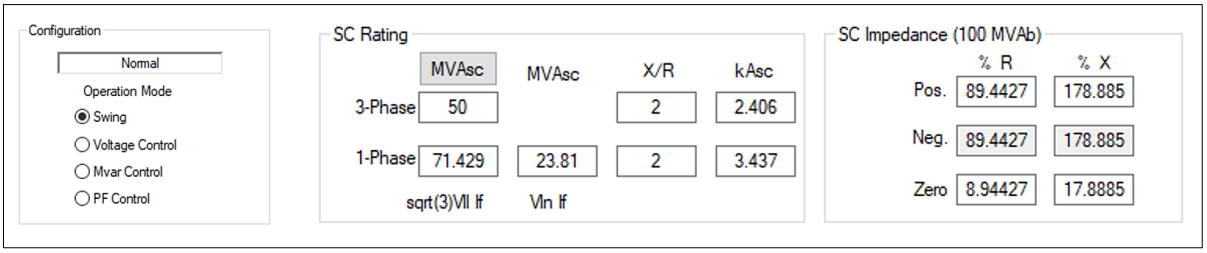

Figure 4-6 Grid parameters set for all grid connections in the network

As per the general system requirement, at least generating source should be kept in the swing mode configuration. It was assumed that out of the three main grids operating, MO-6E and PA-5E were kept in the swing mode while PA-23E was kept in the voltage control mode of operation. In this thesis, the power flow from each grid into the network was compared and analyzed for the Energy Management (EMS) purpose.

4.2.2 Diesel Synchronous Generators

Synchronous generator in the model was connected to the system only for the transient stability study. It should be noted that this generator was not part of the Gløshaugen model data received for modelling the campus and was used exclusively for stability study purpose. The generator specifications and ratings were selected similar to the Utility Grid 'MO-6E'. These reason for choosing similar ratings was due to the fact that the generator would act as a grid replacement if the utility connection was down. The complexity of the generator requires accurately specified parameters for achieving the desired results.

ETAP gives its user the option to select in detail various parameters for a single generator such as ratings, capability, impedance model, inertia, governor and power system stabilizer. The software also set typical parameters for the impedance model based on the type of generator selected for the study. The Generator was connected directly to Varmeteknisk (Bus0330 at 12kV). Figure 4-7 illustrates the parameters given to the generator for the network model. The inertia calculator calculates the typical values of the moment of inertia of prime mover, coupling and the generator.

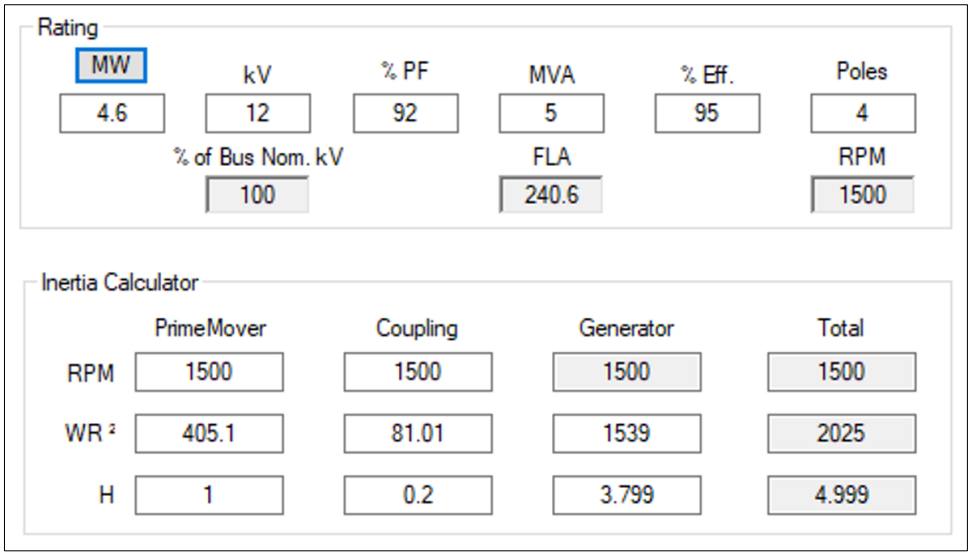

Figure 4-7 Generator and inertia ratings specified and calculated for the model

Once the ratings and inertia were specified for the model, the impedance and dynamic model values were specified from the typical values by ETAP. Three different dynamic models can be chosen for the analysis. Figure 4-8 shows the impedance and dynamic model parameters selected from the typical ETAP data.

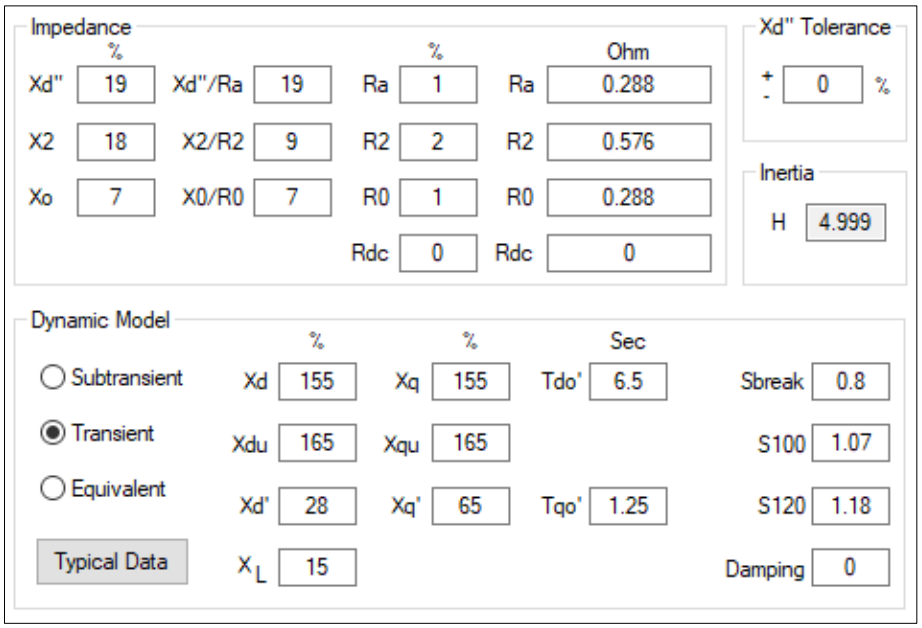

Figure 4-8 Impedance and transient dynamic model parameters for the generator

The above-mentioned settings were the general setting for the generator to operate in a steady-state condition. The control parameters for the generator are required to improve the stability of the system during small or large disturbances within the network. The system model should be completed by specifying the exciter of the generator to add control to the generator. The excitation system for synchronous generators is quite sophisticated. For this model, the IEEE recommended type DC21 exciter was used to improve the stability of the system. The DC1 exciter is a DC commutator type which regulates the voltage on a continuous basis. Figure 4-9 illustrates the logic diagram on the basis of which the exciter was functioning.

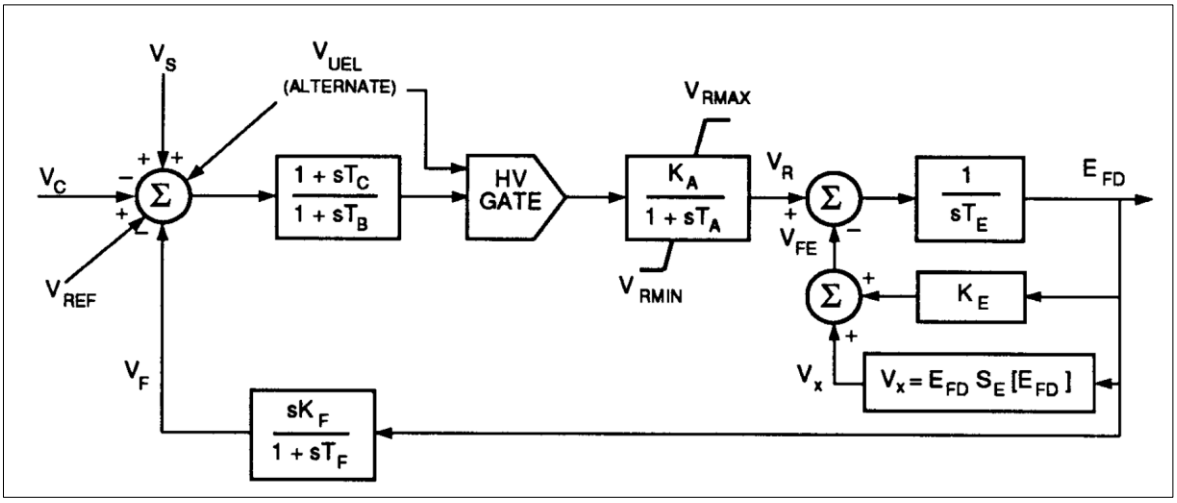

Figure 4-9 Control logic diagram of the DC1 exciter by IEEE

The typical values selected for the time delay and controller gain is shown in Figure 4-10

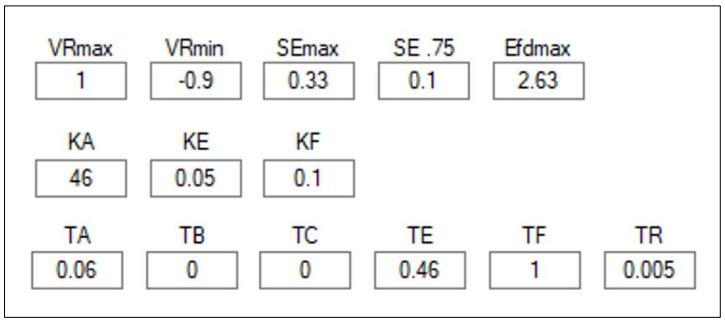

Figure 4-10 DC1 exciter parameter from the ETAP sample data

4.2.3 Transformers

The transformers in the network play a vital role to achieve the desired voltage required by the loads for operation. The Norwegian grid is designed to provide 230 volts and 400 Volt at distribution level for different loads. ETAP allows its users to choose either a 2-winding transformer or a 3-winding transformer for modelling purposes. In the Gløshaugen MG, 41 liquid-fill transformers of different sizes were used to vary the voltage according to the design and load requirements. The main transformers connected to the utility connections were used to step the voltage down from 12kV to 400kV and the transformers within the network, of relatively smaller size, were used to further reduce the voltage to 230 volts for the residential load. The ratings of the transformers were assigned with the help of the data received from the engineers at Gløshaugen. Details regarding the location and capacities of the transformers are given in APPENDIX B. Figure 4-11 represents the 2-winding transformer editor where the values can be changed according to the system requirements. Although the editor comes with various options in different tabs having minor details of the transformer model, only limited tabs were used to model the transformers.

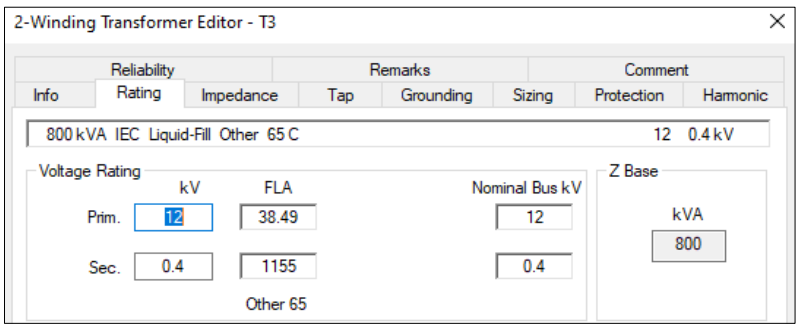

Figure 4-11 ETAP transformer editor for showing parameters for 12/0.4 kV transformer

Another advantage of using ETAP is that it assigns typical impedance, reactance and resistance values according to the ratings and type of the transformer chosen. Figure 4-12 (a) shows the impedance values and the option of selecting the typical Z and X/R values, while Figure 4-12 (b) shows the Load Tap Changer (LTC) also called the voltage regulator.

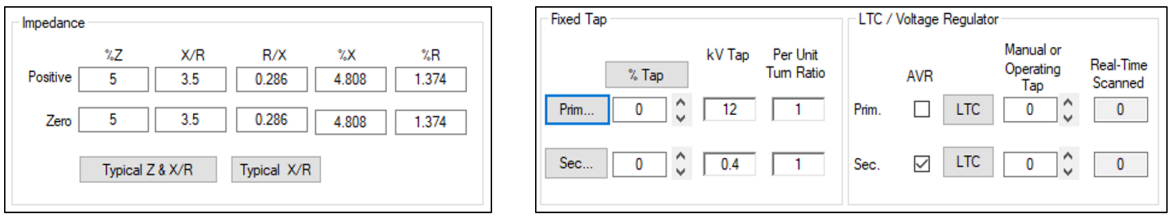

(a) (b)

Figure 4-12 Tabs showing the (a) impendence and (b) transformer tap values according to requirements

The LTC is the most convenient source of operating the system under normal condition by regulating the voltage within the given limits. It helps to regulate the voltage on both the primary and secondary side of the transformer to avoid over or under-voltage conditions at the buses connected directly to the transformer.

4.2.4 AC/DC Buses

AC/DC buses are essential elements of the power system as they provide the path for the power flow. In an electrical system, power is first injected into the bus before it decides the path of the power flow within the network. The Gløshaugen concept was designed to have 57 AC buses and 5 DC buses. All the buildings on campus were expected to have loads operating at both 230V and 400 V. For this purpose, two buses of different voltage levels were associated with each building. The DC buses were used to connect the batteries with the inverters. Bus IDs and the nominal voltages were displayed at all times while carrying out the simulations on ETAP. The letter 'A' was chosen for the 400 V bus IDs, while the letter B was associated with the 230 V buses, making it easier to compare and analyze the model.

The nominal voltages of all the busses were assigned with the help of the ETAP Bus Editor. Elements of AC and DC system were directly connected to the bus, while the interconnections between the buses were either made directly through the cables with CBs or via transformers where buses with different voltages levels were connected together. Depending on the system study case, the bus in ETAP selects automatically in percentage the voltage condition, i.e. initial voltage or operating voltage. Figure 4-13 shows L-N and L-L values for the 12-kV bus at Varmeteknisk building (0330) which is connected to the main grid. At the end of the load flow simulations in ETAP, voltage levels of the buses could be either displayed in kV or in percentage. The voltage limits are specified in the study case to analyze whether the buses are operating within the specified voltage limits. The limits are specified for the marginal and critical condition of the element. The load flow will display the bus in fuchsia colour when it is voltage is within the marginal limits and red, when the voltage is beyond the operating limits.

The marginal limits were specified between 102-105% for overvoltage conditions and 95-98% for the bus operating under voltage limits.

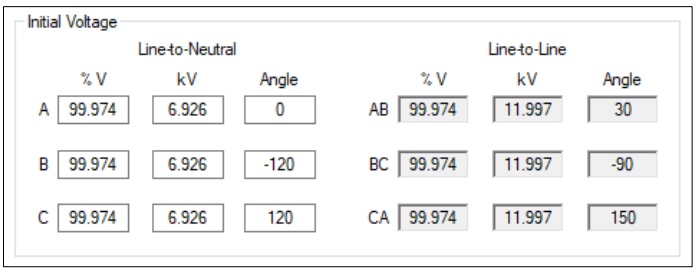

Figure 4-13 ETAP editor showing

4.2.5 Loads

Electrical loads are equipment or component that consumes electric power for its operation. The type of power (active or reactive) consumed are decided by the category under which the load falls. Examples of load in an electrical network are induction motors (requiring reactive power), lighting load, heaters and electronic devices such as computers etc. ETAP has two types of AC load elements in its toolbox for designing, namely 'Static Load' and 'Lump Load'.

4.2.5.1 Static Load

The static loads are used where the power factor of the electrical equipment is 100%. It means that the load will only require active power and no reactive power for its operation. A total of 21 loads were modelled with different ratings depending on the size and energy consumption of the building. All static (resistive) loads were attached to 230V buses in the Gløshaugen campus model. The loads can be given ratings through the Static Load Editor on ETAP. Figure 4-14 shows the Static Editor displaying the load ratings and the loading category. The load category can be specified and adjusted for multiple scenarios and seasons. In this thesis, all the AC and DC elements were kept in the 'Design' loading category for a fair comparison between different scenarios.

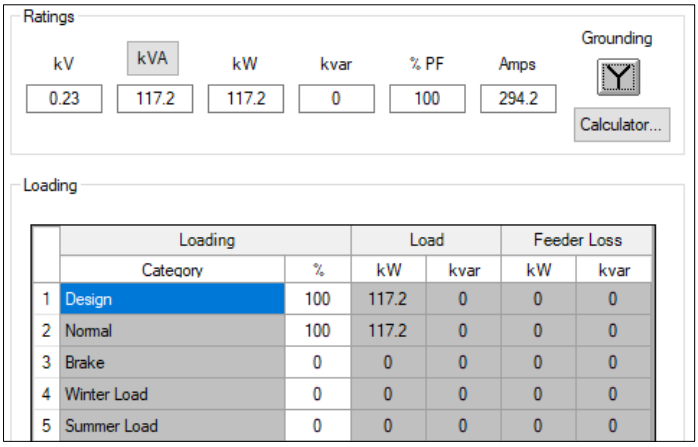

Figure 4-14 Static Load Editor showing the load rating and category

4.2.5.2 Lump Load

Lump load element in ETAP is the most convenient load type to use for modelling any network. The reason lump loads are usually chosen is that the user can specify their power factors. If the power factor is chosen to be as 100%, then the lumped load will be acting as a static load. Unlike static loads, lump loads require reactive power in addition to active power for their operation. Lump load equipment is usually relatively heavy induction motors requiring 400 V for its operation. Seventeen lump loads were attached directly to the 400 V buses of each building depending on the size and consumption of power. The Lump Load Editor provides the option to adjust the active-reactive power of the loads. It can be seen in Figure 4-15 how the parameters were adjusted. Due to the data limitations for Gløshaugen campus loads, it was assumed that all the lump loads modelled had a percentage power factor of 90% and the load was set to 80 kVA inductive (represented as motor load in Figure 4-15) and 20 kW resistive (represented as static load in Figure 4-15).

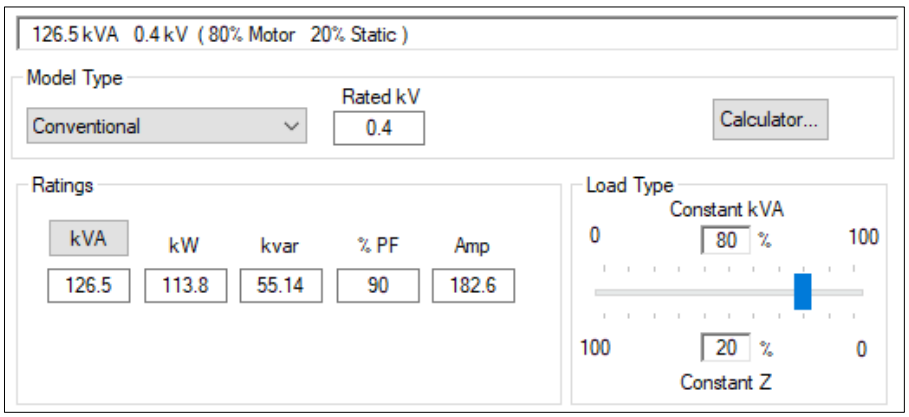

Figure 4-15 Lump Load Editor showing how the power factor and load type are adjusted

4.2.5.3 Load Profiles

To decide the ratings and create the load profiles of the static and lump loads in the Gløshaugen campus, the total energy consumption of the whole campus in a single year was considered. According to [27], the energy requirement for Gløshaugen in the year 2019 was 63.551 GWh. However, due to the unavailability of the data, energy consumption from the year 2012 was used to calculate the rated power of the loads. The annual consumption by each building was taken from [11], and the rated power was calculated for the loads. The complete energy consumption and carbon emission data for the year 2011 – 2012 is attached in APPENDIX C of this report. Energy consumption during working hours is higher compared to consumption at night. All the loads were assumed to be operating at their maximum capacity for a period of 24 hours in order to calculate the ratings to be assigned to each load. Table 3 shows the calculated values in KW for the loads.

Table 3 Gløshaugen Energy consumption and rated load for each building

Building No.	Building Name	Voltage Meter Rating	Energy consumed/year [kWh]	KW Rating (12-Hr)
79	HOVEDBYGNINGEN	230 V	1,374,586	313.83
330	VARMETEKNISK	230 V	1,539,099	351.39
		400 V	452,555	256.89
2020	STROMNINGS TEKNISK	400 V	554,148	126.52
48	METALLURGI	230 V	240,263	54.86
		400 V	248,596	54.76
831	VERKSTEDTEKNISK	410 V	1,074,225	245.26
		400 V	233,476	53.31
297	MATERIALTEKNISK	230 V	1,811,435	413.57
		410 V	633,294	144.59
246	KJEMI 1	230 V	419,147	95.7
		410 V	2,716,962	620.31
830	KJEMI 4	230 V	8,885	2.03
		410 V	762,274	174.04
298	KJEMI 5	230 V	846,480	193.26
299	KJEMIHALL	230 V	585,816	133.75
1122	IT BYGGET	230 V	1,320,179	301.41
150	GAMLE FYSIKK	230 V	279,996	63.93
		410 V	168,178	38.39
300	EFI	230 V	1,005,024	229.46
309	SENTRAL BYG 1	230 V	2,073,725	473.45
932	SENTRAL BYG 2	230 V	2,148,848	490.6
1210	VANNKRAFTLAB	230 V	36,202	8.27
		410 V	25,467	5.81
115	GAMLE ELEKTRO	230 V	758,128	173
1601	ELA	410 V	5,517,944	1260
307	ELEKTRO B, C, D	230 V	1,878,758	429
		410 V	720,018	164.4
1412	BERGAVD	410 V	1,301,972	297.25
832	IDRETT-S BYGGET	230 V	513,340	117.2
1209	BYGNINGSING AVD	230 V	943,715	215.46
		410 V	4,278,825	977
2111	HOGSKOLERINGEN 3	410 V	373,243	85.22
1996	REALFAGBYGGET	410 V	11,633,554	2656
2021	PFI	410 V	976,510	223
308	GEOLOGEN	230 V	601,494	137.32
1983	DRIFTSSENTRALEN	230 V	404,036	92.24
		SUM	**50,460,397 kWh**	**11672.48 kW**

The ratings were given to all the loads based on the load type and operating voltage. To create the load profile for a typical working day (mid-March), The loads were varied in percentage in order to perform the time-domain load flow analysis. The variation made to all the loads were over a period of 24 hours. The detailed explanation of the load profile with visual representation will be presented in chapter 5 of this thesis report.

4.2.6 Photovoltaic Array

PV arrays are the most convenient energy source among renewable energy sources as it is easy to install and maintain. Multiconsult, in their report [27], published in 2018, has carried detailed analysis of the potential of PV generation at the Gløshaugen campus. Since almost all the buildings in Gløshaugen have the tendency and space to install roof-mounted solar panels on top, it was unsure whether the roofs were strong enough to hold the heavy panels on top of them. The PV arrays generate DC power; hence in the older versions of ETAP, the PV array element came separately in the DC toolbox, which was connected to the DC bus. The PV system requires a DC-AC inverter in order to feed AC power into the network. ETAP 16 came with an upgrade where the PV arrays elements come with a built-in inverter, the settings of which can be defined in the PV array Editor.

The existing Gløshaugen campus has only a few PV units installed on Elektro building; the size and choice of location for the panels in the thesis concept model became crucial. The location was decided after running the load flow simulation and analyzing the status of the buses. In this thesis, 5 PV-Panels connected in series-parallel combination were used. The five PV panels connected to respective 400 V buses are presented in Table 4.

Table 4 PV-Panel connection to the buses

PV Panel ID	Bus ID
PVA1	308A
PVA2	831A
PVA3	297A
PVA4	309A
PVA5	1412A

4.2.6.1 PV Panel Design and Parameters

The software comes with a library where PV panels of different ratings can be selected with respect to the manufacturers. From the library, “ART245-60-3-1” model from the manufacturer ‘SUNIVA’ was chosen as the roof-mounted solar panels for the campus. The rating of a single

solar panel was 240 W peak with 1000 Vdc max. Figure 4-16 displays the details of the PV panel and array for the five PV elements used.

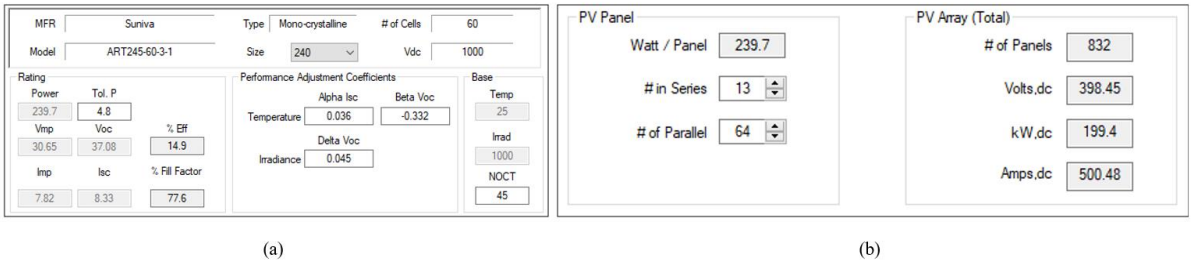

Figure 4-16 Ratings and parameters for the SUNIVA PV panels and array

The 'Power-Voltage' curves and the 'Current-Voltage' curves of the SUNIVA PV panels are represented in Figure 4-17. Figure 4-17(a) represents the P-V curve and Figure 4-17 (b) represents the I-V curve for the panel, respectively.

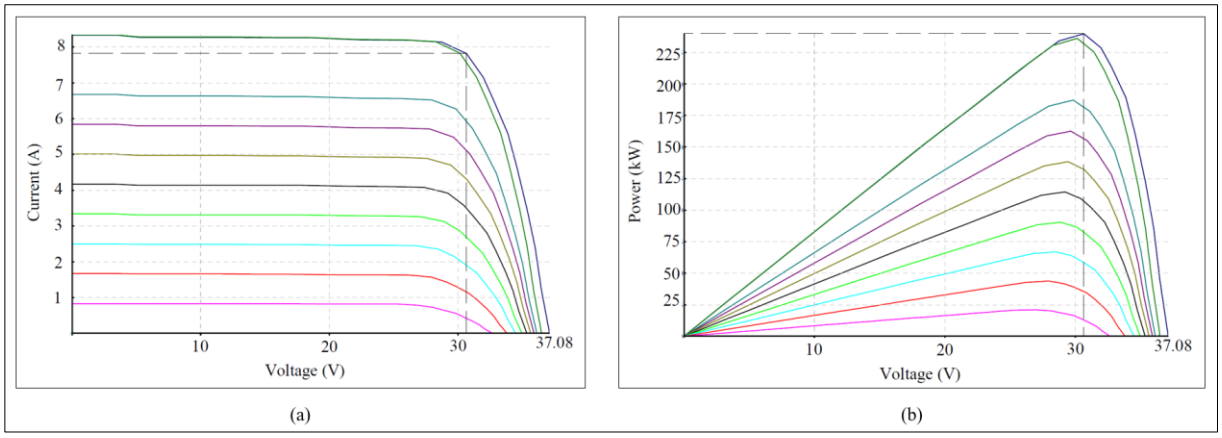

Figure 4-17 P-V and I-V curves for the SUNIVA 1000 Vdc max solar panel

4.2.6.2 PV irradiance

The generation from the PV panels depends entirely on the irradiance and sunlight hours of the location where the PV units are installed. A typical working day in the month of March (16 March 2020) was chosen to carry out the simulations in order to observe significant effects in the behaviour of the system. The sunlight hours in Trondheim for the month of March is approximately 12 hours if the sky is clear. The irradiance on the panels shows variance throughout the day with the maximum during the noon. The irradiance profile was built for all PV panels manually in the library. The maximum irradiance was set as $1000\ W/m^2$ and the minimum was $0\ W/m^2$ at night. Figure 4-18 represents the solar irradiation set for Trondheim over a period of 24 hours for mid of March. The irradiance was set to the maximum with PV giving its peak power from 11:00 – 16:00.

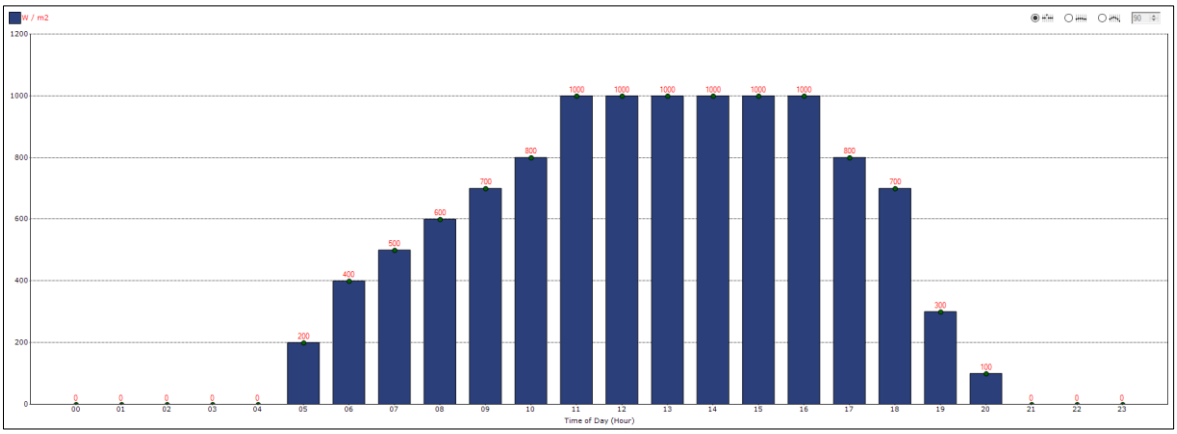

Figure 4-18 Solar irradiance profile of Trondheim for 24 hours

Another vital part of the PV installation is the inverter via which the PV panel is connected to the respective bus. The inverter design and parameters will be discussed in the next sub-section 4.1.6; however, the inverter ratings chosen specifically for the PV is shown in Figure 4-19.

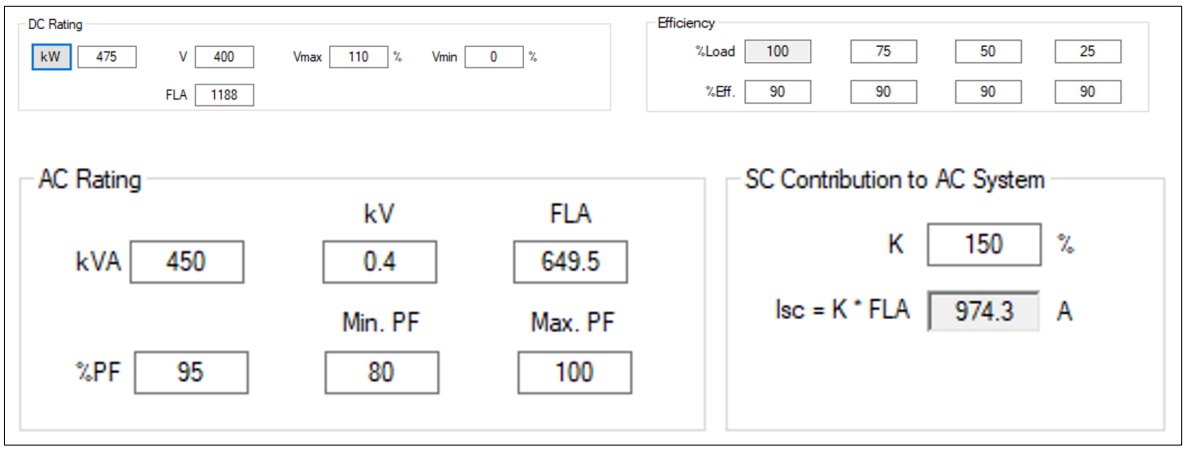

Figure 4-19 PV panel inverter parameters

4.2.7 Energy Storage System (Batteries)

The Energy Storage System is often used for power management through peak-shaving. There are multiple battery models from different manufacturers available in ETAP library. The main difference between these models is the capacity per cell for each battery module. The total number of cells in each string decide the total voltage output of the battery system. Similarly, by keeping output voltage constant, the capacity of the battery system can be easily increased by integrating 'n' number of strings in parallel. The batteries designed for the campus model were selected based on the calculation to assist the main grid during peak load hours. There were ten batteries, each consisting of 6 strings. Figure 4-20 shows the total number of cells per string and the total capacity of the battery for six strings in ampere-hour.

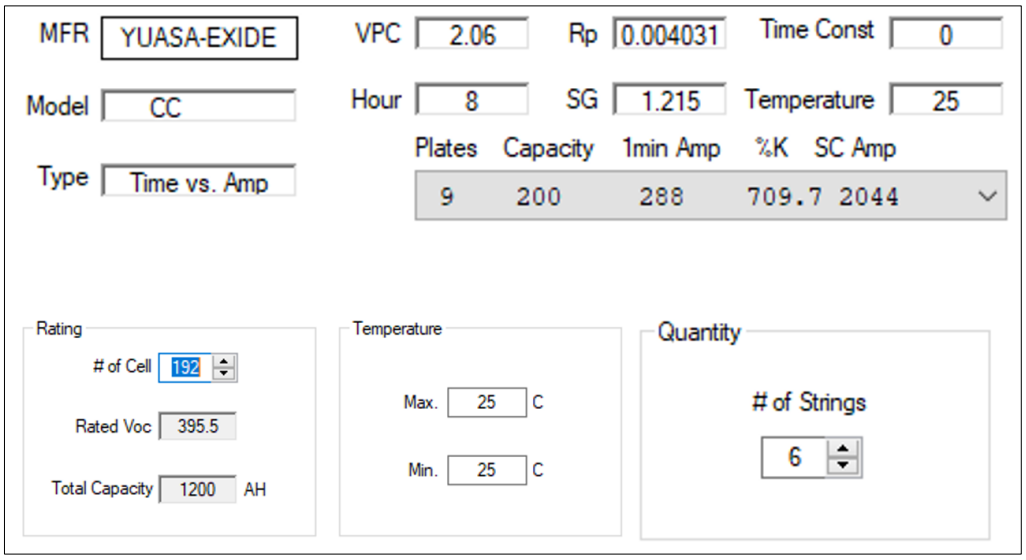

Figure 4-20 Battery ratings for all the batteries in the system

The maximum voltage at 100% state of charge for the battery was set to 400 Vdc. The battery voltage decreases as the state of charge decreases during discharging of the batteries. As shown in Figure 4-20, the batteries for this model can supply constant power for 8 hours without interruption. The batteries can also operate 3-6 times their rated capacity if needed but will have a reduction in the number of hours for discharging. Practically, the battery had been designed for higher power capacity (480 kW), but the power from the batteries was limited to have a relatively smaller depth of discharge, to ensure the optimal use and longer lifetime. The power limitation for the batteries was controlled from the DC-AC inverters. The total power for all the batteries operating at the same time was $250 * 10 = \boldsymbol{2.5MW}$.

4.2.8 DC-AC Converter and DC-DC Converter

The output power from the PVs and the batteries is generated in the DC form. As the load operates with AC power, the DC power should be converted to AC when integrating the PVs and batteries into the network. Similarly, it is equally important to regulate the DC output voltage injected into the DC bus. In this thesis, the RES was integrated with the help of 10 DC-AC inverters and 10 DC-DC converters.

4.2.8.1 DC-DC Converter

The DC-DC converter was selected to keep a constant DC voltage on the DC bus connected to the output side of the converter. Since the voltage of the battery source decreases with state of charge, it is crucial to boost the input voltage to maintain a constant DC voltage. The ratings of the DC-DC converters used for the batteries are shown in

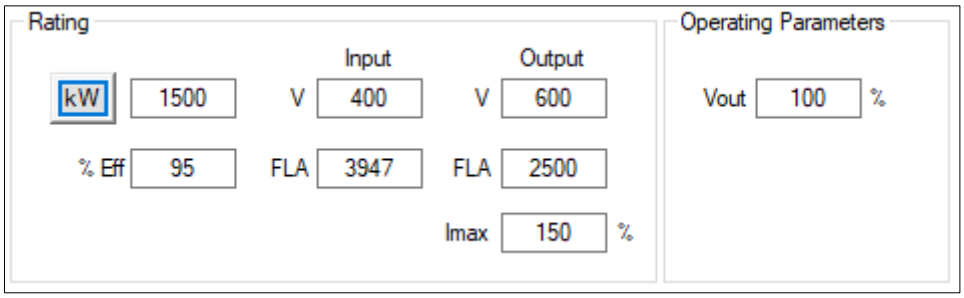

Figure 4-21 DC-DC converter ratings for the batteries

The voltage output of the converter was specified as 600 Vdc. The reason for keeping a higher voltage on the output side of the converter was to boost the input voltage to maintain a constant voltage on the DC bus. The DC-DC converter goes into uncontrolled mode by conducting through the free-willing diodes if both the output and input voltages are kept being of the same magnitude.

4.2.8.2 DC-AC Inverter

Five out of ten inverters were built-in with the PV model. The remaining five inverters were connected to the DC buses with the respective set of batteries. The ratings of the inverters can be seen in Figure 4-22. The inverter AC ratings were selected based on the maximum power from the batteries at 1-C discharge rate. The max power from each battery was 480 kW; thus, the inverter ratings were selected to be marginally higher for allowing discharge rates higher than 1-C.

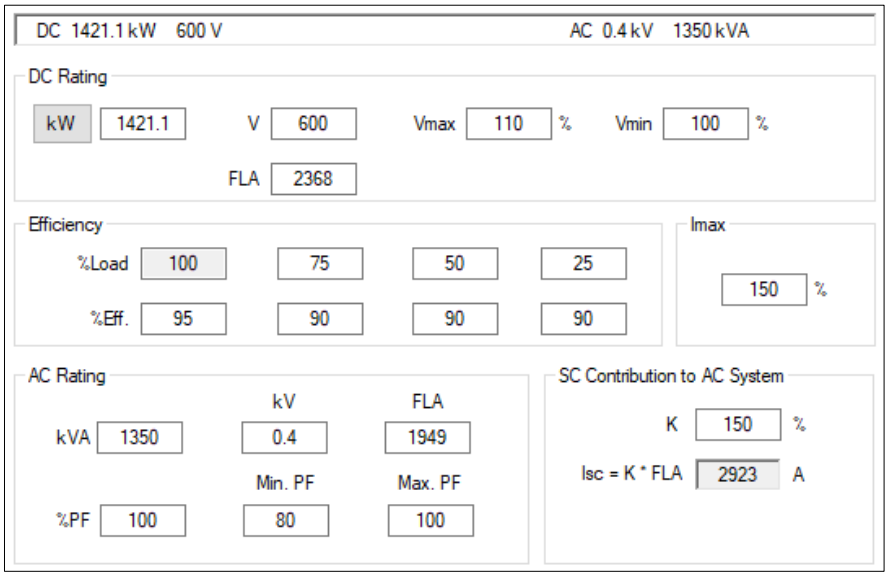

Figure 4-22 DC-AC inverter ratings for battery sets

All the inverters were kept in the voltage control mode of operation in order to maintain constant AC voltages at all buses. Additionally, it allowed the provision of limiting active and reactive from the inverter output.

4.2.9 Cables

To interconnect all the elements of the MG model, aluminium cables of different sizes and dimensions were used along with switches and breakers for protection. ETAP's cable library has a wide range of cables made of aluminium and copper with various voltage ratings and dimensions. Users are also allowed to specify the number of conductors and the insulation type for the cables. The dimensions of the cables were given based on the list of all the connections provided by the technicians. Table 5 shows an example of the cabling data for the Gløshaugen campus. The complete list of all the cables with details of their lengths and dimensions is given in APPENDIX D.

Table 5 Example of cabling data showing the dimensions and lengths of 4 cables

From	To	Length [km]	Rated Voltage [kV]	Cross-Section [mm^2]	Capacitance [µF]	Resistance [Ω]	Reactance [Ω]
NS048	NS1412	0.030	12	150	0.0081	0.00618	0.00264
NS079	NS0307	0.034	12	240	0.01496	0.00425	0.00612
NS079	NS0307	0.165	12	240	0.0726	0.020625	0.0297
NS150	NS1122	0.028	12	120	0.00924	0.007084	0.002016

The rated voltages of all the cables were 12 kV for 50 Hz system. The ETAP cable editor did not have a 12kV cable; however, it has the option of creating a new cable profile. Since the rated voltage of the cables had almost no effect on the system behaviour, 15kV cables were used for connecting the network. Figure 4-23 shows the properties of 165m cable from Hovedbygningen to Elektro Bygning.

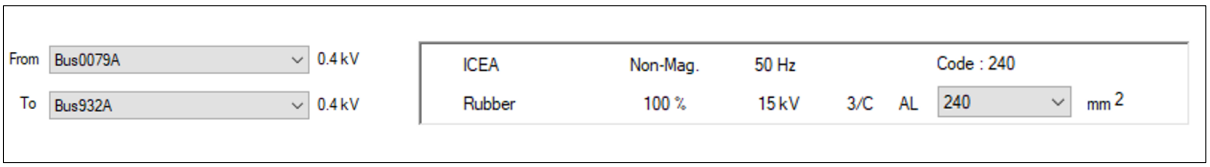

Figure 4-23 Cable properties for the cable connection from Bus0079A to Bus932A

4.2.10 Gløshaugen Microgrid Concept Design on ETAP

Figure 4-24 represents the complete MG concept design after interconnecting all the elements mentioned in the previous sections. All the simulation analysis in this thesis were carried out by using different case studies on this model. The results of EMS and Transient stability have been discussed in the next chapter.

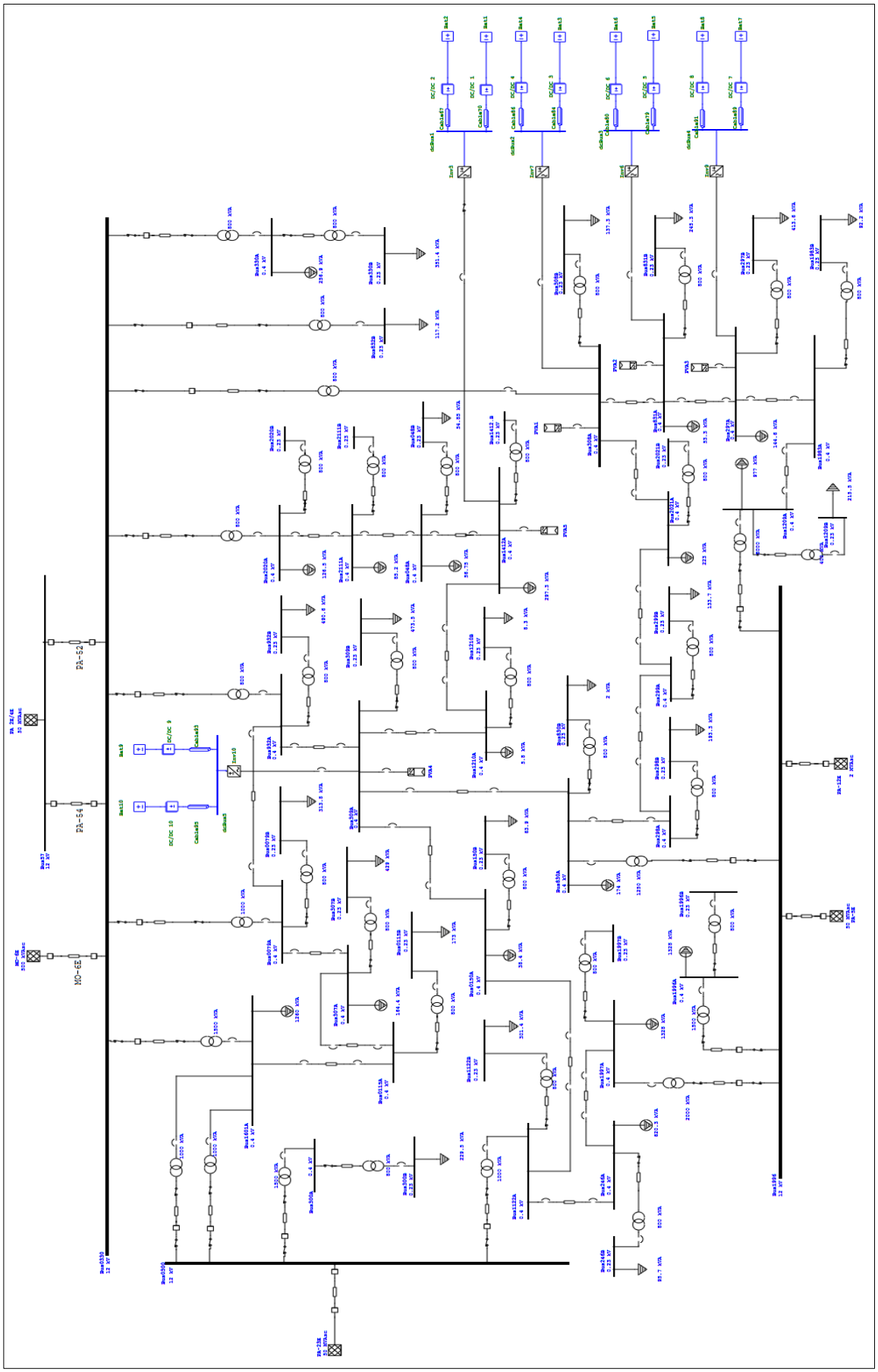

Figure 4-24 Gløshaugen Concept design developed on ETAP

5 RESULTS AND DISCUSSION

In this chapter, the GH model shown in Figure 4-24 has been analyzed by using multiple study cases under different load conditions. For implementing the EMS system and performing transient analysis, the following study cases were chosen:

1. AC Load Flow Analysis
2. DC Load Flow Analysis
3. Time-Domain Load Flow Analysis
4. Transient Stability Analysis

Each study case was based on different scenarios involving connecting and disconnecting of generating sources such as PVs, batteries and utility connection. All the scenarios were based on a typical single week-day load profile of Gløshaugen campus. The load profile was developed using approximations to the rated loads connected on each bus of the campus. The approximations were made on an hourly basis assuming in percentage the energy consumption by all the loads. The daily load profile for a typical weekday is shown in Figure 5-1

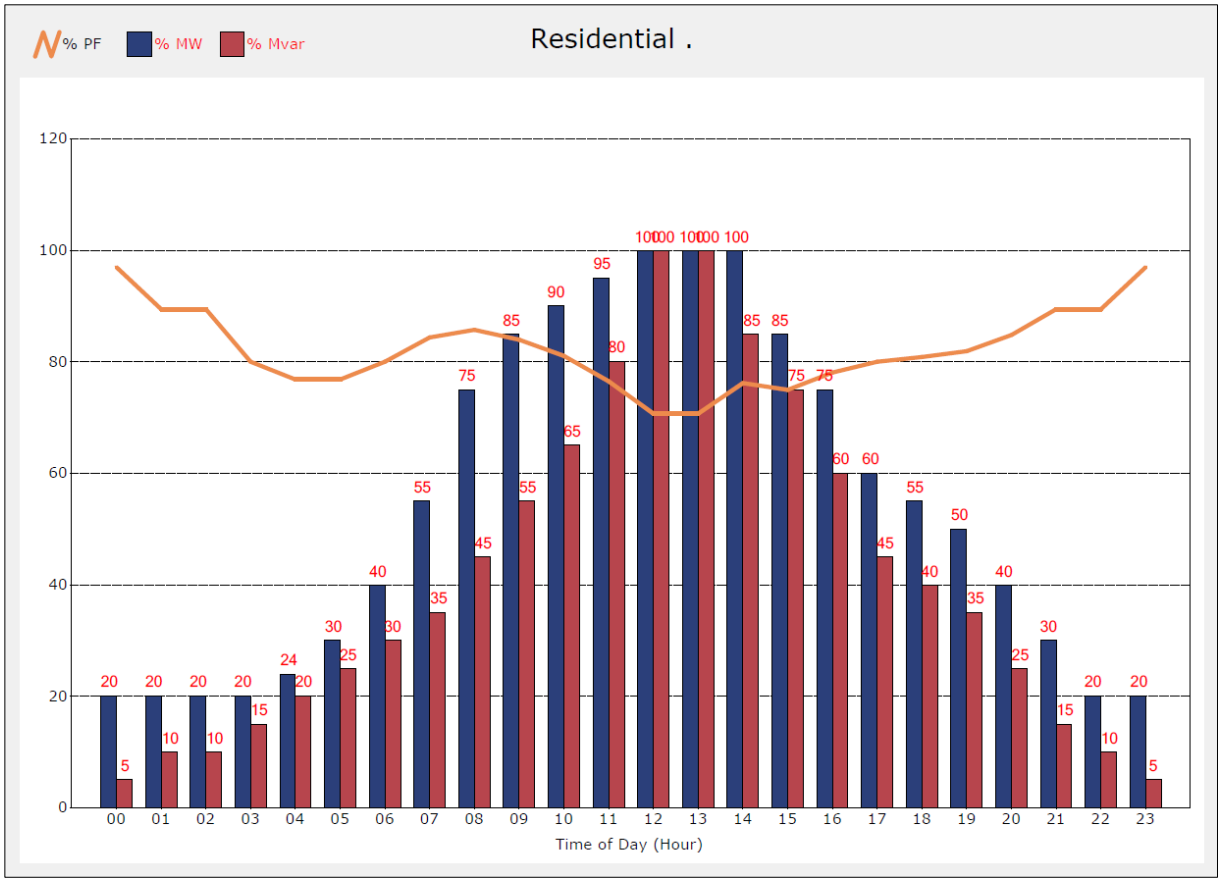

Figure 5-1 Single week-day load profile for Gløshaugen

5.1 Energy Management System of Gløshaugen

In this section, EMS is studied performing simulations using AC load flow, DC load flow and time-based load flow for three different scenarios. The scenarios are classified based on the supply-demand ratio of the campus. The remote-controlled operation for running each scenario has been created on ETAP by using the scenario wizard option. The scenario wizard allows the user to alter the parameters/variables for each equipment in the network assigned to the specific study case. Figure 5-2 shows the scenario wizard window on ETAP. The details of each scenario are described in the following subsections.

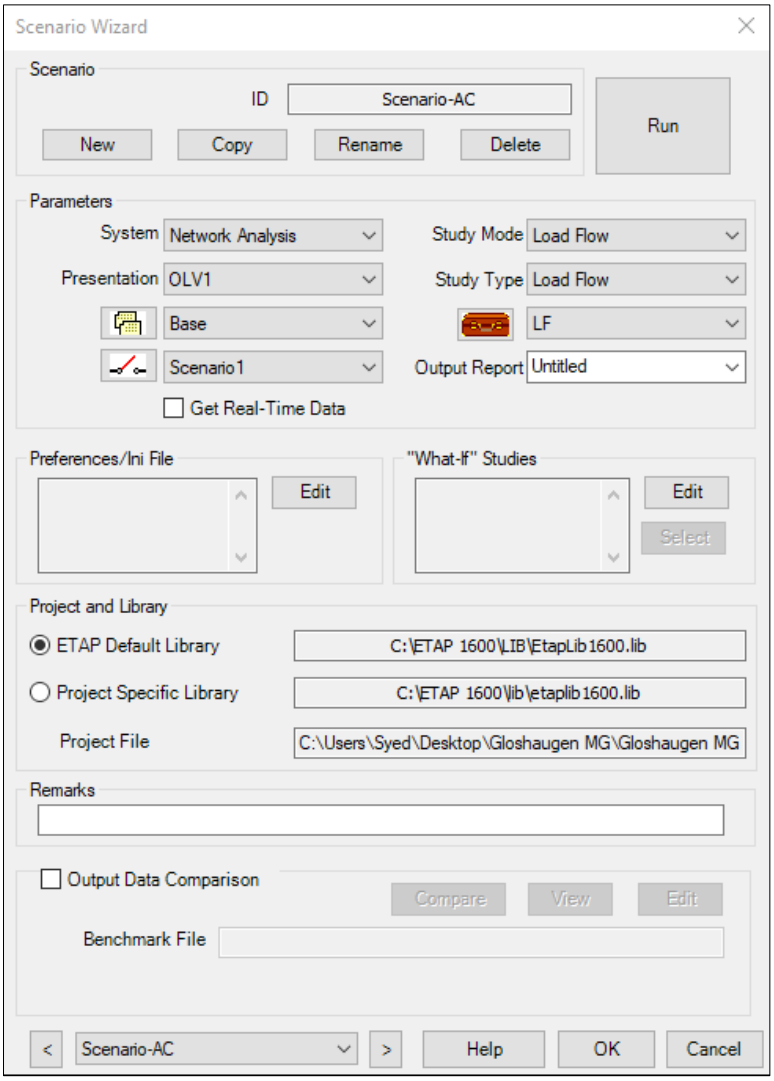

Figure 5-2 ETAP scenario wizard for controlled operations

5.1.1 Scenario 1: System supported only by utility (main grid)

In this scenario, all the loads are supplied by the utility grid alone. It was assumed that two out of five connections from the utility were kept for redundancy purposes. Utility connection "MO-6E", "PA-23E" and "PA-5E" were kept in service for the provision of power to the network. The circuit breakers (CB) for the PVs and inverters (connected to batteries) were kept opened

remotely in order to isolate them from the network. The first case was to run the instantaneous load flow for maximum (rated) loads on each bus. The purpose of running the AC load flow was to observe the active and reactive power flows within the network and from the utility. The second case was to run time-based AC load flow to analyze the active and reactive power flows for varying loads mentioned in the above section (Figure 5-1). This scenario did not require DC load flow analysis as the batteries were isolated from the network. Both studies gave us a clear picture of whether all the system nodes were under reasonable operating limits. A standard operating limit was set for all the equipment within the system, which specified the marginal and critical limits for the equipment. The critical and marginal limits defined in all study cases are represented in Figure 5-3.

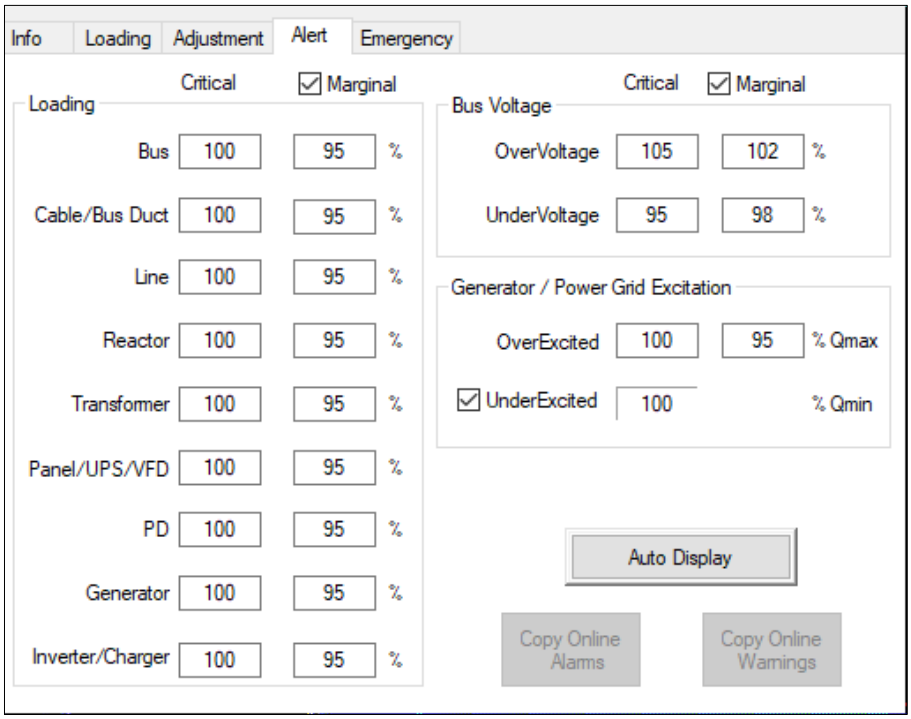

Figure 5-3 Marginal and critical limits for the system

The visual representation of equipment operating beyond their limits is defined by different colours in the system. The marginal operating equipment is visualized by pink, and the critical equipment is displayed in red.

5.1.1.1 AC Instantaneous load Flow (Utility) – Case 1

In the first case of scenario 1, the results of AC load flow are displayed from Figure 5-5 to Figure 5-9. The overall load flow simulation is shown in Figure 5-5, which was divided into four sections (1,2,3 and 4) to clearly visualize the active/reactive power flow and voltage levels at each bus. The most important factor was to analyze the power injected into the main buses (Bus0330, Bus0300 and Bus1996) of the network from all utility sources. Figure 5-4 shows the

power flow from all three utility connections. The values of injections from each utility are of utmost importance as they will be compared with different scenarios having different network conditions (network with PVs and batteries in operation).

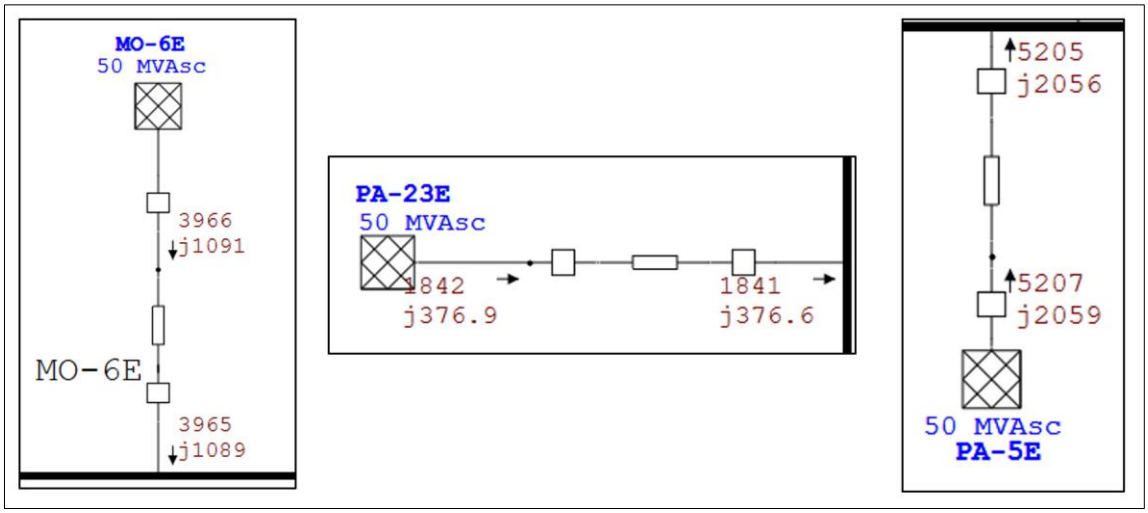

Figure 5-4 Active and reactive power injections from the utilities into the network

The injected power was consumed optimally by all the loads running at their maximum capacity. It can be observed that the majority of buses in the MG network were within their operating limits. However, the voltage at some buses was only marginally under-loaded (buses shown in pink). The range of marginal limit for the voltage levels was set as 95% - 98%. It can be seen from the LF analysis that the undervoltage buses are falling within the marginal range and system is stable. Furthermore, all the equipment was operating below their maximum ratings.

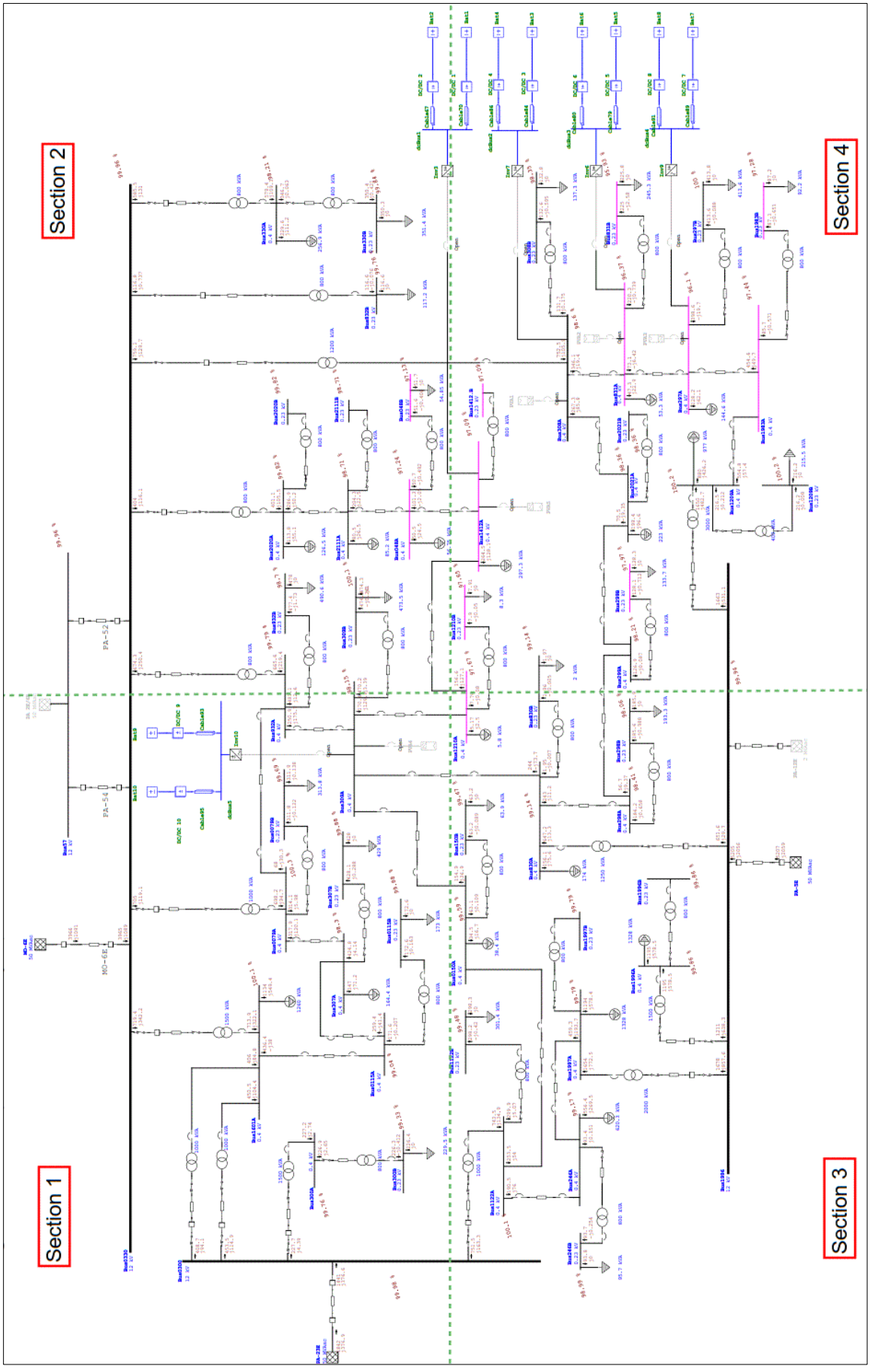

Figure 5-5 Load flow Gløshaugen (complete view)

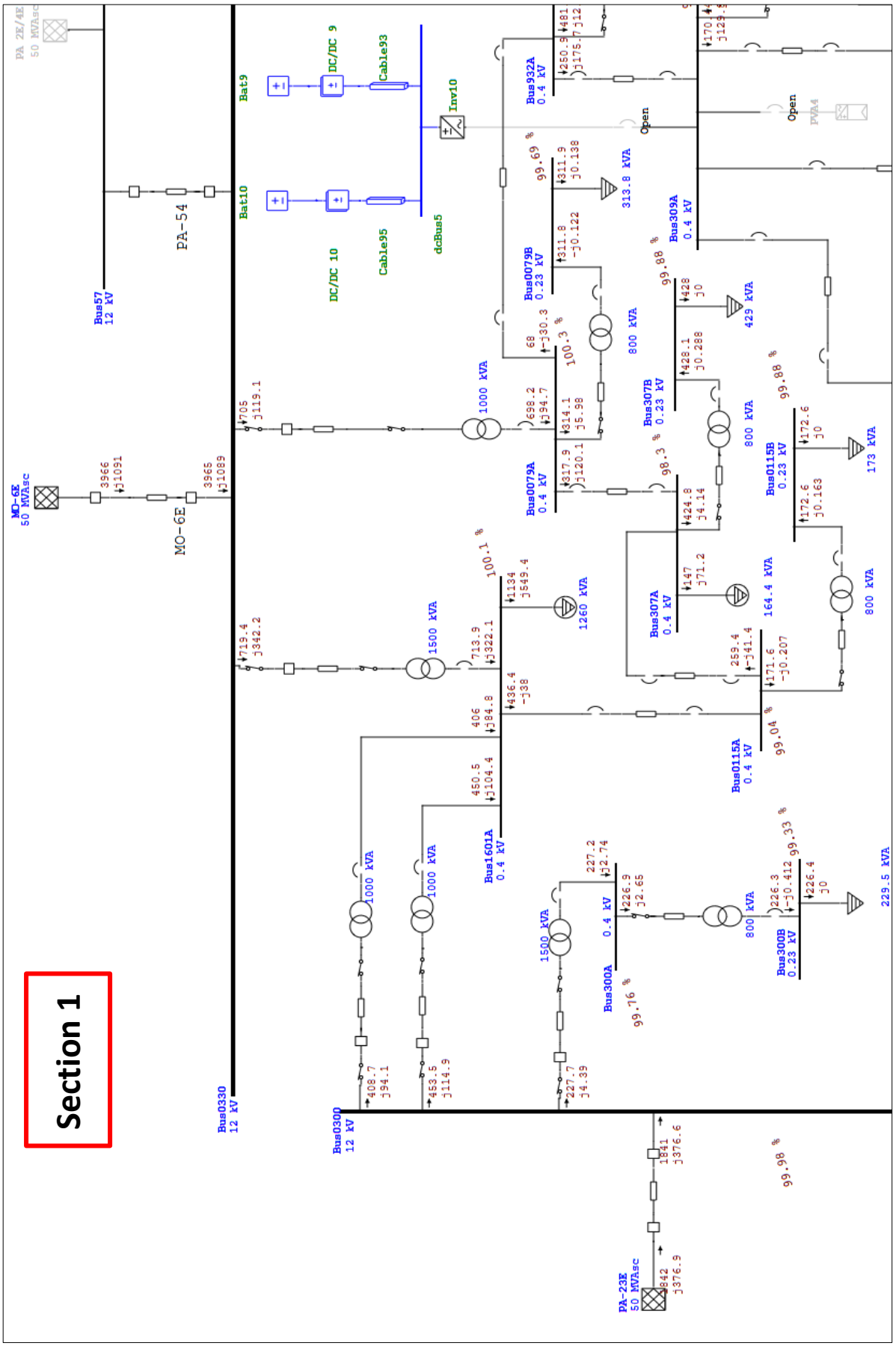

Figure 5-6 Load flow Gløshaugen (Section 1)

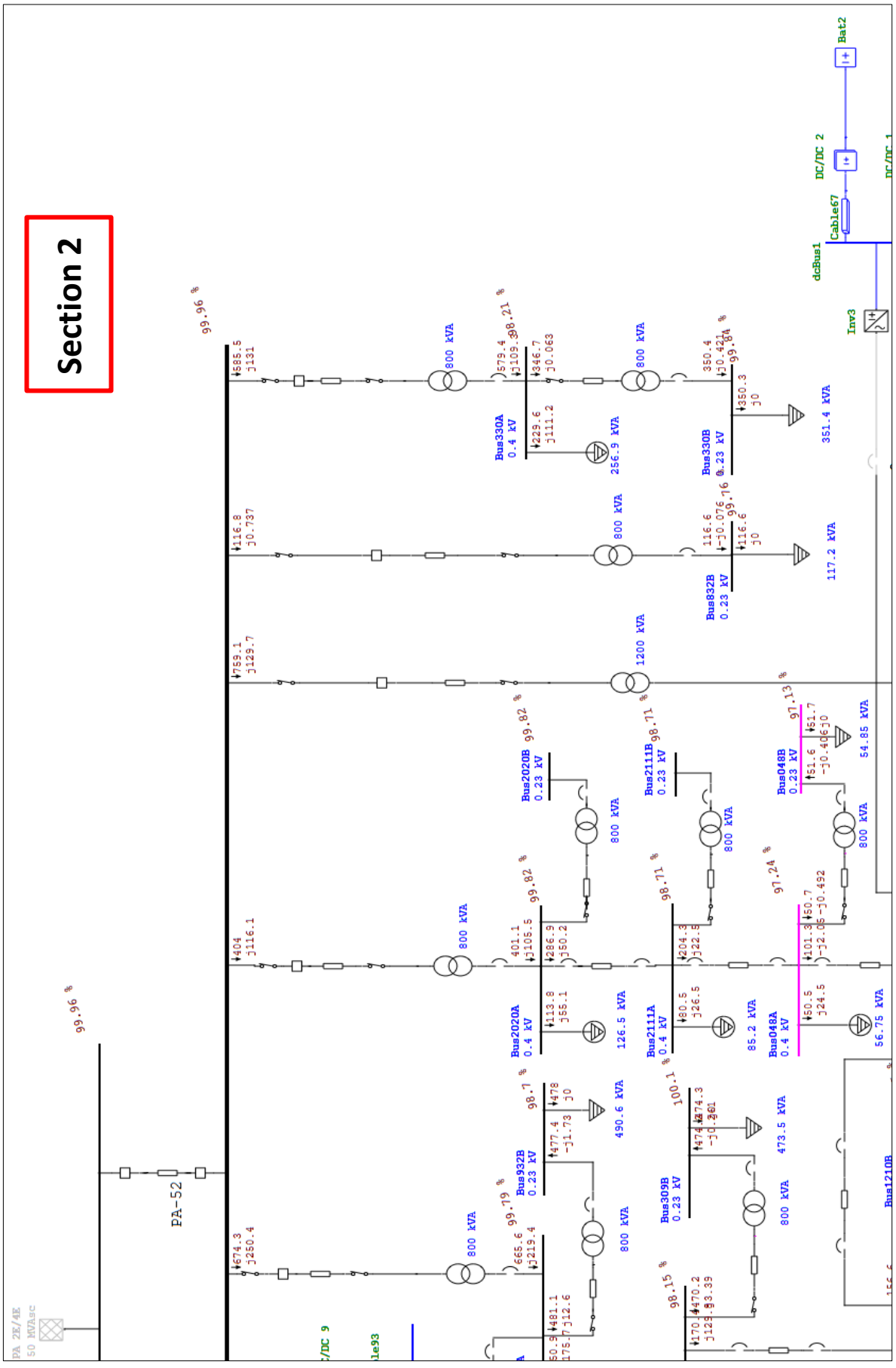

Figure 5-7 Load flow Gløshaugen (Section 2)

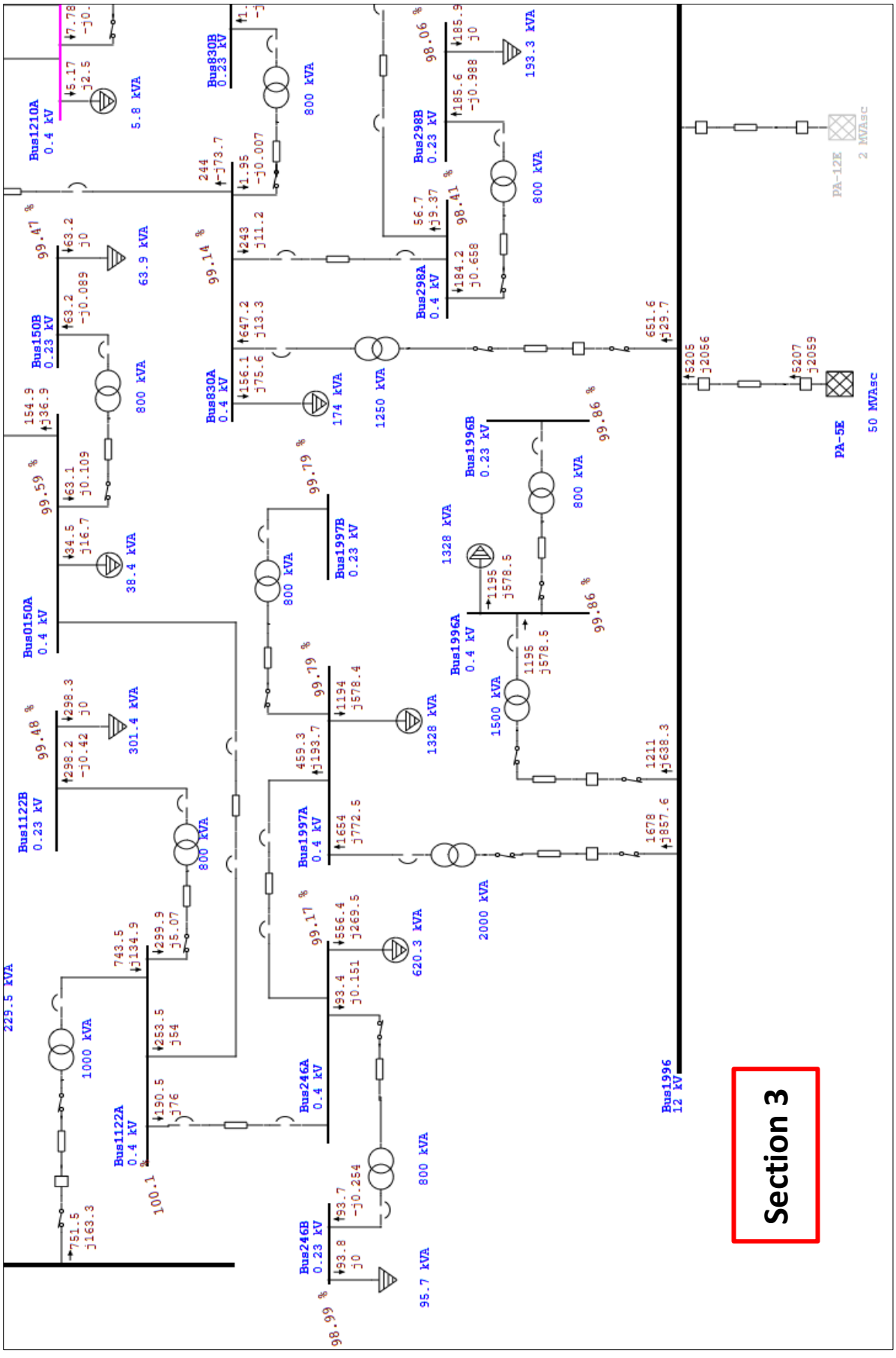

Figure 5-8 Load flow Gløshaugen (Section 3)

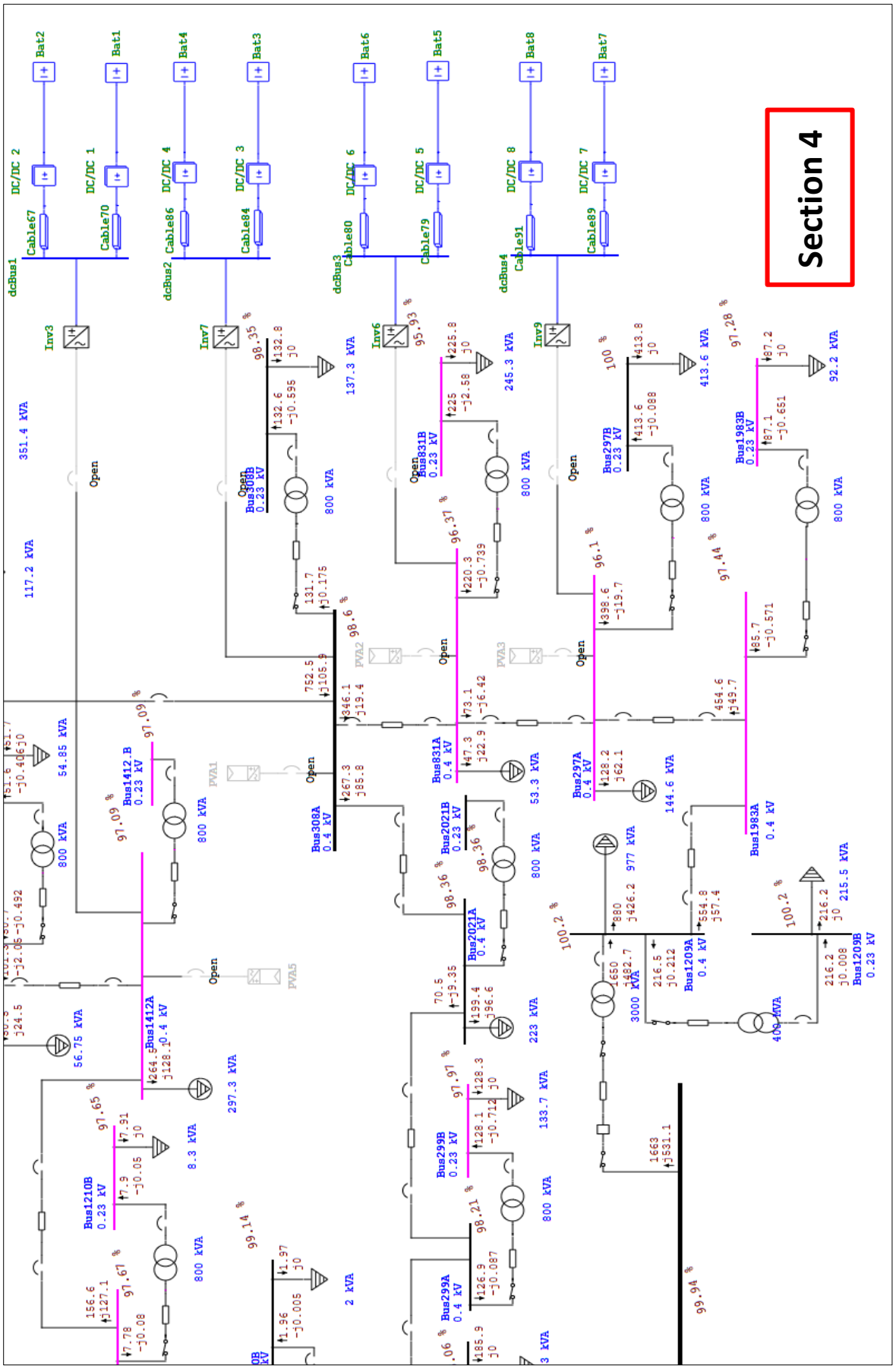

Figure 5-9 Load flow Gløshaugen (Section 4)

5.1.1.2 Time Domain AC Load Flow – Case 2 (Utility)

The second case of the analysis was carried out using the single working day load profile of the power consumption at the Gløshaugen MG. All the assumptions made in case one was also valid for this case. The study case from the scenario wizard was changed to "Time based Load Flow" for this case. The power generation and consumption in the system were analyzed at different hours, depending on the loading profile for a single day. The active and reactive power flow results for this case were graphically represented in Figure 5-10 and Figure 5-11, respectively.

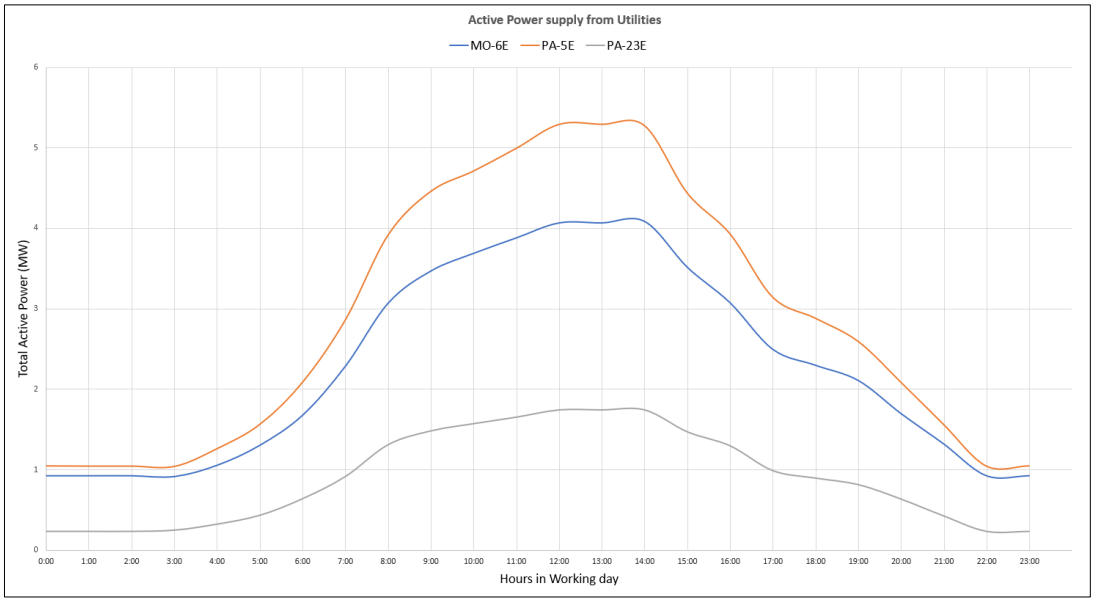

Figure 5-10 Active Power supply from utilities for 24 hours

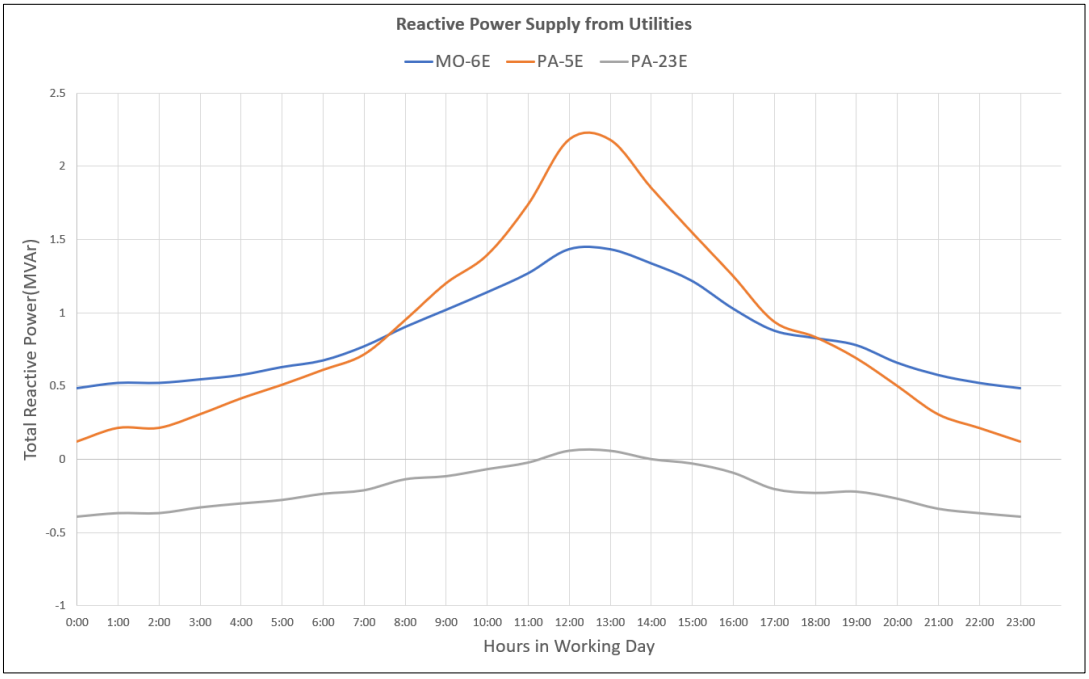

Figure 5-11 Reactive power supply from utilities for 24 hours

The maximum active power at full load during the day (from 11:00 to 14:00) for MO-6E, PA-5E and PA-23E were approximately 4050 kW, 5250 kW and 1750 kW respectively. Similarly, the reactive powers were observed as 1400 kVAr, 2150 kVAr and 50 kVAr, respectively. Table 6 shows the comparison of the resultant power supply from the grids for both the cases from scenario 1.

Table 6 Case comparison for utility power supplies

Utility	AC Load Flow – Case 1		Time-Domain AC Load Flow – Case 2	
	Active Power	**Reactive Power**	**Active Power**	**Reactive Power**
MO-6E	3965 kW	1089 kVAr	4050 kW	1400 kVAr
PA-5E	5205 kW	2059 kVAr	5250 kW	2150 kVAr
PA-23E	1841 kW	377 kVAr	1750 kW	50 kVAr
Total	***11,011 kW***	***3,525 kVAr***	***11,050 kW***	***3,600 kVAr***

It is observed from Table 6 that the sum of total active and reactive powers for the network in both cases was approximately equal during peak hours. The total active/reactive power from the utilities over 24-hours is shown in Figure 5-12. The graph from Figure 5-12 will be compared for analyzing the effect of PV and ESS integration into the network in the next sections.

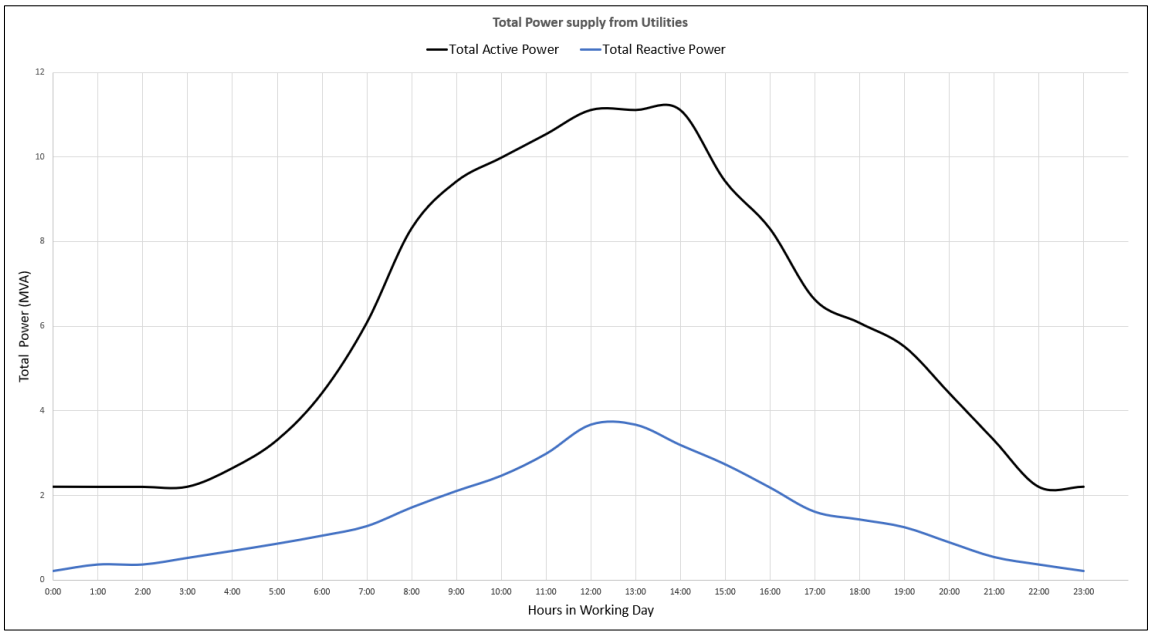

Figure 5-12 Total Active and Reactive Power from the Grids (case 2)

5.1.2 Scenario 2: System supported by utility (main grid) and PVs

In this scenario, all the loads were supplied by the utility grid and the PVs. All the assumption regarding the utility connections were the same for this scenario as well. The PVs were connected to the grid by closing their respective CBs while the CBs for batteries were kept in 'open' position (for isolation). Since the batteries were isolated from the network, the DC load flow simulation was not necessary for this scenario. Similar, to scenario 1, two cases were simulated for scenario 2. The first case was to run the instantaneous load flow of the system including the PVs, and in the second case, time-domain load flow was simulated to study the effect of adding PV to assist the utilities for power supply.

5.1.2.1 AC Instantaneous Load Flow (Utility + PVs) – Case 1

In the first case of scenario 2, the AC instantaneous load flow simulations were carried out. The results were observed for the elements that affected the network due to the integration of the PVs. These factors include power flow in the PV integrated buses, utility power injections and the buses that were marginally underloaded in scenario 1. The PV buses are shown in Figure 5-13, and the utilities are shown in Figure 5-14. The only two buses that were marginally underloaded were Bus831B (230V) and 297A (400 V) while the rest of the buses were operating under specified limits.

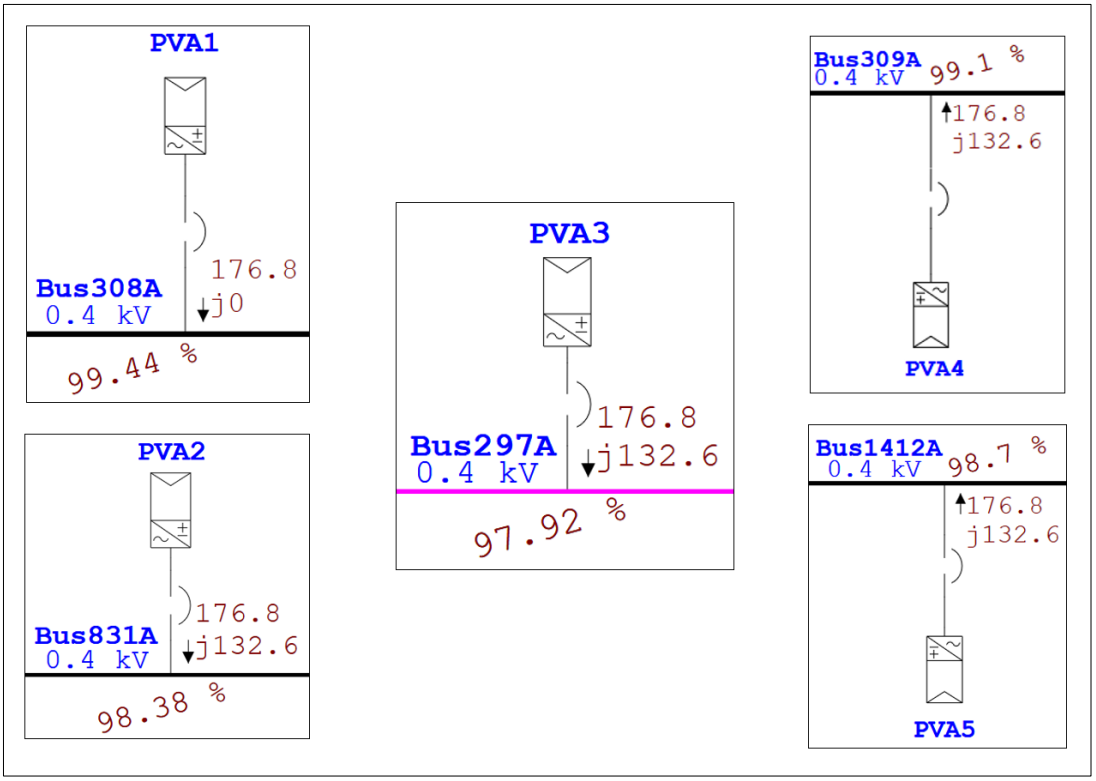

Figure 5-13 PV integrated buses (Power and voltage levels)

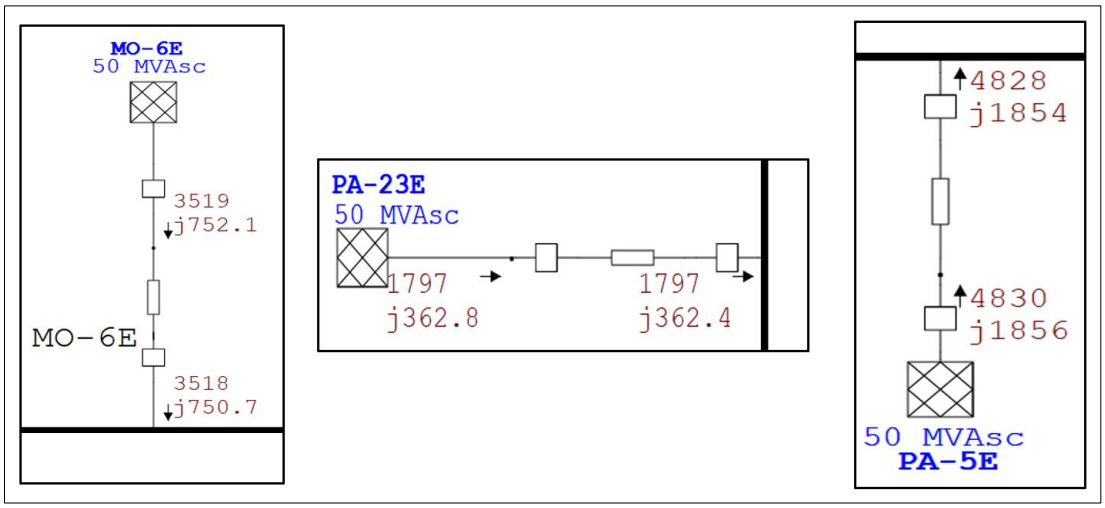

Figure 5-14 Utility injections with PVs connected

The comparison between instantaneous load from the utilities for Scenario 1 and 2 are shown in Table 7.

Table 7 Comparison of scenario 1 and 2 for instantaneous power flow

No.	Total power - Scenario 1	Total power - Scenario 2	
	Utilities	**Utilities**	**PVs**
1	3965 + j1089 kVA	3518 + j750 kVA	176.8 + j0 kVA
2	5205 + j2059 kVA	4828 + j1854 kVA	176.8 + j132.6 kVA
3	1841 + j377 kVA	1797 + j362 kVA	176.8 + j132.6 kVA
4	-	-	176.8 + j132.6 kVA
5	-	-	176.8 + j132.6 kVA
	-	***10,143 + j2,966 kVA***	***884 + j530.4***
Total	***11,011 + j3,525 kVA***	***11027 + j3497 kVA***	

5.1.2.2 Time Domain AC Load Flow – Case 2 (UTILITY + PV)

The second case of the analysis was carried out using load profile (Figure 5-1) of the power consumption at the Gløshaugen MG. All the assumptions made in case one were also valid for this case. The study case from the scenario wizard was switched to “Time based Load Flow”. The power generation and consumption in the system were analyzed at different hours, depending on the loading profile for a single day. The active and reactive power flow results

for this case were graphically represented in Figure 5-15 and Figure 5-16, respectively. The black curve represents the total power supplied from the grid before PV integration, as displayed in Figure 5-12. The yellow curve represents the total solar generation depending on the irradiance profile shown in Figure 4-18.

Consequently, the red curve shows the resultant power generation from the grid after the integration of PVs. It was observed that the power from PVs started to assist the utilities from 07:00 to 17:00. From the graph is can also be seen that the PVs were operating at their maximum capacity during the hours 10:00 - 15:00. The results can be compared with case 1 of this scenario at peak load and maximum PV generation. The resultant active/reactive power at 14:00 was found to be approximately 10.2 MW and 3.15 MVAr, respectively.

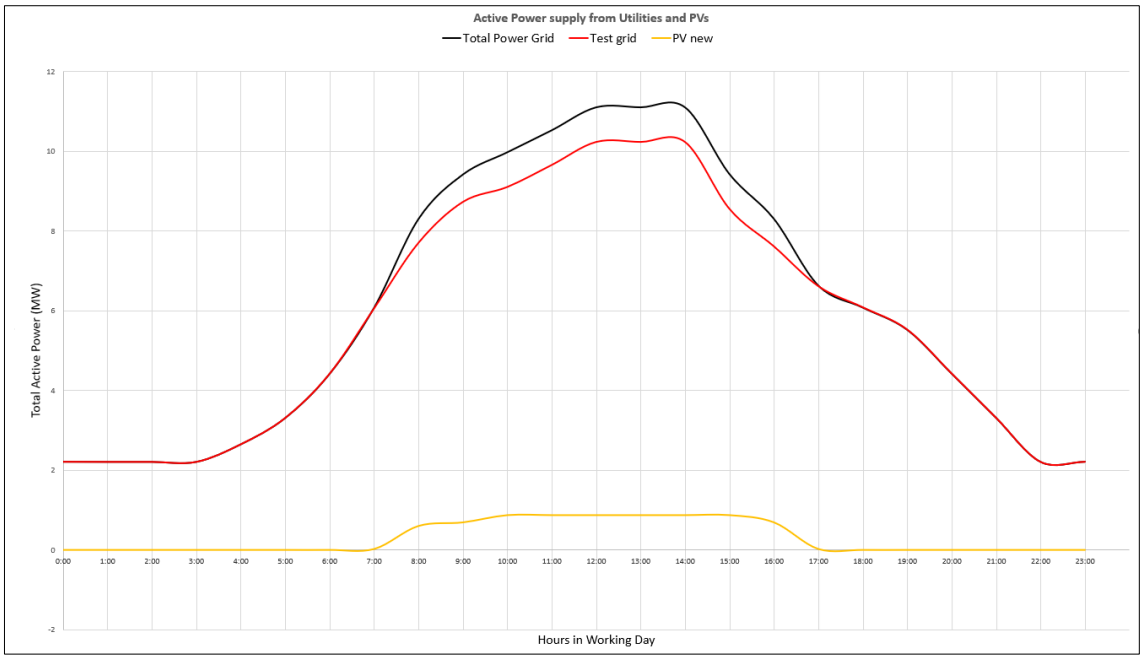

Figure 5-15 Total active power from the grids and PVs

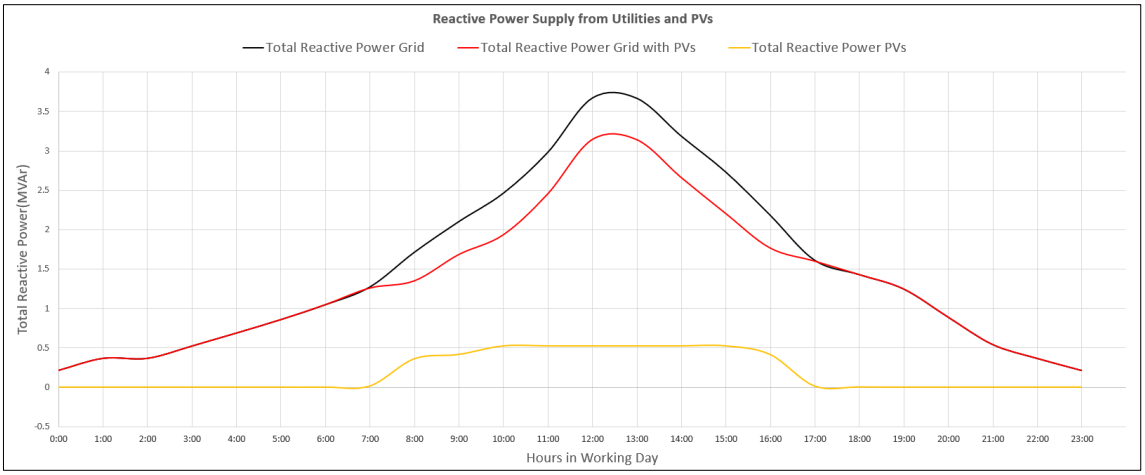

Figure 5-16 Total reactive power from the grids and PVs

5.1.3 Scenario 3: System Supported by UTILITY + PV + Batteries

Batteries were integrated into the network together with the PVs for this scenario to further assist the utilities in supplying power to the loads. Four batteries (2 sets) were kept isolated from the power grid as a backup source of power while the batteries 1 – 6 were connected by closing the CBs of the inverter 3, 6 and 7. A single battery could also be operational from one set using one inverter. This scenario will be divided into three cases. As the batteries were involved, in addition to AC instantaneous and AC time domain load flow, DC load flow was also analyzed. The complete effect of integration of PV and batteries into the network was observed on a single graph to show how the energy management system can be applied. The purpose was to perform peak shaving and flatten the supply/consumption curve.

5.1.3.1 AC Instantaneous Load Flow (Utility + PVs + Batteries) – Case1

The first case of the last scenario represented the power flow results of all the three utility connections when all three types of energy sources were supplying power to the loads. Figure 5-17 shows the power injections into the network from each utility connection. The voltages at all the buses were under operating limits, and the system was running under healthy conditions.

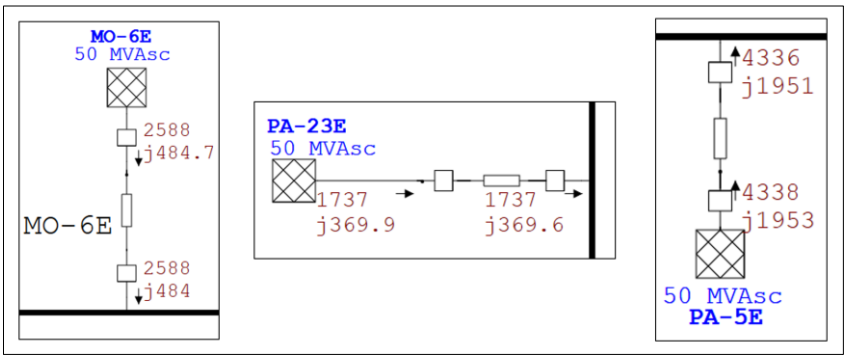

Figure 5-17 Utility injections with PV + Batteries connected

Since the active power was more in demand, the batteries were designed to supply only the active power for peak-shaving. The reactive power in this scenario remained unchanged, and only the active power from the utilities was observed. Figure 5-18 represents the active power injection (circled in red) into the bus via a set of two batteries and an inverter.

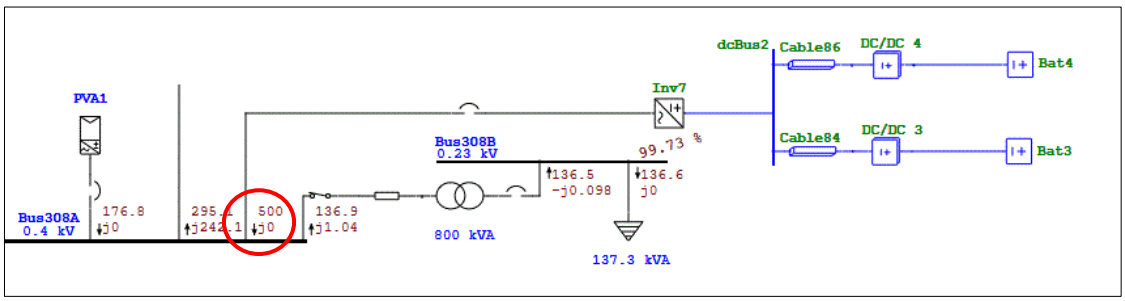

Figure 5-18 Active power injection through a set of two batteries and an inverter

5.1.3.2 DC Instantaneous Load Flow (Batteries) – Case2

The third scenario involves batteries; hence DC load flow simulations were performed in order to show the DC power flow from the batteries to the DC bus and then the inverter. Figure 5-19 represents the DC power flow in kilowatts. It can be seen that the DC bus was maintained at 600 V with the help of the DC-DC inverters and the inverter losses were approximately 14 kW due to 95% efficiency. The inverter losses added up to 26.3 kW; hence the AC power injected into the system was 500 kW. The inverter settings can be adjusted in order to get more power from the batteries at their maximum capacity, but it will result in a higher rate of discharge.

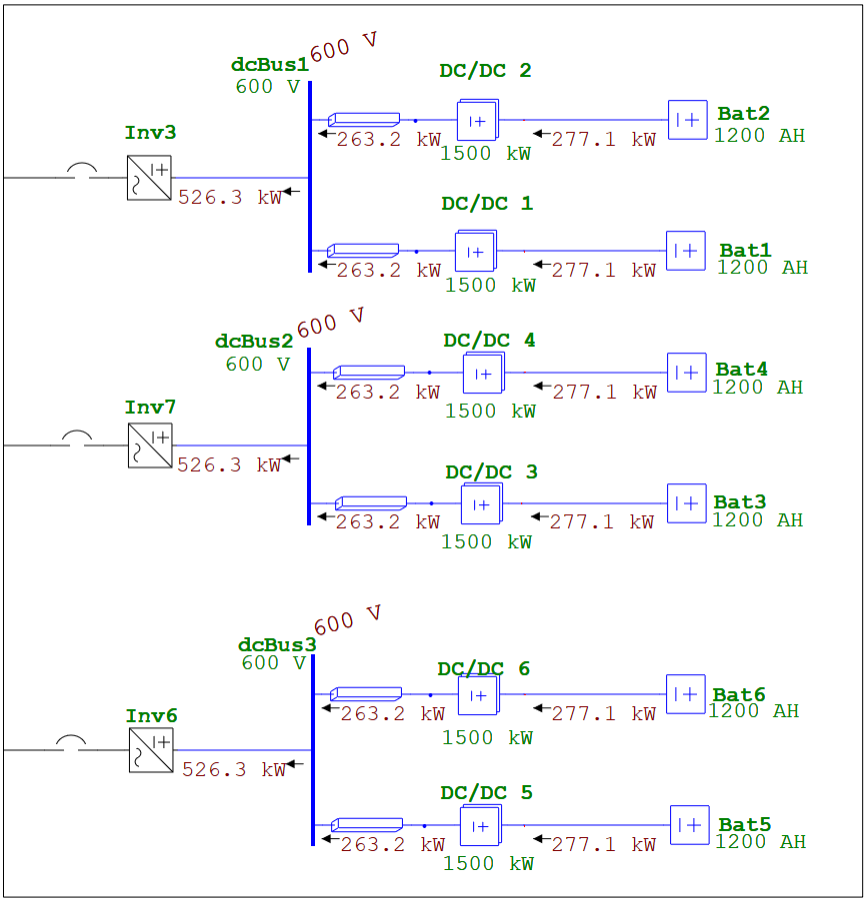

Figure 5-19 DC load flow simulations showing DC power flow from the batteries

The results of case 1 from all three scenarios for the instantaneous load flow during peak hours are compared in Table 8 below. It is clear that at peak hour, i.e. 14:00, the burden on the utility (main grid) is reduced as the power is being generated on-site with the help of PVs and batteries. The active power sum from the three utility connections was reduced by 2350 kW, while the reactive power burden released from the main grid was approximately 718 kVAr during the peak hours when the load at Gløshaugen was maximum.

Table 8 Scenario comparison of instantaneous load flows at peak hours

Scenario 1	Scenario 2		Scenario 3		
Utilities [kVA]	**Utilities [kVA]**	**PVs [kVA]**	**Utilities [kVA]**	**PVs [kVA]**	**Batteries [W]**
3,965 + j1,089	3,518 + j750	176.8 + j0	2,588 + j484	176.8 + j0	500
5,205 + j2,059	4,828 + j1,854	176.8 + j132.6	4,336 + j1,953	176.8 + j132.6	500
1,841 + j377	1,797 + j362	176.8 + j132.6	1,737 + j370	176.8 + j132.6	500
-	-	176.8 + j132.6	-	176.8 + j132.6	-
-	-	176.8 + j132.6	-	176.8 + j132.6	-
11,011 + j3,525	***10,143 + j2,966***	***884 + j530.4***	***8,661 + j2,807***	***884 + j530.4***	***1,500***
11,011 + j3,525 kVA	***11,027 + j3,497 kVA***		***11,045 + j 3,337 kVA***		

5.1.3.3 Time Domain Load Flow – Case 3 (Utility + PV + Batteries)

Case 3 of scenario 3 was similar to the second case of scenario 2, except the batteries in case 3 was also in operation. Time-based load flow simulations were performed to analyze the effect of PVs and battery integration over a period of 24 hours. The load profile and the PV irradiance were kept the same as in the previous section, while the batteries were switched 'ON', one at a time in order to obtain a smooth flat curve for peak-shaving. Since the batteries only assisted the utility with the active power, the reactive power was not affected in this scenario. Figure 5-20 shows the graphical representation of the active power result plots for all the sources in the network. The green curve shows the active power generation from the batteries, and the red curve represents the resultant active power from the grid after the PVs and the batteries were integrated into the network. The sequence of turning the batteries 'ON' at different hours is given in Table 9

Table 9 Battery operation with respect to hours of the day

Hour	Power Supplied by Batteries	No. of Batteries 'ON'
09:00	0.25 kW	1 Battery
10:00	0.5 kW	2 Batteries
11:00	1 kW	4 Batteries
12:00	1.5 kW	6 Batteries
13:00	1.5 kW	6 Batteries
14:00	1.5 kW	6 Batteries
15:00	0.25 kW	1 Battery

This pattern of switching batteries provided a smooth and flat "resultant power from the utility" curve from 09:00 – 15:00 hr. The curve was maintained approximately around 8.6 MW throughout these hours.

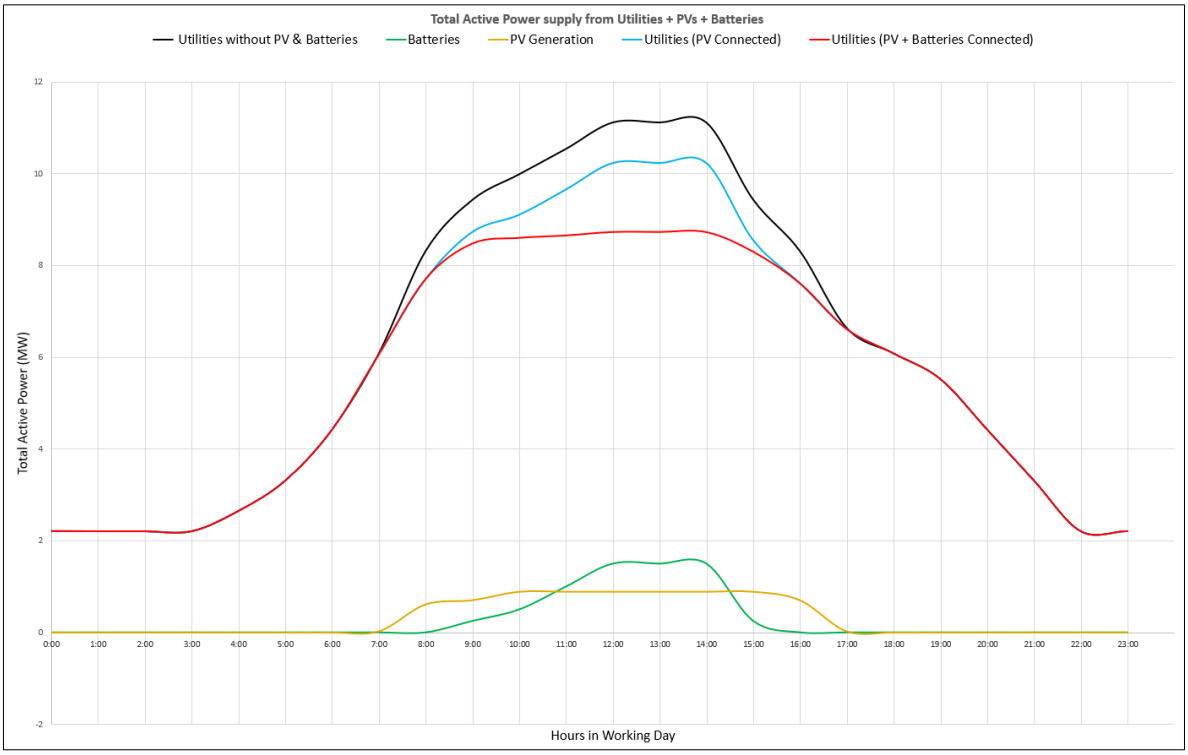

Figure 5-20 Resultant power from the utilities before and after the integration of PV and batteries

5.2 Transient Stability Analysis

In this section, the stability of the system was analysed under different conditions. The complexity of the system would result in various numbers of studies regarding the stability of the model. Therefore, two of the most common stability study scenarios were performed, namely:

1. Load Step Change (Load Impact)
2. Fault Analysis at a Bus

For performing adequate stability study, a weaker grid was selected by changing its short circuit ratings in both the scenarios. To observe significant results, the grid connection MO-6E was isolated from the system by opening the main 12 kV circuit breaker. A synchronous diesel generator was integrated into the system as a replacement of the grid at 'Bus0330'. The purpose of adding the generator to the model was to observe the transient stability of the system due to mechanical rotating mass. The generator was chosen nearly similar to the MO-6E utility grid (5 MVA with 92% P.F), with the specifications mentioned in section 4.2.2.

5.2.1 Load Step Change

The short circuit ratings for the utility grid PA-23E and PA-5E were specified as 2 MVAsc to analyse the behaviour of the system with a relatively unhealthier grid. The simulations were carried out with all the PVs and batteries connected to the system, and all the equipment operating at their maximum capacity (kl 12:00).

The load change was carried out at two different time instants while the voltage and frequency at Bus0330 were observed. For this purpose, two events at 4.00 and 20.00 seconds with different load variations were created. In this case, the stability results were analysed with and without the generator control (Exciter, governor and PSS). Similarly, the total simulation time was set as 50 seconds, and the load disturbance was applied on four random loads, as shown in Table 10.

Table 10 Events created for load variation

Event ID	Time	Device Type	Device ID	Action
1	4.00	Lumped Load	Lump 1	Load Impact +20%
		Lumped Load	Lump 2	Load Impact +10%
		Lumped Load	Lump 3	Load Impact +10%
		Lumped Load	Lump 12	Load Impact +10%
2	20.00	Lumped Load	Lump 12	Load Impact –20%

5.2.1.1 Bus Voltage and Frequency without Generator Control

This subsection presents the graphical results of the bus voltage and frequency without the generator control.

1. **Bus 0300 Voltage**

It can be observed from Figure 5-21, that due to the load change (increase) at 4.0s, the bus voltage drops significantly and the generator was unable to recover the voltage within the stable operating limits. At 20.00s, it can be seen that the bus voltage was slightly increased when the lump12 was reduced by 20%. Finally, the bus voltage gets a new steady-state value with an unreasonable margin of 2kV.

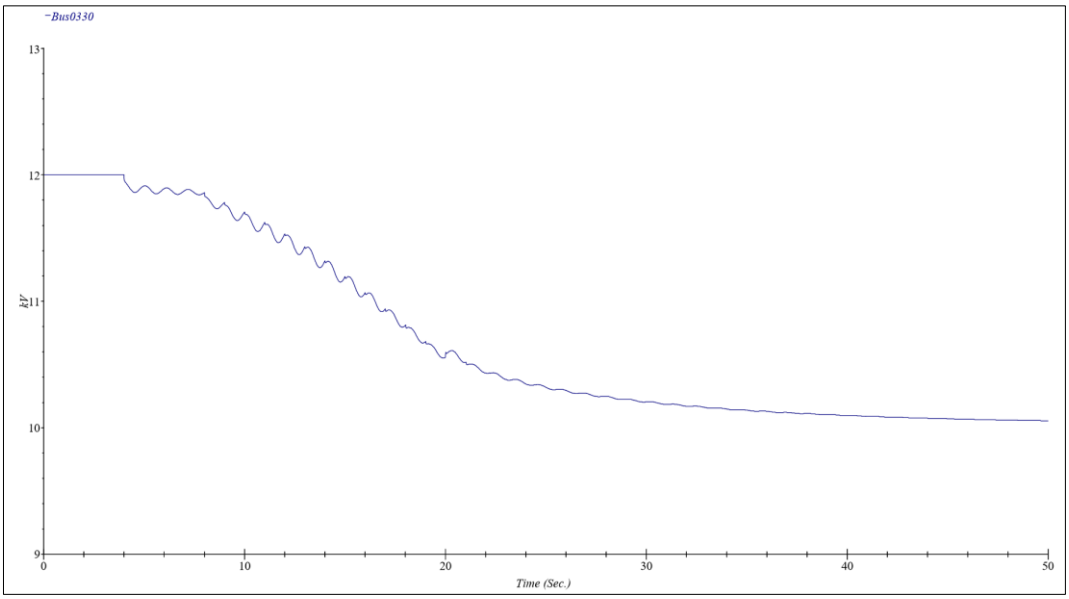

Figure 5-21 Bus voltage variation at Bus0330 without generator control

2. Bus 0300 Frequency

There was no significant impact on the bus frequency by the load variation as the magnitude of the disturbance was comparatively low with respect to the size of the whole Gløshaugen campus network. The frequency was observed to be the same with and without the implementation of generator controls. Figure 5-22 represents the frequency of the Bus0330 without implying generator controls. A straight line without any disturbance at 4.00 and 20.00 seconds was observed. The frequency was maintained at 100% (50Hz) throughout 50 seconds of simulation time.

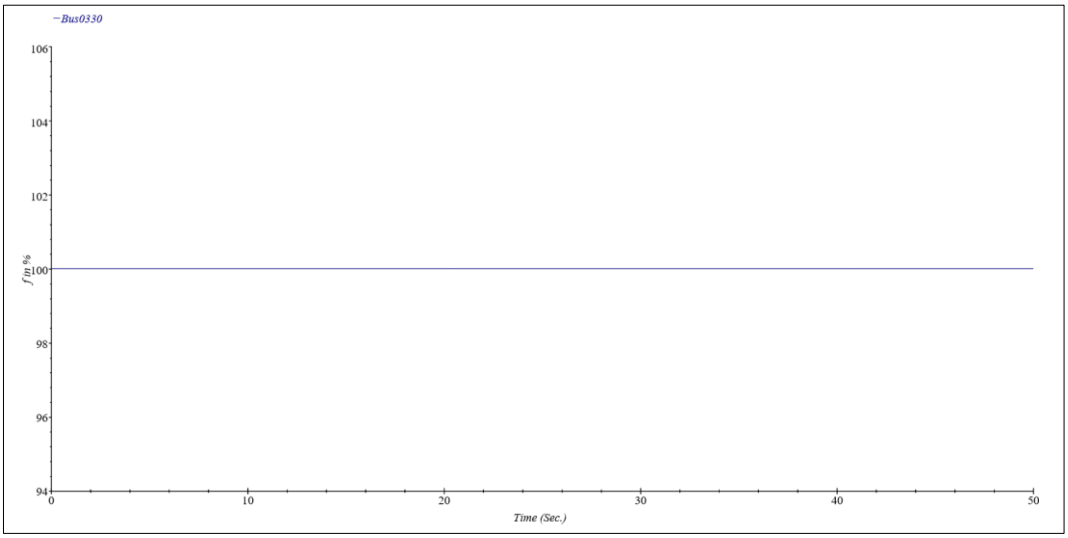

Figure 5-22 Frequency of Bus0330 without generator control

5.2.1.2 Bus Voltage and Frequency with Generator Control

After adding the generator control using an exciter AVR model, a significant improvement was observed in the bus voltage. In Figure 5-23, it can be seen that after the load disturbances, at 4.0s and 20.00s, the bus voltage gets back to the nominal steady-state value. The voltage response was improved by adding generator control and the voltage dip and rise was well within the defined acceptable operating limits.

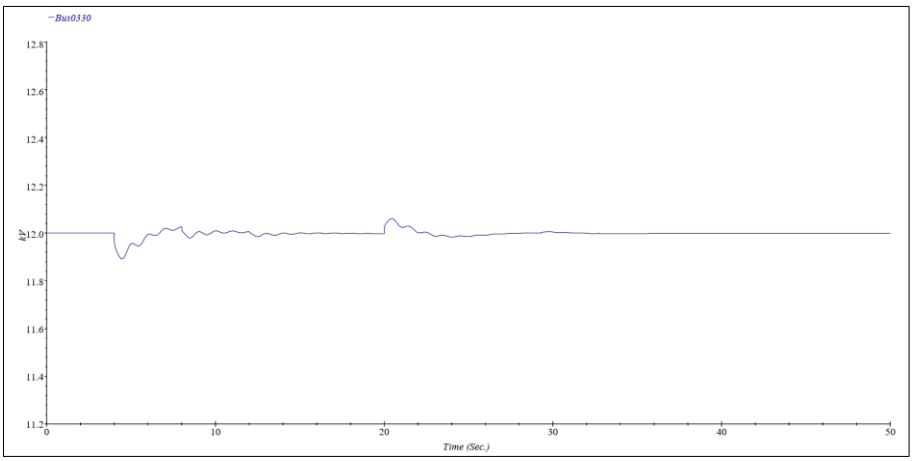

Figure 5-23 Bus voltage at Bus0330 with generator control

As shown in the figure, a small voltage dip occurred at 4.0s because of the load increment. The voltage was stabilized, reaching the steady-state value at approximately 15 – 18 seconds. Similarly, at 20.00 s, the voltage rises slightly before getting back to steady-state at 38 seconds. The supervisory control for the whole system decides, based on the protection schemes, whether to limit the output power from the generator or send a trip signal to the generator.

5.2.2 Transient Stability at Fault Condition

To perform transient stability analysis, a large disturbance was initiated at the centre of the system in the form of a 3-phase fault. Bus308A of 400 V was chosen for testing as it had both PVs and batteries connected to it. The objective of this scenario was to analyze the main bus330A and the generator during pre and post fault conditions. As this scenario dealt with large disturbance, the behaviour of the generator was also considered by analysing some of the important factors. Similar to the first study scenario, the simulation results for the fault conditions were also divided by considering two different conditions, i.e. with and without the generator control. The short circuit capability of PA-5E and PA-23E was reduced further to 0.5 MVAsc, to observe the effect significantly. The factors that were studied for this scenario for both the bus and the generator are given as follows:

A) Bus0330
    1. Bus Voltage Angle

2. Bus Voltage
3. Bus Frequency

B) Generator 1

1. Absolute Power Angle
2. Reactive Power from the Generator
3. Electrical Power from the Generator
4. Generator Terminal Current

Two events were created for this scenario. A 3-phase fault was initiated at Bus308A at 4.00 seconds and was cleared at 4.10 seconds, having a total fault time of 0.1 sec.

5.2.2.1 Bus and Generator Analysis without Generator Control

All simulations in the following subsections were carried out in the similar sequence, as in the above sub-section. So, the variation at Bus0330 was analysed, followed by the generator behaviour.

A) Bus 0330 Analysis

In addition to the bus voltage and frequency, the voltage angle was also studied for this analysis as it is important for stability analysis due to large disturbances.

1. Bus 0330 Voltage

The bus voltage was plotted over a simulation time of 50 seconds. Figure 5-24 illustrates the effect of short circuit fault on the main 12 kV bus voltage. It is evident that the voltage was highly unstable post fault clearance.

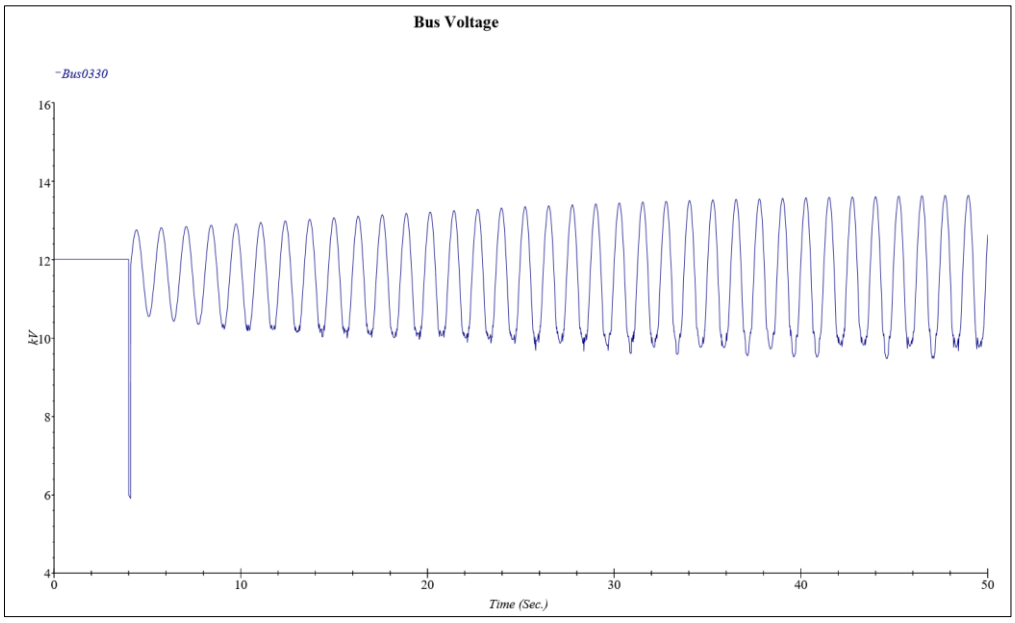

Figure 5-24 Bus voltage fluctuations without generator control

A severe voltage drop from 12 kV to 6 kV can be observed exactly at the time of fault (4.00 seconds). After the fault clearance, the voltage tends to rise back to the nominal ratings, but the uncontrolled synchronism of the generator with the system did not allow the bus voltage to adjust at a certain level. The voltage started to oscillate, and the magnitude of the oscillations was seen to be increasing with time. As a result, the generator protection scheme will trip the generator to avoid any damages to the equipment.

2. Bus 0330 Frequency

The frequency of the bus was disturbed at the instant of the fault and kept oscillating even after the fault was recovered. Figure 5-25 illustrates the fluctuations in the frequency of the bus after the occurrence of the fault.

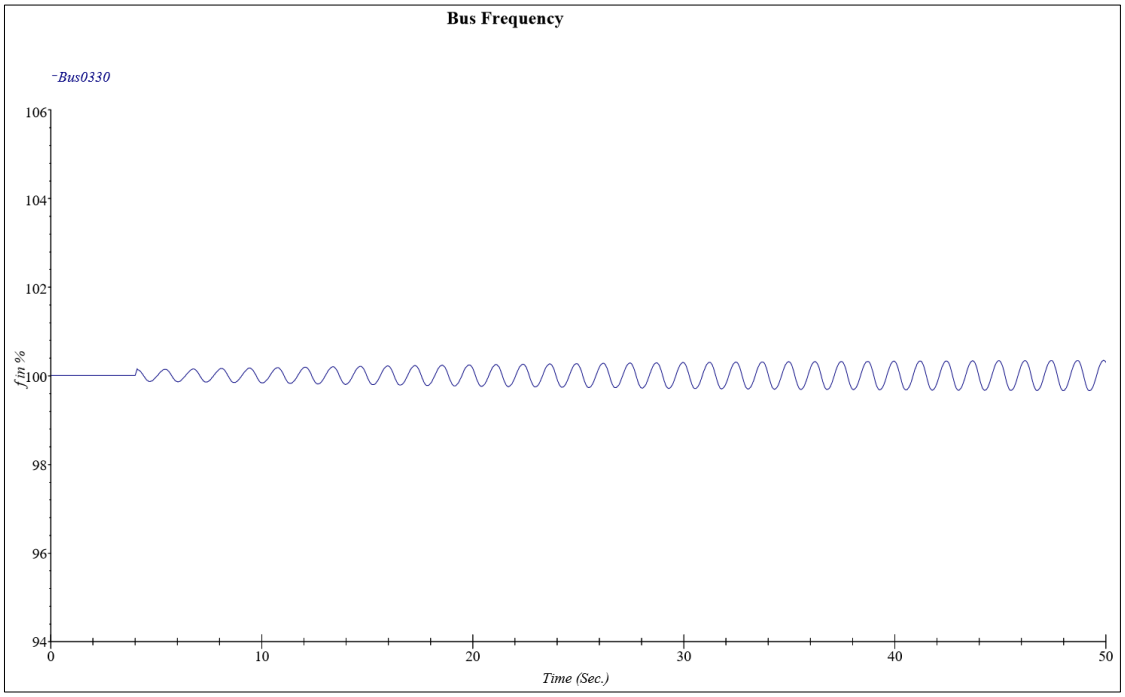

Figure 5-25 Bus frequency fluctuations after fault without generator control

The bus frequency depends highly on the generator speed. The results for the generator speed showed a similar pattern as the frequency after the fault. The amplitude of the fluctuations can be seen increasing over the period, which showed high instability in the frequency without the generator control.

3. Bus Voltage Angle

Figure 5-26 illustrates how the amplitude of oscillations kept increasing with time due to instability. The initial bus voltage angle prior to the fault was at - 40 degrees. The generator control was not implemented; hence the voltage angle could not settle at a fixed value through damping.

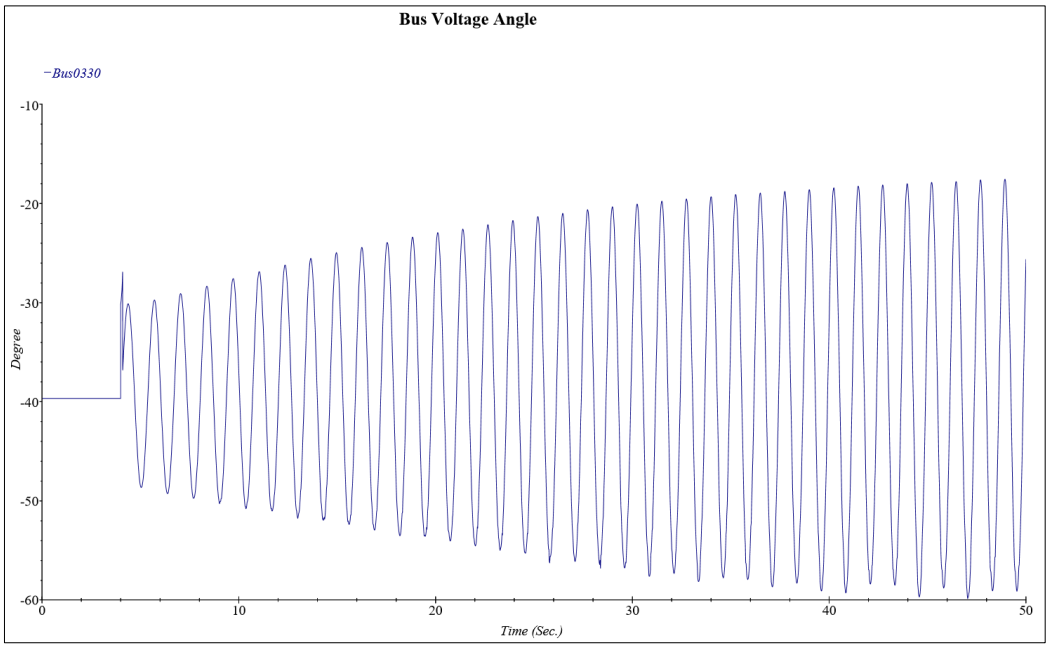

Figure 5-26 Bus voltage angle after fault given no generator control

B) Generator 1 Analysis

The power angle, reactive power, electrical power and short circuit response was observed and discussed in this subsection.

1. Generator Absolute Power Angle

Similar to the voltage angle, the generator absolute power angle shown in Figure 5-27, starts oscillating after the fault occurrence, which was set around 5 degrees prior to the fault.

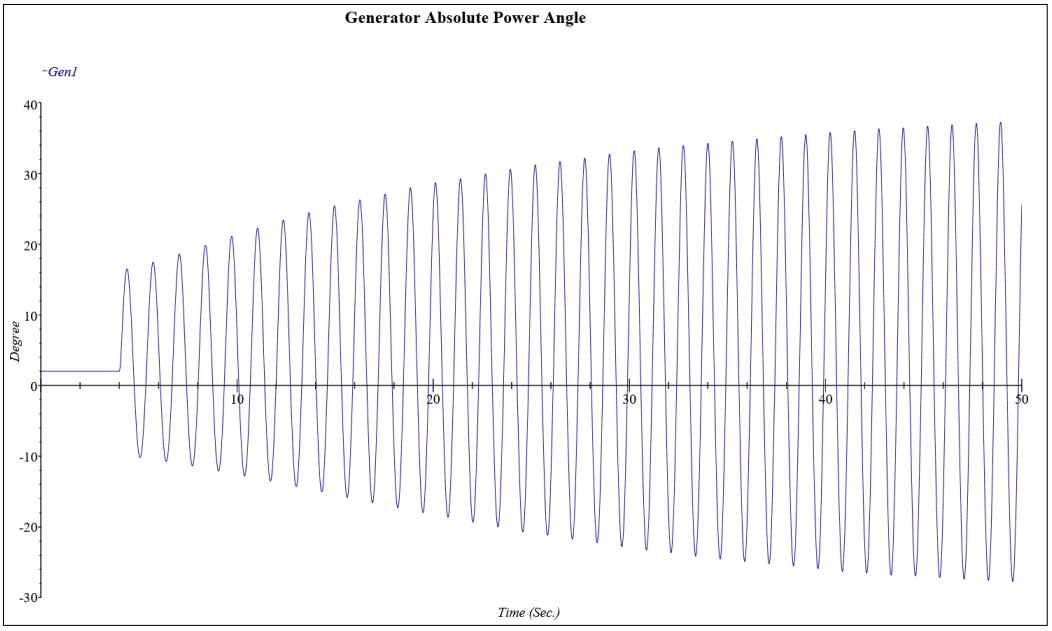

Figure 5-27 Generator absolute power angle without generator control

2. Generator Reactive Power

In addition to the power angle, the electrical and reactive power of the generator as shown in Figure 5-28 and Figure 5-29 also starts increasing unstably with large oscillation after the fault occurrence, which is due to an uncontrolled generator.

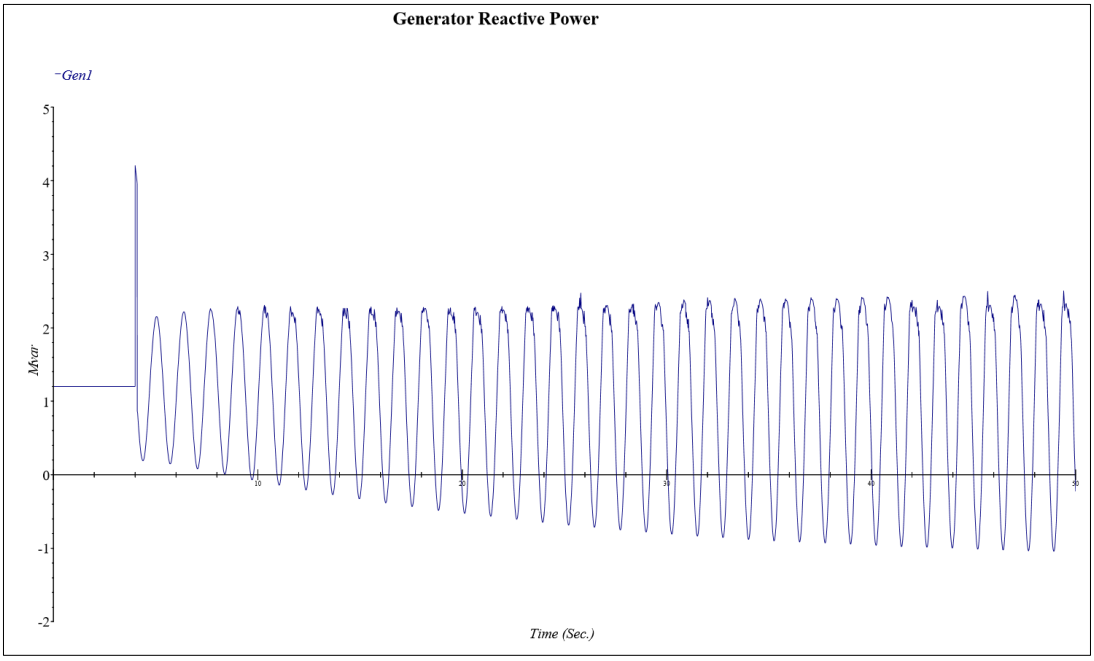

Figure 5-28 Generator's reactive power generation without control

3. Generator Electrical Power

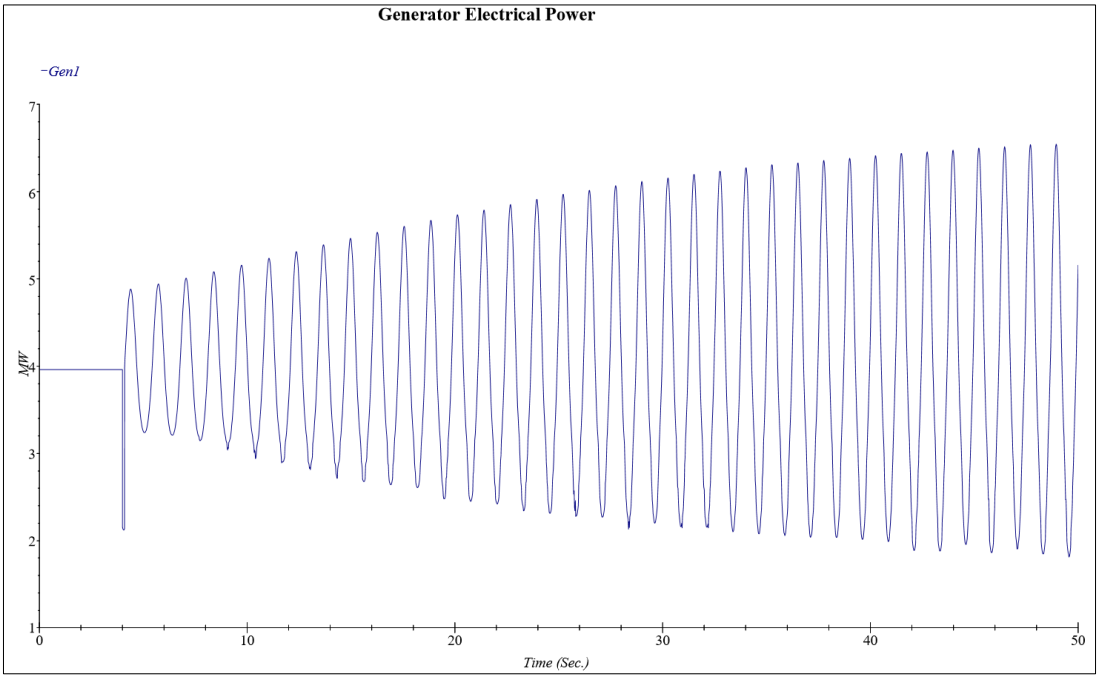

Figure 5-29 Generator's electrical power output without control

4. Generator Terminal Current

The generator terminal current is one of the crucial parameters to analyse since it provides the information regarding the total short circuit contribution of the generator after the occurrence of a three-phase fault. The short circuit contribution from the generator, in this case, is around 450 amperes at the instant of fault (4.0 seconds). Figure 5-30 represents the generator terminal current before adding controls to the generator.

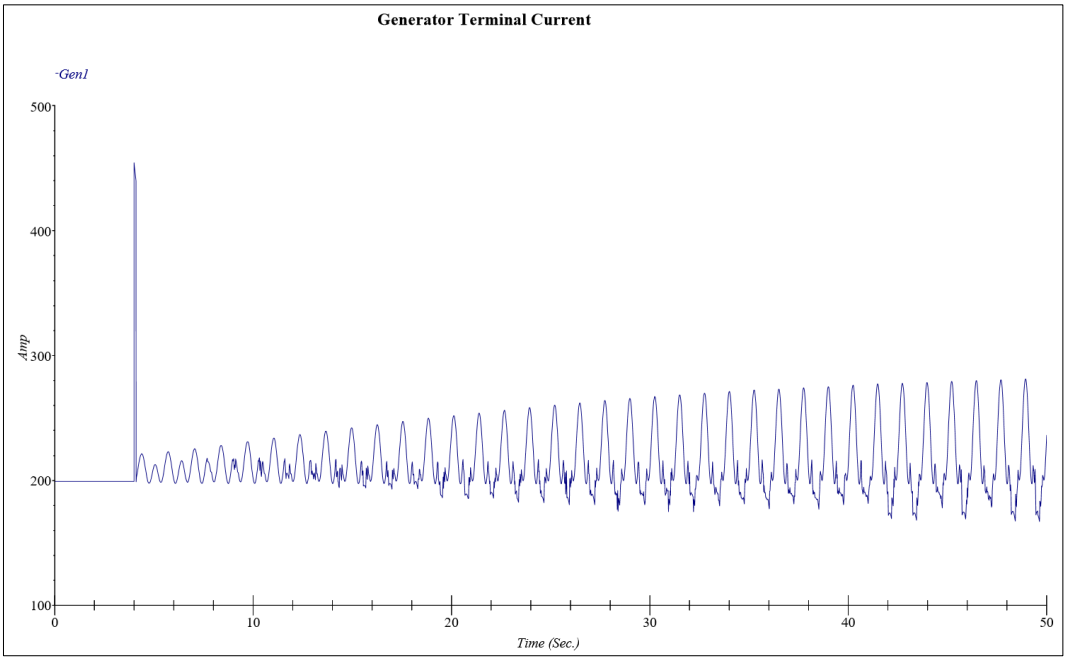

Figure 5-30 Generator terminal current without control

5.2.2.2 Bus and Generator Analysis with Generator Control

The simulation results discussed in this section is carried out in the same sequence as in section 5.2.2.1.

A) Bus 0330 Analysis

The bus voltage, frequency and voltage angle for this case was analysed as it was done for the previous section.

1. Bus 0330 Voltage

After introducing the exciter AVR control, it was observed in Figure 5-31, that the voltage at bus330 rises and take few oscillations after the fault clearance. Consequently, the voltage stabilizes at the nominal steady-state value within 10 seconds after the fault. The stability in voltage occurred due to the implemented generator exciter control.

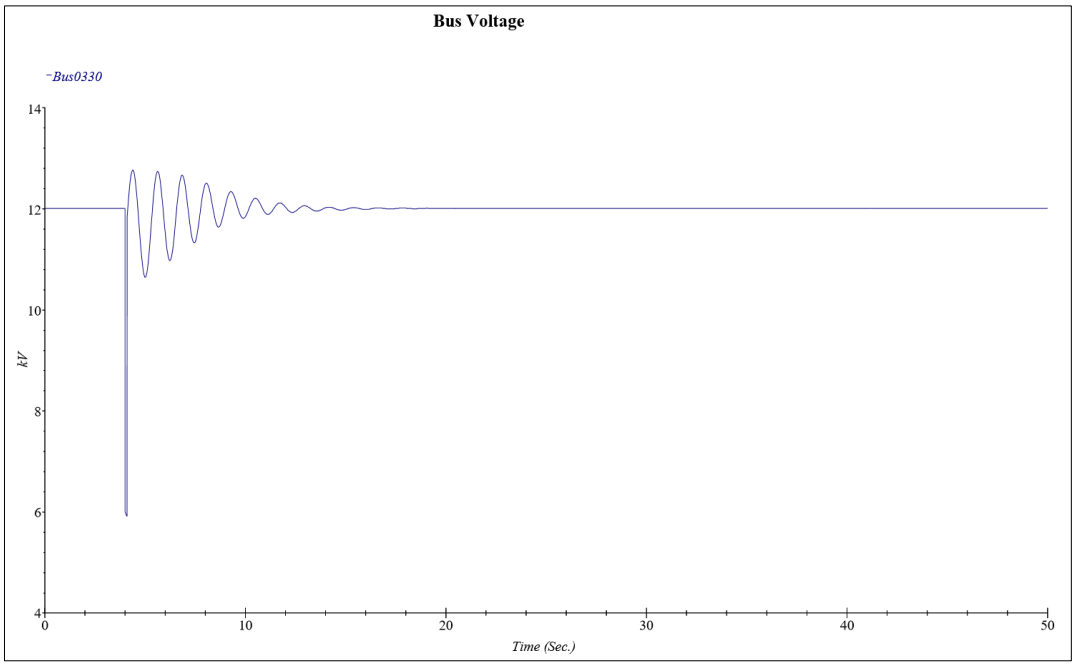

Figure 5-31 Bus voltage after addition of generator control

2. Bus 0330 Frequency

It was observed from Figure 5-32, that the frequency of the bus330 was slightly disturbed at the fault instant and set back to 50Hz, which proves the stability of the system after the fault clearance. As mentioned earlier, the bus frequency depends on the generator speed, which starts to accelerate and results in some speed oscillations after the faulted bus is recovered.

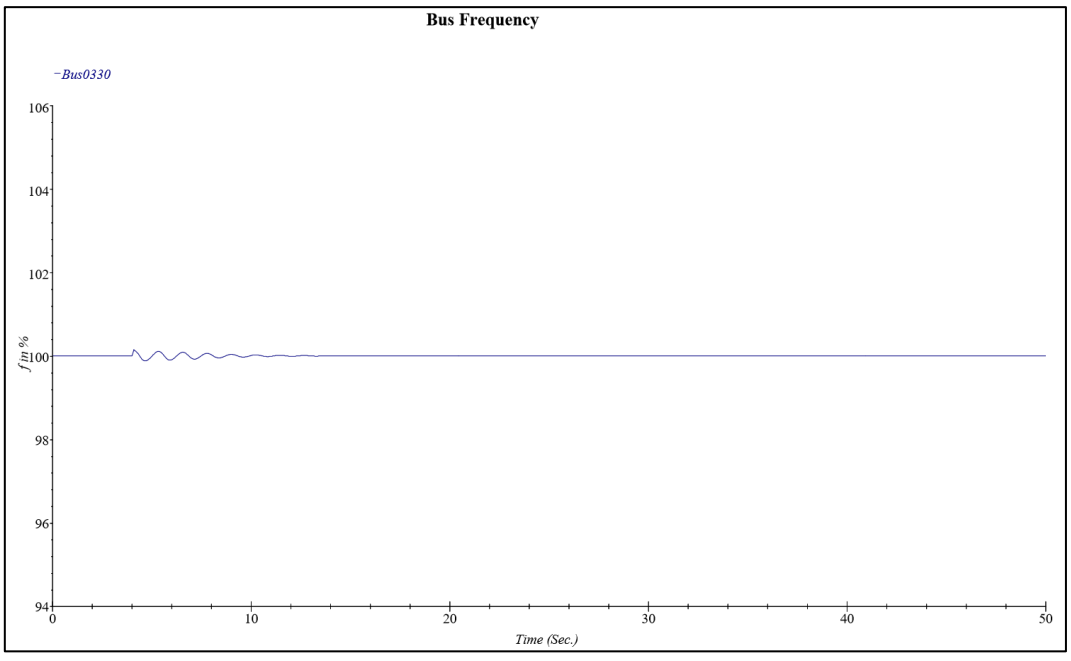

Figure 5-32 Bus frequency after adding generator control

3. Bus 0330 Voltage Angle

The voltage angle of the bus330, as shown in Figure 5-33, gets a steady-state value of 40 degrees after some oscillation, which also indicates that stability of the system after a fault disturbance.

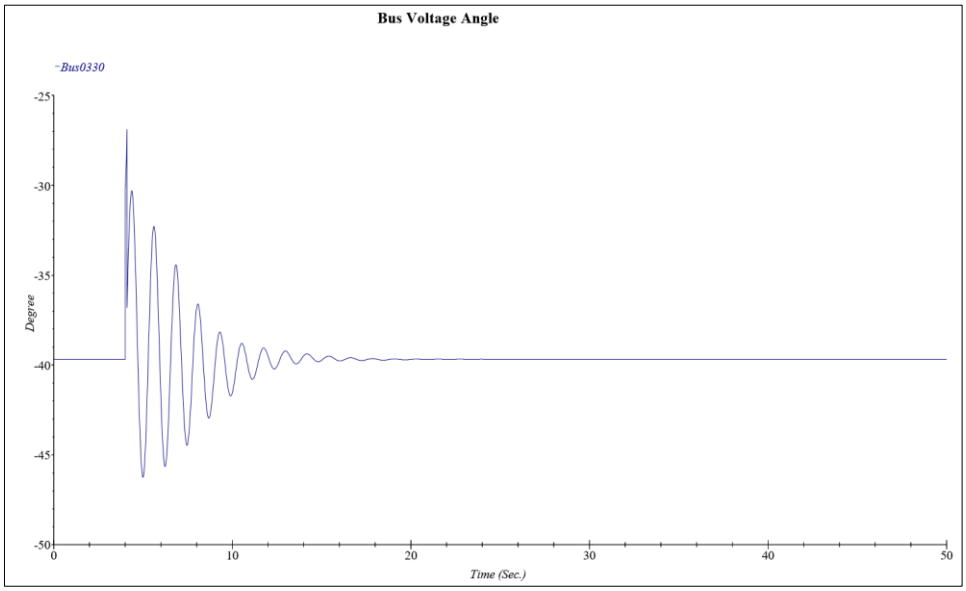

Figure 5-33 Bus voltage angle after generator control

B) Generator Fault Analysis

As in the previous section, the power angle, reactive power, electrical power and short circuit response was observed and discussed for this subsection.

1. Generator Absolute Power Angle

The generator absolute power angle given in Figure 5-34, stabilizes at 5 degrees after the fault is cleared.

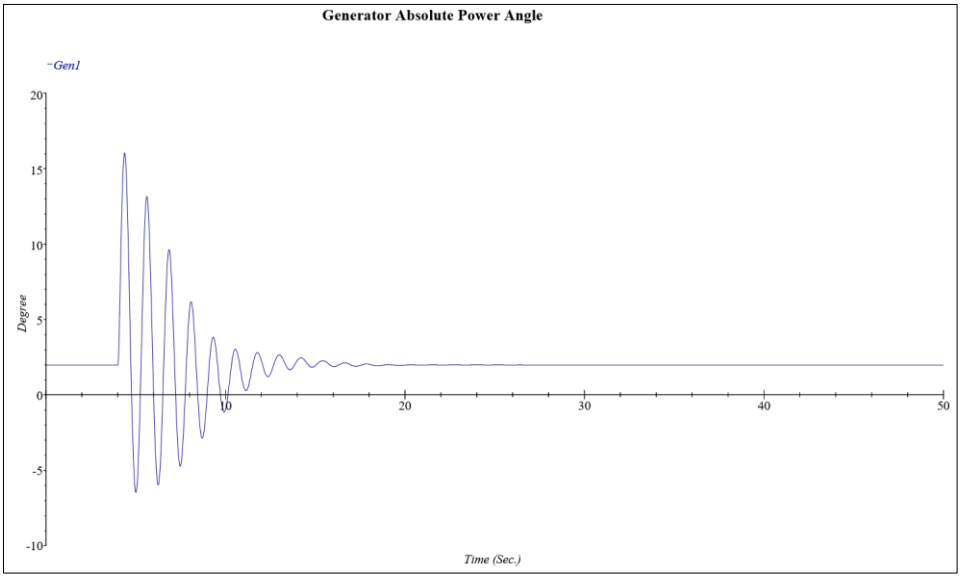

Figure 5-34 Generator Absolute power angle showing stability after applying controls

2. Generator Reactive Power

The reactive and electrical power of the generator can be observed in Figure 5-35 and Figure 5-36, respectively. The power delivered by the generator after the fault was nearly equivalent to the pre-fault value. From the figures, it was observed that the reactive power of the generator was approximately 1.2 MVAr and electrical power was 4 MW as per the consumption requirement.

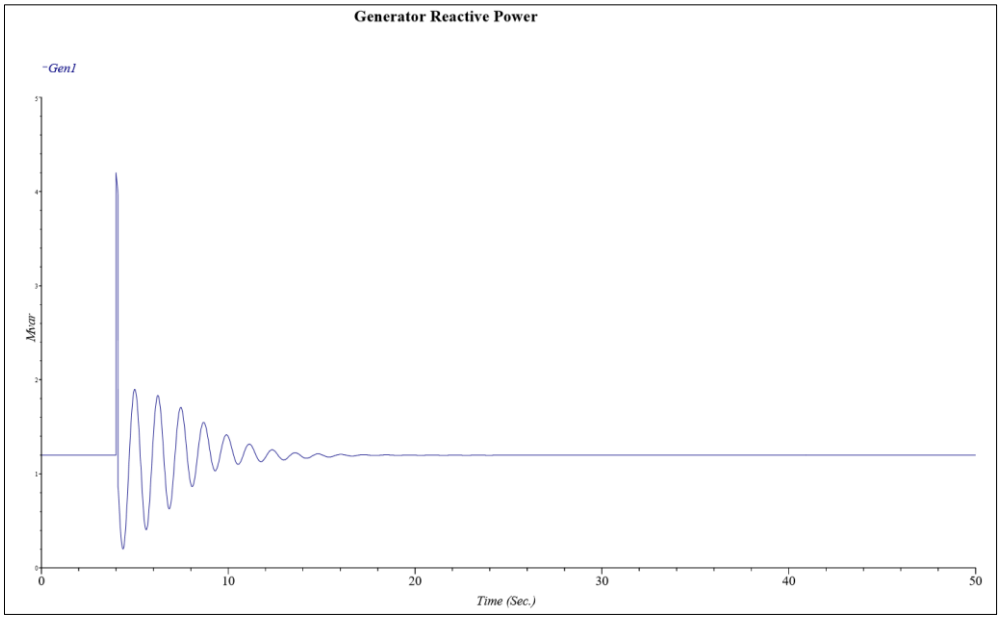

Figure 5-35 Generator reactive power output stabilized after adding control

3. Generator Electrical Power

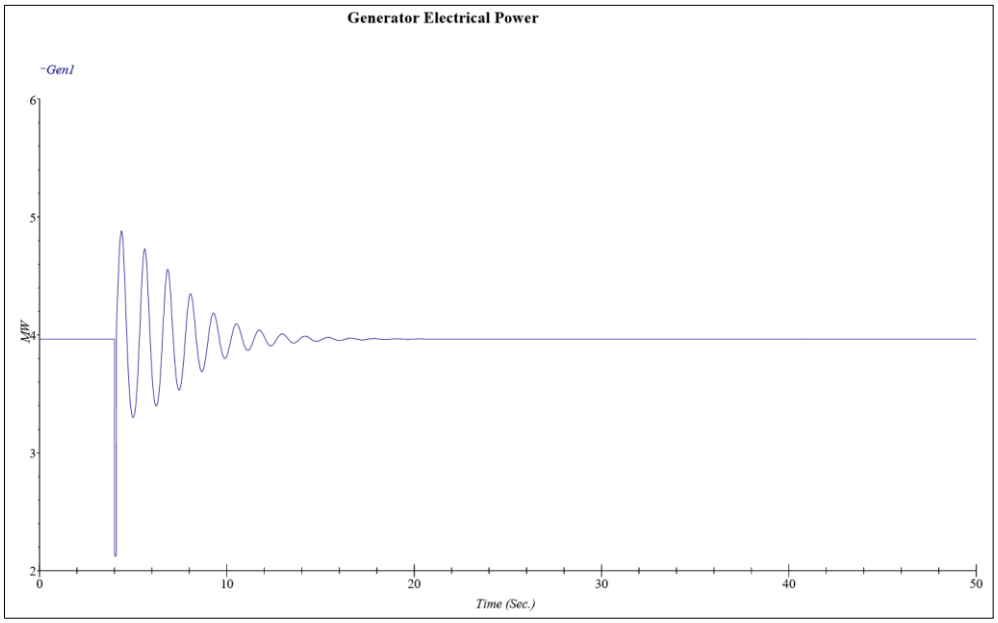

Figure 5-36 Generator electrical power output stabilized after adding control

4. Generator Terminal Current

The magnitude of the short circuit contribution (450 A) from the generator, as shown in Figure 5-37 is approximately equal to the value as described in the previous section.

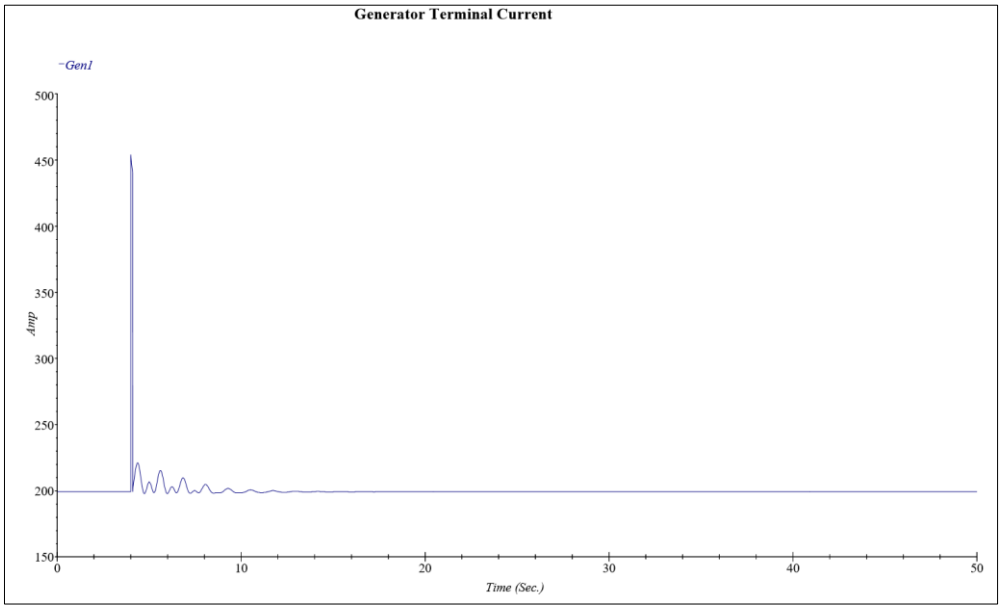

Figure 5-37 Generator terminal current stabilized at 200 A after control addition

6 CONCLUSION AND FUTURE WORK

6.1 Conclusion

In this master thesis, the Gløshaugen distribution network has been developed as a concept design of a typical grid-connected microgrid. The main objectives of the thesis were:

1. To study the overall MG system for varying loads over 24 hours and study its behaviour with RES integration.
2. To analyse the transient stability of the GLØSHAUGEN campus microgrid during load variation and fault conditions at a particular point within the network.

A background study was carried out regarding the MG system overview and the contribution of different components within the MG. A thorough literature review for analysing the Transient Stability and EMS was studied. The data from the existing network was used for the development of campus MG. The system was modelled on ETAP by integrating renewable energy sources and energy storage system using power electronic converters.

The load profile and the solar irradiance for a typical working day was predicted, and three different scenarios were created to observe the effect of RES integration through power flow analysis by connecting and disconnecting the micro-generating units. It was concluded that load peak-shaving could be achieved by connecting and operating the RES and ESS adequately. The results of active and reactive power from the utility grids were analysed and compared for the three scenarios, and it was observed that the burden on the utility was reduced with increasing irradiance during peak hours. The battery sets were operated manually to achieve a flat curve during peak hours.

Transient stability was studied by adding a generator to the grid at the 12kV bus. The generator acted as a replacement for the grid considering the worst-case scenario. The effect of disturbances during load variation and fault condition was analyzed. Load impact and fault events were created on ETAP at different time instants over a period of 50 seconds. The generator controller, in the form of an exciter, was added to improve the stability of the system. The voltage angle, voltage level and the frequency of the bus were stabilized by adding a controller to the generator. The steady-state condition of generator exciter current, power angle and reactive power output was also achieved within 14 seconds after the occurrence of the fault. From the stability studies, it was concluded that the generator exciter improved the stability of the system by synchronising the generator with the system to achieve steady-state condition within a reasonable time.

Key takeaways

- The bus voltages can be improved through load sharing by choosing an optimal location for integrating the RES.
- The active/reactive power can be controlled at different locations by limiting the PE converters.
- Multiple DC power generating units can be connected to a single DC bus to create a hybrid microgrid system.
- The adequate operation of batteries can result in a flat curve for peak shaving.
- Assigning control parameters to the generator allows the system to achieve steady-state condition after the occurrence of fault at any location.

6.2 Future Work

The master thesis was studied comprehensively by modelling the network with RES integration. Due to the limited time and availability of data, the thesis work was constrained with certain boundaries. The thesis work can be further investigated and improved by taking it to various possible directions regarding future work. Some of the possible improvements regarding the model are listed as follows;

- The energy management can be implemented on a yearly basis with various scenarios by creating yearly based load profiles and generation sources.
- The accuracy of the model can be improved by attaining more realistic and accurate data related to the power system and weather conditions.
- The design is a concept design and can be tested on the field to observe any changes that would require any modification within the network.
- The supervisory control for microgrid energy management system and battery management system can be enhanced using the microgrid controller, a toolbox recently introduced in the latest version of ETAP20.
- The concept model in this thesis was not applied to any protection scheme. The protection scheme for this model can be designed after performing short circuit studies on the network model. The circuit breakers and the switches can be given ratings according to short circuits current.
- The campus microgrid can be made more hybrid by connecting many DC components on a single DC bus with a couple of inverters. DC loads can also be connected directly

to the DC bus with regulated voltage for operation. Fewer inverters, converters and DC loads will result in fewer losses.

- Load shifting and load shedding were not considered here for peak-shaving. The loads can be divided into two categories, critical and non-critical, and the controller can manage the operations by swathing the non-critical loads ‘off’ during peak hours or when the demand is higher than the supply.
- Energy prices and power markets can be studied, and costs can be evaluated based on energy consumption of Gløshaugen campus on a timely basis.
- Transient Stability of the model can be analysed under various conditions by initiating faults at different locations within the network.
- The generator controls can be further improved by specifying the governor and power system stabilizer according to the system requirements.
- A very large model was designed in this thesis, and the analysis could take place on parts of the system. The same procedure can be followed to evaluate other parts or buses within the system to analyse the behaviour of the system. Furthermore, various other studies that can also be performed on ETAP for this model are:
    1. Short Circuit Analysis
    2. Arc Flash Analysis
    3. Harmonics Studies
    4. Protection Analysis
    5. Optimal Power Flow
    6. Reliability Assessment

7 REFERENCES

[1] NASA. "Global Mean Estimates based on Land and Ocean Data." https://data.giss.nasa.gov/gistemp/graphs/ (accessed.

[2] M. Hasanuzzaman, U. S. Zubir, N. I. Ilham, and H. Seng Che, "Global electricity demand, generation, grid system, and renewable energy polices: a review," *WIREs Energy and Environment,* vol. 6, no. 3, p. e222, 2017, doi: 10.1002/wene.222.

[3] S. Mujtaba, "NTNU Specialization Project - Microgrid Concept for Future Energy System," 2019.

[4] Statkraft, "Global energy trends - Statkraft's Low Emissions Scenario," 2019.

[5] P. A. Daly and J. Morrison, "Understanding the potential benefits of distributed generation on power delivery systems," in *2001 Rural Electric Power Conference. Papers Presented at the 45th Annual Conference (Cat. No.01CH37214)*, 29 April-1 May 2001 2001, pp. A2/1-A213, doi: 10.1109/REPCON.2001.949510.

[6] N. Hatziargyriou, H. Asano, R. Iravani, and C. Marnay, "Microgrids," *IEEE Power and Energy Magazine,* vol. 5, no. 4, pp. 78-94, 2007, doi: 10.1109/MPAE.2007.376583.

[7] L. E. Zubieta, "Are Microgrids the Future of Energy?: DC Microgrids from Concept to Demonstration to Deployment," *IEEE Electrification Magazine,* vol. 4, no. 2, pp. 37-44, 2016, doi: 10.1109/MELE.2016.2544238.

[8] M. K. Buckholm. "Norway's first and only full-scale microgrid." Smart Innovation Norway. https://en.smartinnovationnorway.com/news/norways-first-full-scale-microgrid/ (accessed.

[9] C. X. EU. "Our project and work." https://cityxchange.eu/ (accessed.

[10] +CityXChange. "Objectives of EU Horizon 2020 smart innovation project - Positive City ExChange." https://cityxchange.eu/objectives/ (accessed.

[11] A. Sretenovic, "Analysis of energy use at university campus," Master, Department of Energy and Process Engineering, Norwegian university of Science & Technology, Trondheim, 2013.

[12] O. Fosso, M. Molinas, K. Sand, and G. Coldevin, *Moving towards the Smart Grid: The Norwegian Case*. 2014.

[13] H. Y. Lai, W. Mai, and C. Chung, "Educational simulation platform for micro-grid," in *2014 IEEE PES Asia-Pacific Power and Energy Engineering Conference (APPEEC)*, 2014: IEEE, pp. 1-7.

[14] D. T. Ton and M. A. Smith, "The U.S. Department of Energy's Microgrid Initiative," *The Electricity Journal,* vol. 25, no. 8, pp. 84-94, 2012/10/01/ 2012, doi: https://doi.org/10.1016/j.tej.2012.09.013.

[15] E. Bullich-Massagué, F. Díaz-González, M. Aragüés-Peñalba, F. Girbau-Llistuella, P. Olivella-Rosell, and A. Sumper, "Microgrid clustering architectures," *Applied Energy,* vol. 212, pp. 340-361, 2018/02/15/ 2018, doi: https://doi.org/10.1016/j.apenergy.2017.12.048.

[16] C. Marnay *et al.*, "Microgrid Evolution Roadmap," in *2015 International Symposium on Smart Electric Distribution Systems and Technologies (EDST)*, 8-11 Sept. 2015 2015, pp. 139-144, doi: 10.1109/SEDST.2015.7315197.

[17] T. S. E. I. Association. "MICROGRID-GRAPHIC." https://events.solar/midwest/smart-energy-microgrid-marketplace/microgrid-graphic/ (accessed.

[18] I. Series, "Microgrids and active distribution networks," *The institution of Engineering and Technology*, 2009.

[19] T. Messo *et al.*, "Using High-Bandwidth Voltage Amplifier to Emulate Grid-Following Inverter for AC Microgrid Dynamic Studies," *Energies*, vol. 12, pp. 1-18, 01/25 2019, doi: 10.3390/en12030379.

[20] M. Jariso, B. Khan, D. Tesfaye, and J. Singh, "Modeling and designing of stand-alone photovoltaic system: CaseStudy: Addis Boder health center south west Ethiopia," in *2017 International conference of Electronics, Communication and Aerospace Technology (ICECA)*, 20-22 April 2017 2017, vol. 1, pp. 168-173, doi: 10.1109/ICECA.2017.8203665.

[21] C. Papadimitriou, E. Zountouridou, and N. Hatziargyriou, "Review of hierarchical control in DC microgrids," *Electric Power Systems Research*, vol. 122, pp. 159-167, 2015.

[22] C. Phurailatpam, B. Rajpurohit, and N. Pindoriya, "Embracing Microgrids: Applications for Rural and Urban India," in *10th National Conference on Indian energy sector*, 2015.

[23] R. A. University. "Hybrid AC/DC Microgrids: A Bridge to Future Energy Distribution Systems." https://www.acs.eonerc.rwth-aachen.de/cms/E-ON-ERC-ACS/Forschung/Abgeschlossene-Projekte/~euwe/HYBRID-AC-DC-MICROGRIDS-A-BRIDGE-TO-FUT/lidx/1/ (accessed.

[24] O. Mohammed, T. Youssef, M. H. Cintuglu, and A. Elsayed, "Chapter 12 - Design and simulation issues for secure power networks as resilient smart grid infrastructure," in *Smart Energy Grid Engineering*, H. A. Gabbar Ed.: Academic Press, 2017, pp. 245-342.

[25] P. S. R. Murty, "Chapter 23 - Voltage and Reactive Power Control," in *Electrical Power Systems*, P. S. R. Murty Ed. Boston: Butterworth-Heinemann, 2017, pp. 731-781.

[26] Z. Salam, K. Ishaque, and H. Taheri, "An improved two-diode photovoltaic (PV) model for PV system," in *2010 Joint International Conference on Power Electronics, Drives and Energy Systems & 2010 Power India*, 2010: IEEE, pp. 1-5.

[27] Multiconsult, "Campus Gløshaugen – Egenproduksjon av energi," 2018.

[28] S. Hajiaghasi, A. Salemnia, and M. Hamzeh, "Hybrid energy storage system for microgrids applications: A review," *Journal of Energy Storage*, vol. 21, pp. 543-570, 2019/02/01/ 2019, doi: https://doi.org/10.1016/j.est.2018.12.017.

[29] S. X. Chen and H. B. Gooi, "Sizing of energy storage system for microgrids," in *2010 IEEE 11th International Conference on Probabilistic Methods Applied to Power Systems*, 14-17 June 2010 2010, pp. 6-11, doi: 10.1109/PMAPS.2010.5528720.

[30] M. Shahabi, M. R. Haghifam, M. Mohamadian, and S. A. Nabavi-Niaki, "Microgrid Dynamic Performance Improvement Using a Doubly Fed Induction Wind Generator," *IEEE Transactions on Energy Conversion*, vol. 24, no. 1, pp. 137-145, 2009, doi: 10.1109/TEC.2008.2006556.

[31] K. M. G. Y. Sewwandi *et al.*, "Wind turbine emulator for a microgrid," in *2017 Innovations in Power and Advanced Computing Technologies (i-PACT)*, 21-22 April 2017 2017, pp. 1-6, doi: 10.1109/IPACT.2017.8244901.

[32] M. Shahbazi and A. Khorsandi, "Chapter 10 - Power Electronic Converters in Microgrid Applications," in *Microgrid*, M. S. Mahmoud Ed.: Butterworth-Heinemann, 2017, pp. 281-309.

[33] M. Akter, S. Mekhilef, N. Tan, and H. Akagi, "Model Predictive Control of Bidirectional AC-DC Converter for Energy Storage System," *Journal of Electrical Engineering and Technology*, vol. 10, pp. 165-175, 01/01 2015, doi: 10.5370/JEET.2015.10.1.165.

[34] A. Mohamed, M. Nizam, and A. Salam, "Performance Evaluation of Fuel Cell and Microturbine as Distributed Generators in a Microgrid," *European Journal of Scientific Research*, vol. 30, 05/01 2009.

[35] Y. T. Shah, *Chemical Energy from natural and Synthetic Gas*. Boca Raton, FL 33487, USA: Taylor & Francis Group, 2017.

[36] D. Gaonkar and S. Nayak, "Modeling and performance analysis of microturbine based Distributed Generation system,“a review”," in *IEEE 2011 EnergyTech*, 2011: IEEE, pp. 1-6.

[37] P. Kundur *et al.*, "Definition and classification of power system stability IEEE/CIGRE joint task force on stability terms and definitions," *IEEE Transactions on Power Systems*, vol. 19, no. 3, pp. 1387-1401, 2004, doi: 10.1109/TPWRS.2004.825981.

[38] T. Taufik, M. Guevara, A. Shaban, and A. Nafisi, "Modeling and Load Flow Analysis of a Microgrid Laboratory," *International Journal of Smart Grid and Sustainable Energy Technologies*, vol. 3, pp. 103-111, 12/23 2019, doi: 10.36040/ijsgset.v3i2.1178.

[39] D. Mondal, A. Chakrabarti, and A. Sengupta, "Chapter 1 - Concepts of Small-Signal Stability," in *Power System Small Signal Stability Analysis and Control*, D. Mondal, A. Chakrabarti, and A. Sengupta Eds. Boston: Academic Press, 2014, pp. 1-14.

[40] A.-A. Fouad and V. Vittal, *Power system transient stability analysis using the transient energy function method*. Pearson Education, 1991.

[41] N. M. Tabatabaei, E. Kabalci, and N. Bizon, *Microgrid architectures, control and protection methods*. Springer, 2019.

[42] F. Katiraei, R. Iravani, N. Hatziargyriou, and A. Dimeas, "Microgrids Management," *Power and Energy Magazine, IEEE*, vol. 6, pp. 54-65, 06/01 2008, doi: 10.1109/MPE.2008.918702.

[43] G. Karmiris and T. Tengnér, "Peak shaving control method for energy storage," *Corporate Research Center, Vasterås, Sweden*, 2013.

[44] Q.-U. Ain, S. Iqbal, and N. Javaid, "User Comfort Enhancement in Home Energy Management Systems using Fuzzy Logic," 2019.

[45] C.-K. Chang, S.-H. Lee, R.-N. Wu, C.-H. Lee, and J.-H. Chang, "The use of the peak-clipping method for energy management in households with energy storage equipment," *Journal of the Chinese Institute of Engineers*, vol. 43, no. 3, pp. 257-268, 2020/04/02 2020, doi: 10.1080/02533839.2019.1708807.

[46] H. Saadat, "Power system analysis," ed: WCB/McGraw-Hill, 1999.

[47] T. K. Y. Hase, K. Kameda, *Power System Dynamics with Computer-Based Modeling and Analysis*. John Wiley & Sons Ltd, 2020.

APPENDIX A: COMPLETE OVERVIEW OF GLØSHAUGEN SLD

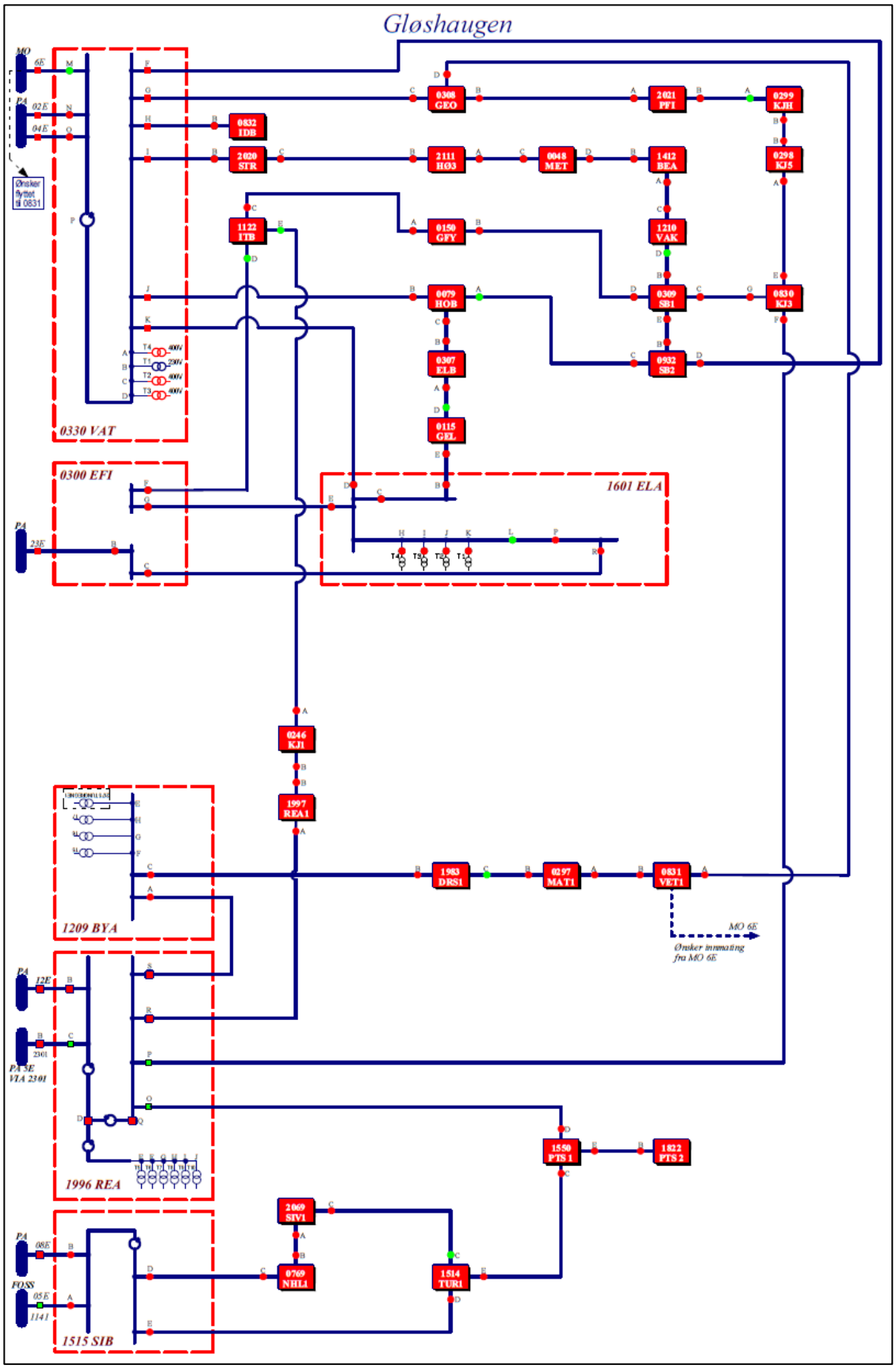

APPENDIX B: LOCATION AND CAPACITIES OF THE TRANSFORMERS AT GLØSHAUGEN

TRAFO-KAPASITET GLØSHAUGEN - SOUTH AREA.					
NS: nr.	Building	Fab.nr	Trafo nr.	Trafo kVA	Comments
0048-MET	Metallurgen	12659	T - 1	500	230 V
0048-MET	Metallurgen	420-40334	T - 2 A	260	Smelting
0048-MET	Metallurgen	24208	T - 2	150	Smelting
0048-MET	Metallurgen	8158 B1	T - 3	500	230 V Beneficiation
0048-MET	Metallurgen	001-10677	T - 4	800	230 V Smelting
0048-MET	Metallurgen	269704 / AOV	T - 5	1250	690 V Smelting
0048-MET	Metallurgen	K2-41214	T - 6	315	365 V Smelting
0079-HOB	Hovedbygget	410-09857	T - 1	800	230 V
0115-ELM	Elektro. M	230866	T - 1	800	230 V
0115-ELM	Elektro. M	100607	T - 2	800	400 V
0150-GFY	Gamle Fysikk	230864	T - 1	800	230 V
0150-GFY	Gamle Fysikk		T - 2	1000	400 V
0246-KJ1	Kjemi 1.	230867	T - 1	800	400V
0246-KJ1	Kjemi 1.	500708	T - 2	800	400 V
0297-MAT	Materialteknisk	8713655	T - 1	800	400 V
0297-MAT	Materialteknisk	8713656	T - 2	800	230 V
0298-KJ5	Kjemi 5	8815548	T - 1	800	230 V
0299-KJH	Kjemi Hall	230869	T - 1	800	230 V
0299-KJH	Kjemi Hall	410 - 09400	T - 2	800	230 V
0300-EFI	EFI		T - 1	250	230 V
0307-ELB	Elektro. B	420 - 41269	T - 1	800	400 V
0307-ELB	Elektro. B	410 - 02891	T - 2	800	230 V
0308-GEO	Geologen	771159	T - 1	500	230 V
0309-SB1	Sentralbygg 1.	012 - 01166	T - 1	800	230 V
0330-VAT	Varmeteknisk	410 - 09398	T - 1	800	230 V
0330-VAT	Varmeteknisk	96 1 3699	T - 2	800	400 V Kjelhuset
0330-VAT	Varmeteknisk	410 - 04292	T - 3	800	400 V
0330-VAT	Varmeteknisk	610283	T - 4	1000	400 V Research
0830-KJ4	Kjemi 3	T 930924	T - 1	800	400 V
0831-VET	Verkstedtekn.	230863	T - 1	800	230 V
0831-VET	Verkstedtekn.	70131	T - 2	800	400V
0832-IDB	Idrettsbygget	230865	T - 1	800	230 V
0932-SB2	Sentralbygg 2.	8611028	T - 1	800	230 V
1122-ITB	IT-Bygget	710825	T - 1	500	230 V
1209-BYA	Bygningsavd.	201015	T - 1	800	400 V
1209-BYA	Bygningsavd.	70289	T - 2	1000	230 V
1209-BYA	Bygningsavd.		T - 3	500	400 V
2175-BYA	Bygningsavd.	530 - 51508	T - 3	1600	400V
2175-BYA	Bygningsavd.			1250	400V
1210-VAK	Vannkrafta	202366	T - 1	1250	400 V
1210-VAK	Vannkrafta	70283	T - 2	500	230 V
1412-BEA	Bergavdelingen	12 - 00872	T - 1	800	400 V Bygget
1412-BEA	Bergavdelingen		T-2	500	230 V Oppredningen
1601-ELA	ELA	410 - 06375	T - 1	800	230 V Lab.trafo. E
1601-ELA	ELA	410 - 06376	T - 2	800	400 V Lab.trafo. D
1601-ELA	ELA	410 - 06377	T - 3	800	400 V Lab.trafo. C
1601-ELA	ELA	410 - 06379	T - 4	800	400 V
1601-ELA	ELA	410 - 06378	T - 6	800	400 V Lab.trafo. B
1983-DRS	Driftsentralen	410 - 04639	T - 1	800	230 V
1996-REA	Realfagbygget	K7 48645	T - 1	1250	400 V HU4.0100
1996-REA	Realfagbygget	K7 48644	T - 2	1250	400 V HU4.0200
1996-REA	Realfagbygget	K7 48643	T - 3	1250	400 V HU4.0300
1996-REA	Realfagbygget	K7 48641	T - 4	1250	400 V HU4.0400
1996-REA	Realfagbygget	K7 48646	T - 5	1250	400 V HU4.0500
1996-REA	Realfagbygget	K7 48642	T - 6	1250	400 V HU4.0600
1997-REA	Realfagbygget	K7 48640	T - 1	1250	400 V HU2.0100

2020-STR	Strømn.tekn.	T961262	T - 1	1000	400 V
2021-PFI	Papir.Ind.Forkn.	T971467	T - 1	1000	400 V
			Sum side 1	48375	
, TRAFO-KAPASITET GLØSHAUGEN - NORTH AREA.					
NS: nr.	Bygg	Fab.nr	Trafo nr.	Trafo kVA	Bemerkninger
2111-HØ3	Høyskolering. 3	200412	T - 1	800	400 V
0769-NHL	Vassdr.lab	961706	T - 1	1000	230 V
1514-TUR	Turbinlab.	410 - 04933	T - 1	1250	400 V
1514-TUR	Turbinlab.	410 - 04932	T - 2	800	400 V
1515-SIB	Silobygget	410 - 04934	T - 1	800	230 V
1515-SIB	Silobygget		T - 2	1000	400 V
1550-PTS	Petro.tek.sen.	410 - 05048	T - 1	800	230 V
1550-PTS	Petro.tek.sen.	410 - 05049	T - 2	800	230 V
1822-IKU	IKU - Bygget	410 - 08968	T - 1	800	400 V
2069-SIV	Sintef Valgr.	99 05736	T - 1	1000	400 V
			Sum side 1 og 2	57425	

APPENDIX C: GLØSHAUGEN ENERGY CONSUMPTION BY BUILDING

ANNUAL ELECTRICITY CONSUMPTION AND CO2 EMISSION IN NTNU GLØSHAUGEN					
Building		Meter/Submeter	year	Eel [kWh]	[Tonnes] CO2
HOVEDBYGNINGEN		RE01 230 V	2011 2012 2010	1,175,706 1,374,586 1,217,981	636.76 744.48 659.66
		RE01 230 V	2011 2012 2009 2010 2007 2008	1,539,099 936,725 560,655 258,875 147,389 159,120	833.58 507.33 303.65 140.21 79.80 86.18
		RE03 400 V	2012 2010 2011 2008 2009 2007	257,721 452,555 112,137 51,773 31,824 29,451	139.58 245.10 60.73 28.04 17.24 15.95
		RE01 400V	2011 2012 2010	214,683 263,994 199,752	116.27 142.98 108.19
METALLURGI		RE01 230V	2012 2010 2011	240,263 245,639 236,941	130.13 133.04 128.33
		RE01 400V	2011 2012 2010	132,688 248,596 83,430	71.86 134.64 45.19
		RE01 230V	2011 2012 2010	275,435 330,408 257,749	149.18 178.95 139.60
		RE01 230V	2011 2012 2010	469,832 601,494 515,480	254.46 325.77 279.18
VERKSTEDTEKNISK	RE01 230V	2011 2012 2009 2010 2007 2008	1,259,829 1,074,225 1,313,300 1,283,856 1,311,719 1,182,413	682.32 581.80 711.28 695.34 710.23 640.39	186.09 158.67 193.99 189.64 193.70 174.65

	RE02 400V	1/2 2011 2012	161,782 233,476	87.62 126.45	23.90 34.49
	RE03 400V	1/2 2011 2012	6,310 10,356	5.61 3.42	1.53 0.93
	RE04 400V	2012 1/22011	4,326 2,114	2.34 1.14	0.64 0.31
MATERIALTEKNISK	RE01 400V	2012 2010 2011	620,975 1,147,615 394,720	336.32 621.55 213.78	91.72 169.51 58.30
	RE02 230V	2012 2010 2011	1,269,292 290,567 1,081,948	687.45 157.37 585.98	159.81 187.49 42.92
	RE03 230V	1/2 2011 2012	75,207 99,146	40.73 53.70	11.11 14.64
	RE04 230V	1/2 2011 2012	169,753 303,742	91.94 164.51	25.07 44.87
	RE05 230V	1/2 2011 2012	74,507 139,255	40.35 75.42	11.01 20.57
	RE06 400V	2012 2010 2011	12,319 4,063 5,216	6.67 2.20 2.82	1.82 0.60 0.77
	RE07 400V	2010	293,005	158.69	43.28
DRIFTSSENTR.	RE01 230V	2011 2012 2010	298,522 404,036 346,246	161.68 218.83 187.53	44.09 59.68 51.14
KJEMI 1	M1 400V	1/2 2011 2012	366,159 953,768	198.31 516.56	140.88 54.09
	M2 400V	1/2 2011 2012	825,342 1,366,111	447.01 739.89	121.91 201.79
	M3 230V	1/2 2011 2012	104,049 112,289	56.35 60.82	15.37 16.59
	M4 230V	1/2 2011 2012	95,990 213,767	51.99 115.78	14.18 31.58
	M5 400V	1/2 2011 2012	270,269 397,083	146.38 215.06	39.92 58.65
	M6 230V	2012 1/2 2011	93,091 33,490	50.42 18.14	13.75 4.95
KJEMI 3	RE03 230V	2011 2012 2010	1,286,603 1,164,742 1,437,860	696.82 630.82 778.74	190.04 172.04 212.38

KJEMI 4	RE01 400V	2012 2010 2011	762,274 2,472,846 1,881,038	412.85 1,339.29 1,018.77	112.59 365.26 277.85
	RE02 230V	2012 2011	8,885 6,583	4.81 3.57	1.31 0.97
KJEMI 5	RE01 230V	2011 2012 2010	764,199 846,480 797,462	413.89 458.45 431.91	112.88 125.03 117.79
KJEMIHALL	RE01 230V	2012 2010 2011	336,605 958,209 223,203	182.31 518.97 120.89	49.72 141.54 32.97
	RE02 230V	2012 2011	249,211 12	134.97 0.01	36.81 0.00
IT BYGGET	RE01 230V	2011 2012 2010	848,027 876,547 823,381	459.29 474.74 445.94	125.26 129.47 121.62
IT BYGGET SYDFLØY	RE01 230V	2012 1/2 2011	443,632 143,571	240.27 77.76	65.53 21.21
GAMLE FYSIKK	RE01 230V	2012 2010 2011	279,996 667,070 374,514	151.65 361.29 202.84	41.36 98.53 55.32
	RE02 400V	2012 1/2 2011	168,178 75,854	91.09 41.08	24.84 11.20
EFI	RE01 230V	2011 2012 2010	970,576 1,005,024 1,003,788	525.66 544.32 543.65	143.36 148.45 148.27
SENTRALBYGG 1	RE01 230V	2012 2010 2011	1,790,217 1,424,125 1,514,848	969.58 771.31 820.44	264.43 210.36 223.76
	RE02 230V	2011 2012 2010	267,216 283,508 272,512	144.72 153.55 147.59	39.47 41.88 40.25
SENTRALBYGG 2	RE01 230V	2011 2012 2010	1,811,520 2,148,848 1,708,815	981.12 1,163.82 925.49	267.58 317.40 252.41
GAMLE KJEMI	RE01 230V	2011 2012 2010	302,170 323,658 323,220	163.66 175.29 175.06	44.63 47.81 47.74
VANNKRAFTLAB	RE01 400V	2012 2010 2011	25,467 43,963 57,416	13.79 23.81 31.10	3.76 6.49 8.48
	RE02 230V	2011 2012 2010	36,202 2,206 191,814	19.61 1.19 103.89	5.35 0.33 28.33

GAMLE ELEKTRO	RE01 230V	2011 2012 2010	742,337 758,128 757,287	402.05 410.60 410.15	109.65 111.98 111.86
ELEKTRO A	RE01 230V	2012 2010 2011	540,520 467,448 484,151	292.75 253.17 262.22	79.84 69.05 71.51
	RE02 400V	2012 1/2 2011	102,379 54,780	55.45 29.67	15.12 8.09
ELEKTRO B ELEKTRO C	RE01 400V	2012 2010 2011	508,102 1,358,162 787,435	275.19 735.58 426.47	75.05 200.61 116.31
	RE010 TP	2012	109,537	59.33	16.18
	RE02 230V	2011 2012	703,533 1,338,238	381.03 724.79	103.92 197.67
BERG AVD	RE01 400V	2012 2010 2011	703,482 1,265,590 1,026,106	381.01 685.44 555.74	103.91 186.94 151.57
	RE02 400V	2012 1/2 2011	598,490 380,961	324.14 206.33	88.40 56.27
IDRETTSBYGGET	RE01 230V	2011 2012 2010	335,844 513,340 183,275	181.89 278.03 99.26	49.61 75.83 27.07
BYGGTEKNISK	RE01 400V	2012 1/2 2010 1/2 2011	534,880 2,247,718 174,822	289.69 1,217.36 94.68	79.01 332.01 25.82
	RE010 TP	2012	196,339	106.34	29.00
	RE02 230V	2012 2010 2011	862,209 802,070 866,914	466.97 434.40 469.52	127.36 118.47 128.05
	RE03 230V	2012 1/2 2010 1/2 2011	81,506 98,180 39,150	44.14 53.17 21.20	12.04 14.50 5.78
	RE04 400V	2011 2012 2010	2,773,298 3,743,945 42,161	1,502.02 2,027.72 22.83	409.64 553.01 6.23
ELA (ELEKTRO E+F)	RE05 400V RE01 400V	2012 2012 2011 2010 2011	2,423,064 2,622,985 2,099,957 2,363,324 2,351,882	1,312.33 1,420.61 1,137.34 1,279.98 1,273.78	357.91 387.44 310.18 349.08 347.39
	RE02 400V	2012 2010 2011	305,827 30,988 156,501	165.64 16.78 84.76	23.12 45.17 4.58

	RE03 400V	2011? 2012? 2010	89 178,266 173	0.05 96.55 0.09	0.01 26.33 0.03
	RE05 400V	2012 1/2 2011	166,068 137,590	89.94 74.52	24.53 20.32
KJELHUSET	RE02 400V	2011 2012 2010	659,737 672,613 619,357	357.31 364.29 335.44	97.45 99.35 91.48
PRODUKT DESIGN	RE02 400V	2011 2012 2010	263,169 290,154 247,676	142.53 157.15 134.14	38.87 42.86 36.58
HØGSKOLERINGEN	RE01 400V	2012 1/2 2011	373,243 222,832	202.15 120.69	55.13 32.91
REALFAGBYGGET	RE01 400V	1/2 2011 2012 2010	693,712 1,524,616 10,331,835	375.71 825.73 5,595.72	225.20 1,526.11 102.47
	RE02 400V	2012 2010 2011	1,451,640 1,083,241 1,229,071	786.21 586.68 665.67	214.42 160.00 181.55
	RE03 400V	1/2 2011 2012	1,379,021 1,916,459	746.88 1,037.95	283.08 203.69
	RE04 400V	1/2 2011 2012	888,711 1,364,918	481.33 739.24	131.27 201.61
	RE05 400V	1/2 2011 2012	1,044,062 1,399,870	565.46 758.17	206.77 154.22
	RE06 400V	1/2 2011 2012	2,435,217 2,863,090	1,318.91 1,550.65	359.70 422.90
	RE07 400V	1/2 2011 2012	732,635 1,112,961	396.80 602.78	108.22 164.39
	WM02 KJ04	1/2 2011 2012	7,578 11,247	4.10 6.09	1.12 1.66
	WM02 KJ05	1/2 2011 2012	4,874 6,828	3.70 2.64	1.01 0.72
	WM201	2012 1/2 2011	337,709 210,556	182.90 114.04	49.88 31.10
PFI	RE01 400V	2012 1/2 2011	976,510 671,905	0.00 0.00	0.00 0.00
MAIN METER		2011 2012 2009 2010 2008	61,286,821 62,405,546 57,495,284 60,839,328 55,621,396	33,192.94 33,798.84 31,139.45 32,950.58 30,124.55	9,052.62 9,217.87 8,492.58 8,986.52 8,215.79

From	To	Length	Rated Voltage	Cross-Section	Capacitance	Resistance	Reactance
		km	kV	mm2	uF	ohm	ohm
NS0048	NS1412	0.030	12	150	0.0081	0.00618	0.00264
NS0079	NS0307	0.034	12	240	0.01496	0.00425	0.00612
NS0079	NS0307	0.165	12	240	0.0726	0.020625	0.0297
NS0150	NS1122	0.028	12	120	0.00924	0.007084	0.002016
NS02111	NS0048	0.020	12	240	0.01056	0.003	0.00432
NS02111	NS0048	0.071	12	240			
NS02111	NS0048	0.020	12	240	0.03476	0.009875	0.01422
NS0246	NS1122	0.032	12	240	0.01408	0.004	0.00576
NS0246	NS1122	0.140	12	240	0.0616	0.0175	0.014
NS0297	NS0831	0.004	0	0	0	0	0
NS0297	NS0831	0.117	12	240			
NS0298	NS0299	0.038	12	240	0.0114	0.00475	0.003344
NS0298	NS0299	0.125	12	240	0.0375	0.015625	0.011
NS0300	NS1601	0.091	12	240	0.0273	0.011375	0.008008
NS0300	NS1122	0.160	12	150	0.0528	0.03296	0.0192
NS0307	NS0115	0.098	12	240	0.04018	0.01225	0.01078
NS0308	NS2021	0.009	0	0	0	0	0
NS0308	NS2021	0.015	0	0	0	0	0
NS0308	NS0831	0.197	12	240			
NS0309	NS0830	0.007	12	240	0.0021	0.000875	0.000616
NS0309	NS0150	0.040	12	120	0.0132	0.01012	0.00288
NS0309	NS1210	0.062	12	240	0.02728	0.00775	0.01116
NS0309	NS0150	0.139	12	120	0.04587	0.035167	0.010008
NS0309	NS0830	0.155	12	240	0.0465	0.019375	0.01364
NS0330	NS1601	0.085	12	240	0.04428	0.0135	0.01188
NS0330	NS1601	0.109	12	240	0.0327	0.013625	0.009592
NS0330	NS1601	0.055	12				
NS0330	NS0079	0.090	12	240			
NS0330	NS0079	0.058	12	240			
NS0330	NS0308	0.414	12	240			
NS0330	NS0832	0.125	12	120	0.05875	0.035955	0.02068
NS0330	NS0832	0.145	12	240			
NS0330	NS0932	0.267	12	240			
NS0330	NS0932	0.267	12	240			
NS0330	NS2020	0.154	12	240			
NS0668	NS0797	0.009	12	240	0.00396	0.001125	0.00162
NS0668	NS0797	0.089	12	185	0.02492	0.014596	0.007832
NS0830	NS0298	0.007	12	240	0.0021	0.000875	0.000616
NS0830	NS1996	0.101	12	240	0.04141	0.012625	0.01111
NS0830	NS0298	0.113	12	240	0.04972	0.014125	0.02034
NS0932	NS0079	0.021	12	240	0.00924	0.002625	0.00378
NS0932	NS0079	0.074	12	120	0.02442	0.018722	0.005328

From	To	Length	Rated Voltage	Cross-Section	Capacitance	Resistance	Reactance
		km	kV	mm2	uF	ohm	ohm
NS0932	NS0309	0.149	0	0	0	0	0
NS1209	NS1983	0.016	12	240	0.00656	0.002	0.00176
NS1209	NS2175	0.039	24	95	0.0078	0.01248	0.00468
NS1209	NS1983	0.040	12	240	0.012	0.005	0.00352
NS1209	NS1983	0.150	0	0	0	0	0
NS1249	NS0797	0.006	12	240	0.00264	0.00075	0.00108
NS1249	NS1394	0.012	12	240	0.00528	0.0015	0.00216
NS1249	NS1527	0.059	12	95	0.01357	0.01888	0.005369
NS1249	NS1394	0.061	12	185	0.01708	0.010004	0.005368
NS1249	NS1394	0.083	12	185	0.02324	0.013612	0.007304
NS1249	NS0797	0.115	12	185	0.0322	0.01886	0.01012
NS1249	NS0797	0.318	12	185	0.08904	0.052152	0.027984
NS1313	NS2126	0.451	12	240	0.19844	0.056375	0.08118
NS1394	NS1395	0.008	12	240	0.00352	0.001	0.00144
NS1395	NS0668	0.005	12	240	0.0022	0.000625	0.0009
NS1395	NS0668	0.009	12	240	0.00396	0.001125	0.00162
NS1395	NS0668	0.181	12	185	0.05068	0.029684	0.015928
NS1412	NS1210	0.063	12	185	0.01764	0.010332	0.005544
NS1625	NS1313	0.076	12	240	0.0228	0.0095	0.006688
NS1625	NS1313	0.117	12	240	0.05148	0.014625	0.02106
NS1983	NS0297	0.018	12	240	0.00792	0.00225	0.00324
NS1983	NS0297	0.086	12	240	0.0258	0.01075	0.007568
NS1996	NS1997	0.015	0	0	0	0	0
NS1996	NS1997	0.078	12	240	0.03198	0.00975	0.00858
NS1996	NS1209	0.084	12	240	0.03444	0.0105	0.00924
NS1996	NS1997	0.093	12	240	0.04092	0.011625	0.01674
NS1997	NS0246	0.009	12	240	0.00396	0.001125	0.00162
NS1997	NS0246	0.015	12	240	0.0066	0.001875	0.0027
NS1997	NS0246	0.041	12	240	0.01804	0.005125	0.00738
NS2020	NS02111	0.015	12	240	0.011	0.003125	0.0045
NS2020	NS02111	0.112	12	240			
NS2020	NS02111	0.060	12	240	0.0264	0.0075	0.0108
NS2021	NS0299	0.009	0	0	0	0	0
NS2021	NS0299	0.091	12				
NS2126	NS1625	0.104	12	240	0.04576	0.013	0.01872
NS2126	NS1625	0.140	12	240	0.0616	0.0175	0.0252

APPENDIX D: CABLE DATA INTERCONNECTING THE CAMPUS GRID

From	To	Object Number	Operational Labeling	Length	Type designation	Rated Voltage	Operating Capacitance	From-address	Max. OperatingCurrent (A)	CrossSection	Node 1	Node 2	Earthing capacitance	Resistance	Reactance
				km		kV	uF		A	mm2			uF	ohm	ohm
NS0048	NS1412	1359090	NR.2201	0.030	DKBA 1X3X150 AL	12	0.0159	ALFRED GETZ' VEI 2A	265	150	0048	1412	0.0081	0.00618	0.00264
NS0079	NS0307	1372325	NR.3719	0.034	TSLE 3X1X240 AL	12	0.01394	HØGSKOLERINGEN 1	465	240	0079	0307	0.01496	0.00425	0.00612
NS0079	NS0307	1343579	NR.3719	0.165	TSLE 3X1X240 AL	12	0.06765	HØGSKOLERINGEN 1	465	240	0307	0079	0.0726	0.020625	0.0297
NS0150	NS1122	1331251	NR.1276	0.028	DKBA 1X3X120 AL	12	0.00924	SEM SÆLANDS VEI 5	0	120	1122	0150	0.00924	0.007084	0.002016
NS02111	NS0048	1343948	NR.4462	0.020	TSLE 3X1X240 AL	12	0.00984	HØGSKOLERINGEN 3	465	240	2111	0048	0.01056	0.003	0.00432
NS02111	NS0048		NR.6317	0.071	TSLF 3X1X240 AL	12		HØGSKOLERINGEN 3	465	240	0048	2111			
NS02111	NS0048	1370339	NR.3810	0.020	TSLE 3X1X240 AL	12	0.03239	HØGSKOLERINGEN 3	465	240	0048	2111	0.03476	0.009875	0.01422
NS0246	NS1122	1332659	NR.4846	0.032	TSLF 3X1X240 AL	12	0.01312	SEM SÆLANDS VEI 14	465	240	1122	0246	0.01408	0.004	0.00576
NS0246	NS1122	1358863	NR.3494	0.140	TXSP 1X3X240 AL	12	0.0616	SEM SÆLANDS VEI 14	400	240	1122	0246	0.0616	0.0175	0.014
NS0297	NS0831	1318233	NR.3379	0.004		0	0	RICHARD BIRKELANDS VEI 1E	0	0	0297	0831	0	0	0
NS0297	NS0831		NR.6320	0.117	TSLF 3X1X240 AL	12		RICHARD BIRKELANDS VEI 1E	465	240	0297	0831			
NS0298	NS0299	1317565	NR.3496	0.038	DKBA 1X3X240 AL	12	0.0228	SEM SÆLANDS VEI 4	345	240	0298	0299	0.0114	0.00475	0.003344
NS0298	NS0299	1345863	NR.3496	0.125	DKBA 1X3X240 AL	12	0.075	SEM SÆLANDS VEI 4	345	240	0298	0299	0.0375	0.015625	0.011
NS0300	NS1601	1330618	NR.3062	0.091	DKBA 1X3X240 AL	12	0.0546	SEM SÆLANDS VEI 11	345	240	0300X	1601Y	0.0273	0.011375	0.008008
NS0300	NS1122	1318302	NR.3002	0.160	TXSE 1X3X150 AL	12	0.0528	SEM SÆLANDS VEI 11	310	150	1122	0300Y	0.0528	0.03296	0.0192
NS0307	NS0115	1330612	NR.3959	0.098	TXSE 1X3X240 AL	12	0.04018	O.S. BRAGSTADS PLASS 2C	400	240	0307	0115	0.04018	0.01225	0.01078
NS0308	NS2021	1357290	NR.4216	0.009		0	0	HØGSKOLERINGEN 6A	0	0	0308	2021	0	0	0
NS0308	NS2021	1357250	NR.3624	0.015		0	0	HØGSKOLERINGEN 6A	0	0	2021	0308	0	0	0
NS0308	NS0831		NR.6319	0.197	TSLF 3X1X240 AL	12		HØGSKOLERINGEN 6A	465	240	0308	0831			
NS0309	NS0830	1319292	NR.3956	0.007	DKBA 1X3X240 AL	12	0.0042	ALFRED GETZ' VEI 3	345	240	0830	0309	0.0021	0.000875	0.000616
NS0309	NS0150	1305080	NR.1365	0.040	DKBA 1X3X120 AL	12	0.0132	ALFRED GETZ' VEI 3	0	120	0150	0309	0.0132	0.01012	0.00288
NS0309	NS1210	1331242	NR.3958	0.062	TSLE 3X1X240 AL	12	0.02542	ALFRED GETZ' VEI 3	465	240	1210	0309	0.02728	0.00775	0.01116
NS0309	NS0150	1358391	NR.1365	0.139	DKBA 1X3X120 AL	12	0.04587	ALFRED GETZ' VEI 3	0	120	0150	0309	0.04587	0.035167	0.010008
NS0309	NS0830	1306162	NR.3956	0.155	DKBA 1X3X240 AL	12	0.093	ALFRED GETZ' VEI 3	345	240	0830	0309	0.0465	0.019375	0.01364
NS0330	NS1601	1398437	NR.3001	0.085	TXSE 1X3X240 AL	12	0.04428	KOLBJØRN HEJES VEI 1B	400	240	0330	#1001630	0.04428	0.0135	0.01188
NS0330	NS1601	1398587	NR.3001	0.109	DKBA 1X3X240 AL	12	0.0654	KOLBJØRN HEJES VEI 1B	345	240	0330	#1001630	0.0327	0.013625	0.009592
NS0330	NS1601		NR.6411	0.055	TSLF 3X1X240 AL	12		KOLBJØRN HEJES VEI 1B	465		0331	1601			
NS0330	NS0079	1383091	NR.3160	0.090	DKBA 1X3X240 AL	12	0.0768	KOLBJØRN HEJES VEI 1B	345	240	0330	0079			
NS0330	NS0079		NR.6410	0.058	TSLF 3X1X240 AL	12		KOLBJØRN HEJES VEI 1B	465	240	0330	0079			
NS0330	NS0308		NR.6412	0.414	TSLF 3X1X240 AL	12		KOLBJØRN HEJES VEI 1B	465	240	0330	0308			
NS0330	NS0832	1369959	NR.1133	0.125	DKBA 1X3X120 CU	12	0.11515	KOLBJØRN HEJES VEI 1B	305	120	0330	0832	0.05875	0.035955	0.02068
NS0330	NS0832		NS.6324	0.145	TSLF 3X1X240 AL	12		KOLBJØRN HEJES VEI 1B	465	240	0330	0832			
NS0330	NS0932		NR.6371	0.267	TSLF 3X1X240 AL	12		KOLBJØRN HEJES VEI 1B	465	240	0330	0932			
NS0330	NS0932		NR.6372	0.267	TSLF 3X1X240 AL	12		KOLBJØRN HEJES VEI 1B	465	240	0330	0932			
NS0330	NS2020		NR.6374	0.154	TSLF 3X1X240 AL	12		KOLBJØRN HEJES VEI 1B	465	240	0330	2020			
NS0668	NS0797	1370431	NR.2132	0.009	TSLE 3X1X240 AL	12	0.00369	PROFESSOR J.H.L. VOGTS VEG 1	465	240	0797	0668	0.00396	0.001125	0.00162
NS0668	NS0797	1358482	NR.2132	0.089	NKBA 1X3X185 AL	12	0.04984	PROFESSOR J.H.L. VOGTS VEG 1	300	185	0668	0797	0.02492	0.014596	0.007832
NS0830	NS0298	1332295	NR.3495	0.007	DKBA 1X3X240 AL	12	0.0042	SEM SÆLANDS VEI 6	345	240	0298	0830	0.0021	0.000875	0.000616

From	To	Object Number	Operational Labeling	Length	Type designation	Rated Voltage	Operating Capacitance	From-address	Max. OperatingCurrent (A)	CrossSection	Node 1	Node 2	Earthing capacitance	Resistance	Reactance
				km		kV	uF		A	mm2			uF	ohm	ohm
NS0830	NS1996	1344329	NR.4255	0.101	TXSE 1X3X240 AL	12	0.04141	SEM SÆLANDS VEI 6	400	240	0830	1996	0.04141	0.012625	0.01111
NS0830	NS0298	1358446	NR.4977	0.113	TSLF 3X1X240 AL	12	0.04633	SEM SÆLANDS VEI 6	465	240	0830	0298	0.04972	0.014125	0.02034
NS0932	NS0079	1357116	NR.1107	0.021	TSLE 3X1X240 AL	12	0.00861	ALFRED GETZ' VEI 1	465	240	0932	0079	0.00924	0.002625	0.00378
NS0932	NS0079	1398394	NR.1107	0.074	DKBA 1X3X120 AL	12	0.02442	ALFRED GETZ' VEI 1	0	120	0932	0079	0.02442	0.018722	0.005328
NS0932	NS0079	1397000	NR.1107	0.139	DKBA 1X3X120 AL	12	0.04587	ALFRED GETZ' VEI 1	0	120	0932	0079	0.04587	0.035167	0.010008
NS0932	NS0309	1383087	NR.3957	0.149		0	0	ALFRED GETZ' VEI 1	0	0	0932	0309	0	0	0
NS1209	NS1983	1304965	NR.4033	0.016	TXSE 1X3X240 AL	12	0.00656	HØGSKOLERINGEN 7A	400	240	1983	1209	0.00656	0.002	0.00176
NS1209	NS2175	1385199	NR.4735	0.039	TXSE 1X3X95 AL	24	0.0078	HØGSKOLERINGEN 7A	240	95	2175	1209	0.0078	0.01248	0.00468
NS1209	NS1983	1357292	NR.3492	0.040	DKBA 1X3X240 AL	12	0.024	HØGSKOLERINGEN 7A	345	240	1983	1209	0.012	0.005	0.00352
NS1209	NS1983	1305122	NR.4321	0.150		0	0	HØGSKOLERINGEN 7A	0	0	1209	1983	0	0	0
NS1249	NS0797	1319334	NR.5020	0.006	TSLF 3X1X240 AL	12	0.00246	OTTO NIELSENS VEG 10	465	240	0797	1249	0.00264	0.00075	0.00108
NS1249	NS1394	1319888	NR.4888	0.012	TSLF 3X1X240 AL	12	0.00492	OTTO NIELSENS VEG 10	465	240	1394	1249	0.00528	0.0015	0.00216
NS1249	NS1527	1318047	NR.2403	0.059	DKBA 1X3X95 AL	12	0.02655	OTTO NIELSENS VEG 10	205	95	1249	1527T1	0.01357	0.01888	0.005369
NS1249	NS1394	1370430	NR.1792	0.061	DKBA 1X3X185 AL	12	0.03416	OTTO NIELSENS VEG 10	300	185	1249	1394	0.01708	0.010004	0.005368
NS1249	NS1394	1383583	NR.2129	0.083	DKBA 1X3X185 AL	12	0.04648	OTTO NIELSENS VEG 10	300	185	1249	1394	0.02324	0.013612	0.007304
NS1249	NS0797	1306647	NR.1666	0.115	DKBA 1X3X185 AL	12	0.0644	OTTO NIELSENS VEG 10	300	185	1249	0797	0.0322	0.01886	0.01012
NS1249	NS0797	1371758	NR.1666	0.318	DKBA 1X3X185 AL	12	0.17808	OTTO NIELSENS VEG 10	300	185	1249	0797	0.08904	0.052152	0.027984
NS1313	NS2126	1372274	NR.4526	0.451	TSLE 3X1X240 AL	12	0.18491	EDVARD BULLS VEG 1	465	240	1313	2126	0.19844	0.056375	0.08118
NS1394	NS1395	1306703	NR.4890	0.008	TSLF 3X1X240 AL	12	0.00328	TANKVEGEN 22A	465	240	1394	1395	0.00352	0.001	0.00144
NS1395	NS0668	1385430	NR.4889	0.005	TSLF 3X1X240 AL	12	0.00205	TANKVEGEN 22A	465	240	1395	0668	0.0022	0.000625	0.0009
NS1395	NS0668	1383572	NR.2131	0.009	TSLE 3X1X240 AL	12	0.00369	TANKVEGEN 22A	465	240	1395	0668	0.00396	0.001125	0.00162
NS1395	NS0668	1306739	NR.2131	0.181	NKBA 1X3X185 AL	12	0.10136	TANKVEGEN 22A	300	185	0668	1395	0.05068	0.029684	0.015928
NS1412	NS1210	1306126	NR.2288	0.063	DKBA 1X3X185 AL	12	0.03528	ALFRED GETZ' VEI 2B	300	185	1210	1412	0.01764	0.010332	0.005544
NS1625	NS1313	1384823	NR.1754	0.076	DKBA 1X3X240 AL	12	0.0456	48/53	345	240	1625	1313	0.0228	0.0095	0.006688
NS1625	NS1313	1306812	NR.1754	0.117	TSLE 3X1X240 AL	12	0.04797	48/53	465	240	1313	1625	0.05148	0.014625	0.02106
NS1983	NS0297	1331120	NR.4034	0.018	TSLE 3X1X240 AL	12	0.00738	HØGSKOLERINGEN 8	465	240	1983	0297	0.00792	0.00225	0.00324
NS1983	NS0297	1372337	NR.3492	0.086	DKBA 1X3X240 AL	12	0.0516	HØGSKOLERINGEN 8	345	240	1983	0297	0.0258	0.01075	0.007568
NS1996	NS1997	1358947	NR.4129	0.015		0	0	HØGSKOLERINGEN 7G	0	0	1997	1996	0	0	0
NS1996	NS1997	1345628	NR.4129	0.078	TXSE 1X3X240 AL	12	0.03198	HØGSKOLERINGEN 7G	400	240	1996	1997	0.03198	0.00975	0.00858
NS1996	NS1209	1306732	NR.4256	0.084	TXSE 1X3X240 AL	12	0.03444	HØGSKOLERINGEN 7G	400	240	1996	1209	0.03444	0.0105	0.00924
NS1996	NS1997	1372179	NR.4129	0.093	TSLE 3X1X240 AL	12	0.03813	HØGSKOLERINGEN 7G	465	240	1997	1996	0.04092	0.011625	0.01674
NS1997	NS0246	1372137	NR.4324	0.009	TSLE 3X1X240 AL	12	0.00369	GLØSHAUGVEIEN 14	465	240	1997	0246	0.00396	0.001125	0.00162
NS1997	NS0246	1359189	NR.4324	0.015	TSLE 3X1X240 AL	12	0.00615	GLØSHAUGVEIEN 14	465	240	0246	1997	0.0066	0.001875	0.0027
NS1997	NS0246	1385197	NR.4324	0.041	TSLE 3X1X240 AL	12	0.01681	GLØSHAUGVEIEN 14	465	240	1997	0246	0.01804	0.005125	0.00738
NS2020	NS02111	1396681	NR.4461	0.015	TSLE 3X1X240 AL	12	0.01025	KOLBJØRN HEJES VEI 2	465	240	2111	2020	0.011	0.003125	0.0045
NS2020	NS02111		NR.6318	0.112	TSLF 3X1X240 AL	12		KOLBJØRN HEJES VEI 2	465	240	2020	2111			
NS2020	NS02111	1397045	NR.4128	0.060	TSLE 3X1X240 AL	12	0.0246	KOLBJØRN HEJES VEI 2	465	240	2020	2111	0.0264	0.0075	0.0108
NS2021	NS0299	1344151	NR.4217	0.009		0	0	HØGSKOLERINGEN 6B	0	0	0299	2021	0	0	0
NS2021	NS0299		NR.6316	0.091	TSLF 3X1X240 AL	12		HØGSKOLERINGEN 6B	465		0299	2021			
NS2126	NS1625	1345885	NR.4525	0.104	TSLE 3X1X240 AL	12	0.04264	48/53	465	240	2126	1625	0.04576	0.013	0.01872
NS2126	NS1625	1359087	NR.4525	0.140	TSLE 3X1X240 AL	12	0.0574	48/53	465	240	2126	1625	0.0616	0.0175	0.0252

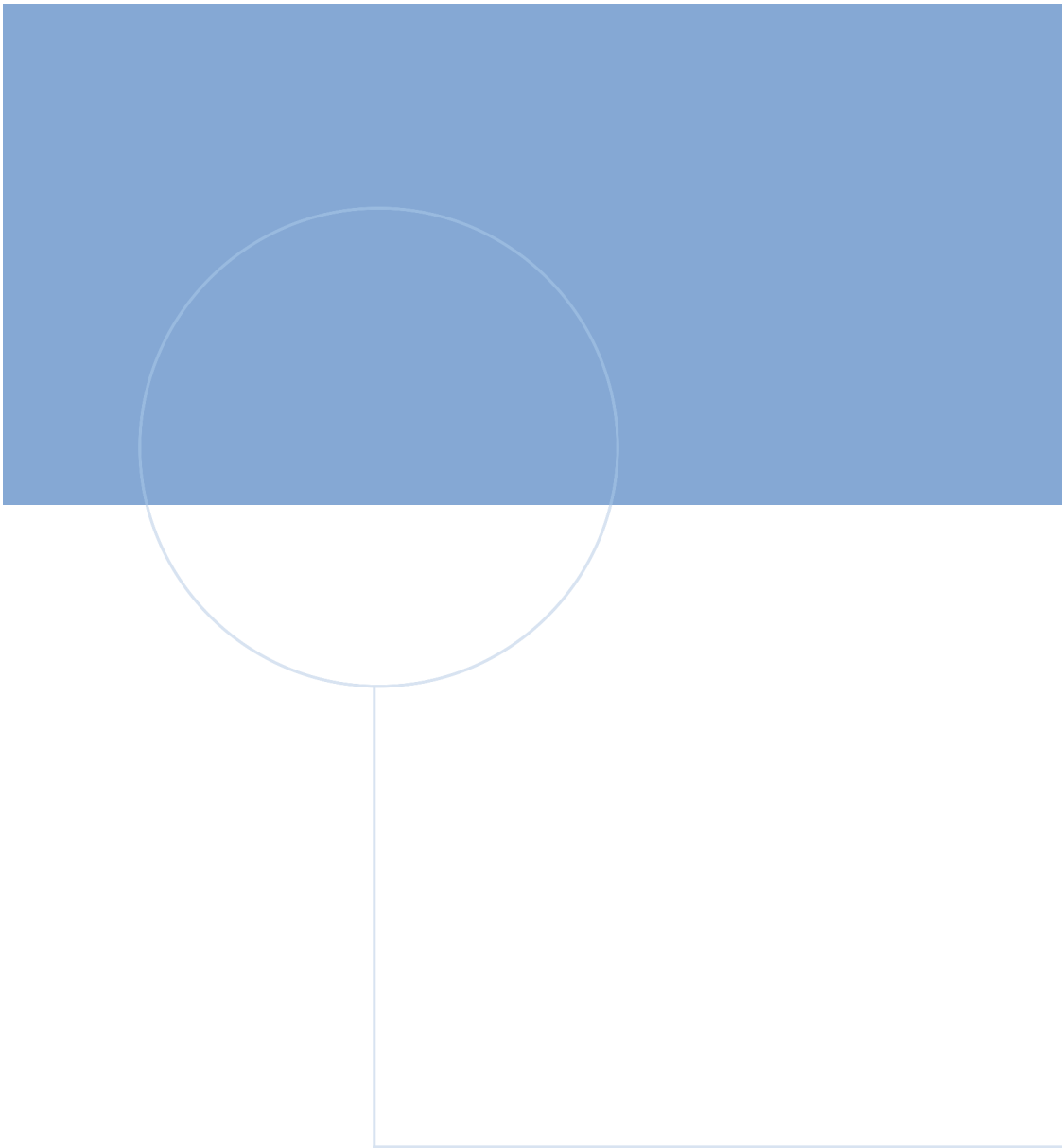

NTNU

Norwegian University of
Science and Technology